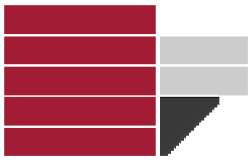

UNIVERSITY OF CALABRIA

Department of Physics

Doctoral School "Archimede" in science, communication and technology

Doctorate in

Physics and Quantum Technologies

XXVIII Cycle

Thesis Title

Physical and Chemical treatments to produce graphene and their related applications

Scientific sector: Nanosciences, nanomaterials and graphene

Coordinator

Prof. Pietro Pantano

PhD Supervisor

Prof. Lorenzo Caputi

PhD Co-supervisor

Dr. Adalgisa Tavolaro

PhD candidate

Gabriela Viviana Tubon Usca

Academic Year: 2012 – 2015

Rende - Italy

TABLE OF CONTENTS

ACKNOWLEDGMENT

First of all to God, though all this time, he protected me and always I felt his love and companionship. I want to thank all the people who have directly or indirectly contributed to the realization of this research. To my tutors Prof. Lorenzo Caputi and Dr. Adalgisa Tavolaro, thanks for the advice and teachings, but above all for the opportunity to work with you. To my colleagues Diana and Cristian who have contributed their knowledge to conduct this research, despite the disadvantages we have never given up. My husband Carlos, because you have always believed in me, by the sacrifice that we have made being away from each other, for your love and your smile that every day have fed my heart, thanks for every special moment you are part of this dream. To my mum Mary, from my birth you've given me your unconditional love, thank you for your words, that fill me in every difficult moment, thank you for believing that this dream was possible, this dream is for you, thank you for your continued support, your smiles and your prayers. My dad Luis for your support from my born until now, I feel your love at each step. My family whose support me in this last time was fundamental especially Alex, Irvin, Ibeth and Jonathan. My friends Jorge, Diana, Estela, Marta, Denia, Fanny you are my family, thanks for the laughs and encouragement to complete this dream.

To my husband, my mum and my dad

you are my reason of life.

There is a driving force
more powerful than steam,
electricity and nuclear
power: "the will"

Albert Einstein

ABSTRACT

In this work Few Layers Graphene (FLG) and Graphene Oxide (GO) were produced by using physical and chemical treatments, and two types of applications were tested with GO. The first application concerns the Drug delivery in the field of nano-medical treatments, while the second regards environmental remediation for removal of pollutants from water.

Few Layers Graphene (FLG) was produced from natural graphite by two methods: i) Sonication in a mixture of solvents, and ii) With the aid of an external agent (zeolite crystals) in the exfoliation process. In the first stage, the mixture was made with two types of solvents: N-methyl-2 pyrrolidone and Dimethylsulfoxide in different ratios. The exfoliation was carried out in that mixtures, then the centrifugation was applied in order to remove unexfoliated graphite. The supernatant suspensions were characterized using Ultraviolet - visible spectroscopy (UV-vis), and Raman Spectroscopy. The Uv-visible analysis and the Raman spectroscopy showed of existence of Few layers Graphene (FLG). In the second stage, the zeolite 4A (Z4A) was selected. The experiments were carried out to improve the exfoliation of graphite, after the exfoliation and centrifugation; the stability was achieved in those that were added the zeolite 4A. Supernatant solutions were characterized by Field Emission Scanning Electron Microscopy (FESEM), Transmission Electron Microscopy (TEM), Electron Diffration, and Raman Spectroscopy. The 3_BS suspension and the 7_F suspension showed the best results; these reached the greatest amount of days in suspension.

The Electrical Characterization (EC) was carried out using 3_BS and 7_F suspensions. The drop-casting technique was used over Al_2O_3 substrates with gold (Au) InterDigitated Electrodes (IDE). The Current–Voltage (I-V) characterization was performed, and the results were averaged for each sample and computed; in order to obtain the 2D resistivity ($\rho 2D$). Finally, an annealing treatment was applied on the Al_2O_3/Au substrates; afterwards, the resistivity improves, for 3_BS ink by a factor of 1.75 and for the 7_F ink by a factor of 1.3.

Graphene Oxide was produced from natural graphite flakes. A chemical treatment was applied in order to produce graphene oxide through the Hummer's method and Improved Hummer's method. At the end of the process, the graphene oxide was recovered under form of colloidal suspensions. The characterization was made by Field Emission Scanning Electron Microscopy (FESEM), Ultraviolet–visible (UV-vis) spectroscopy, Fourier Transform Infrared spectroscopy (FTIR), Energy Dispersive Spectroscopy (EDS), and Raman Spectroscopy. The results showed a good level of oxidation in the material and small flakes of graphene oxide.

Concerning to the adsorption process for drug delivery, a cancer drug was used. Doxorubicin (DOX) hydrochloride was placed in contact with GO to evaluate the capacity of adsorption of the material using the depletion method. The study was carried out by using different initial concentrations of DOX and different pH values. All experiments were placed under agitation in dark conditions at room temperature and different incubation times. Once the results of final concentrations was completed, the quantity loaded onto GO were calculated. Finally, the kinetic adsorption showed a percentage of 95% at pH 3 in only 24 hours of interaction. The GO presented excellent characteristics to be used in nano-medical applications.

Regarding environmental applications, an adsorption study was conducted using commercial Acridine Orange dye (AO). The adsorption process was proved using the depletion method. AO was prepared in aqueous solution at different concentrations, and these were placed under agitation and dark conditions at different contact times to evaluate the kinetic adsorption. The GO was analyzed at different weight using the highest concentration of AO. On the other hand, the temperature and the incubation time were varied, to find out the best conditions for the adsorption process. The kinetic of adsorption showed a percentage of adsorption among 75% to 95% in the first 20 min for higher concentrations and GO showed a better adsorption process to higher temperatures.

SOMMARIO

In questo lavoro, pochi strati di grafene (FLG) e ossido di grafene (GO) sono stati prodotti utilizzando trattamenti fisici e chimici, e due tipi di applicazioni sono stati testati con GO. La prima applicazione relativa al trasporto di farmaci nel settore dei trattamenti nano-medicali. La seconda applicazione è stata fatta per il risanamento ambientale per la rimozione di inquinanti dall'acqua.

Alcuni strati di grafene (FLG) sono stati prodotti dalla grafite naturale in due modi: i) sonicazione in una miscela di solventi, e ii) Con l'aiuto di un agente esterno (cristalli di zeolite) nel processo di esfoliazione. Nella prima fase, la miscela è stata fatta con due tipi di solventi: N-metil-2 pirrolidone e dimetilsolfossido a diversi rapporti. L'esfoliazione è stata effettuata con queste miscele, dopo la centrifugazione è stata applicata al fine di rimuovere la grafite non esfoliata. Le sospensioni surnatanti sono stati caratterizzati con spettroscopia Ultravioleta-visibile (UV-vis), e spettroscopia Raman. L'analisi UV-vis, e la spettroscopia Raman hanno mostrato una esistenza di pochi strati di grafene (FLG). Nella seconda fase, è stata selezionata la zeolite 4A (Z4A). Gli esperimenti sono stati effettuati per migliorare l'esfoliazione della grafite, dopo l'esfoliazione e centrifugazione; la stabilità è stata raggiunta solo in quelli in cui sono state aggiunte le zeoliti 4A. Le soluzioni surnatante sono stati caratterizzati da un Microscopio Effetto di Campo a Scansione Elettronica (FESEM), microscopia elettronica a trasmissione (TEM), Electron Diffration, e spettroscopia Raman. La sospensione 3_BS e la sospensione 7_F hanno mostrato i migliori risultati; questi hanno raggiunto la maggiore quantità di giorni in sospensione.

La caratterizzazione elettrica (CE), è stata effettuata utilizzando le sospensioni 3_BS e 7_F. La tecnica drop casting è stato utilizzato sui substrati di Al_2O_3 con elettrodi interdigitati (IDE) di oro (Au). La caratterizzazione corrente-tensione (I-V) è stata effettuata, ei risultati sono stati calcolati in media per ogni campione; a modo di ottenere la resistività 2D (ρ2D). Infine, un trattamento di annealing fu applicato nei substrati di Al_2O_3/Au; successivamente, la resistività migliora, da un fattore di 1.75 per 3_BS e da un fattore di 1.3 per 7_F.

L'ossido di Grafene è stato prodotto da fiocchi di grafite naturale. Un trattamento chimico è stato applicato per produrre ossido di grafene attraverso il metodo di Hummer e il metodo migliorato di Hummer. Al termine del processo, l'ossido di grafene è stato recuperato sotto forma di sospensioni colloidali. La caratterizzazione è stata fatta da Field Emission Scanning Electron Microscopy (FESEM), Ultraviolet-visibile (UV-vis) spettroscopia, spettroscopia infrarossa in Trasformata di Fourier (FTIR), spettroscopia a dispersione di energia (EDS), e spettroscopia

Raman. I risultati hanno mostrato un buon livello di ossidazione in fiocchi e piccoli materiali di ossido di grafene

Per quanto riguarda al processo di adsorbimento per somministrazione di farmaci, è stato utilizzato un farmaco antitumorale. Doxorubicina (DOX) cloridrato è stato posto in contatto con GO per valutare la capacità di adsorbimento del materiale con il metodo di esaurimento. Lo studio è stato effettuato utilizzando diverse concentrazioni iniziali di DOX e diversi valori di pH. Tutti gli esperimenti sono stati posti sotto agitazione al buio a temperatura ambiente e diferenti tempi di incubazione. Una volta che i risultati delle concentrazioni finali sono stati completati, la quantità caricata su GO è stata ottenuta. Infine, la cinetica di adsorbimento ha mostrato una percentuale del 95% a pH 3 a solo 24 ore di interazione. Il GO presenta ottime caratteristiche per essere utilizzato in applicazioni di nano-medicina

Per le applicazioni ambientali, lo studio di adsorbimento è stato condotto utilizzando un colorante commerciale Acridine Orange (AO). Il processo di adsorbimento è stato dimostrato usando il metodo di esaurimento. AO è stato preparato in soluzione acquosa a diverse concentrazioni, e questi sono stati posti sotto agitazione e buio a diversi tempi di contatto per valutare la cinetica di adsorbimento. Il GO è stato testato a diversi pesi utilizzando la soluzione con concentrazione più alta di AO. Da altra parte la temperatura e il tempo di incubazione erano variate, per determinare le migliori condizioni per il processo di adsorbimento. La cinetica di adsorbimento ha mostrato una percentuale di assorbimento tra il 75% al 95% nei primi 20 min per concentrazioni superiori eppure GO ha mostrato una migliore processo di adsorbimento a temperature più elevate.

OUTLINE

In this work Graphene Oxide (GO) and Few Layers Graphene (FLG) were produced by using chemical and physical treatments, and two applications were tested. The first application concerns the Drug delivery in the field of nano-medical treatments, while the second regards environmental remediation using GO for removal of pollutants from water.

Chapter I

In chapter one is describe a brief introduction to state of art of graphene and top down – approach to produce graphene materials, as well as the methods to characterize Graphene Oxide and Few Layers Graphene. Following by an introduction of nanomedical applications in drug delivery and environmental applications for removal of pollutants from water.

Chapter II

Describe the way to produce Few Layers Graphene by Physical treatments, as well as the different characterization techniques.

FLG was produced by two methods: i) Sonication in a mixture of solvents to reach a considerable amount of FLG after the centrifugation, as well as ii) With the aid of an external agent (zeolite crystals). The characterization was carried out using different techniques: SEM, TEM, UV-vis, Raman and others. To complete the study, the Electrical Characterization (EC) was conducted using the better suspensions obtained.

Chapter III

In chapter III is describes the chemical method to obtain Graphene Oxide, as well as the characterization and techniques.

Graphene Oxide was produced from natural graphite flakes. A chemical treatment was applied in order to produce graphite oxide through the Hummer's method and Improved Hummer's method. The results showed a good level of oxidation in the material and small flakes of graphene oxide.

Chapter IV

The drug delivery using GO as adsorbent material in the adsorption process is described in this chapter. Doxorubicin (DOX) hydrochloride was tested with GO to evaluate the capacity of adsorption of the material using the depletion method. In this chapter you can see the characterization stage as well as the percentage of adsorption reached for GO.

Chapter V

The last chapter presents the environmental application using GO to removal pollutants from water. A commercial dye Acridine Orange (AO) was used to study the adsorption process on GO. The adsorption process was proved using the depletion method. The chapter presents the process to evaluate the kinetic of adsorption, as well as the best conditions to reach a higher capacity of loading.

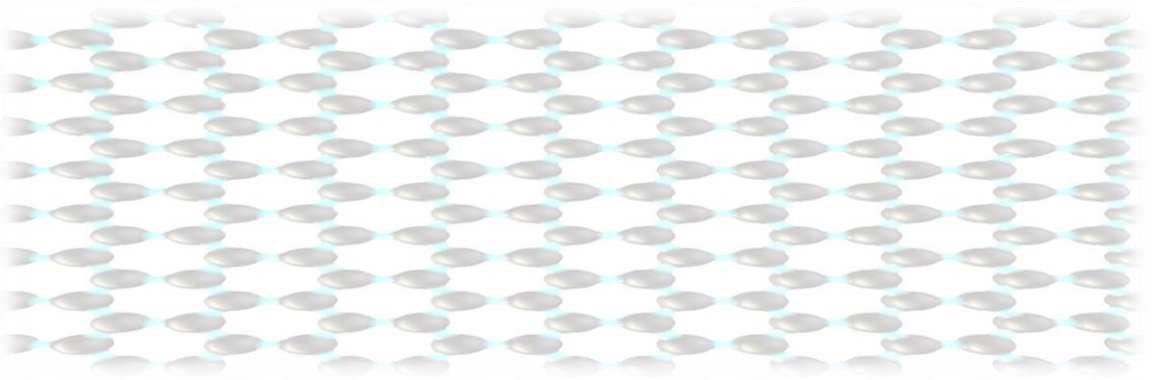

CHAPTER 1

INTRODUCTION

1. Graphene State of Art

Graphene has marked a new age in terms of 2D materials and nanostructures, it has earned great attention due to the fascinating properties (see table 1.), and the possible applications in many areas of science and technology. One of the main problems is the production to large scale. Until now several methods to prepare graphene have been developed, such as thermal decomposition of hydrocarbon gases/liquids by Chemical Vapor Deposition (CVD)[1][2], Epitaxial Growth [3][4], Chemical exfoliation of Graphene Oxide (GO) and Reduced Graphene Oxide (RGO) [5][6][7][8] and Liquid Phase Exfoliation of Graphite (LPEG)[9][10][11]. Among these, GO/RGO and LPEG are the most favorable ways to produce graphene in large quantities with minimal environmental impact.

Graphene oxide can be easily obtained through exfoliation of graphite oxide. The most common method for the oxidation of graphitic planes is the Hummer's method [5], in which a mixture of sulfuric acid, nitric acid and aliquots of potassium permanganate is used to achieve graphite oxide. Once graphite oxide is obtained, graphene oxide is achieved through appropriate exfoliation treatments [12][13] that permit the complete exfoliation of graphite oxide, thus obtaining large quantities of material. After the chemical treatment and exfoliation, the obtained GO presents interesting features due to the functional groups added between graphite layers. The functional groups that decorate the graphitic planes are hydroxyl, carboxyl, carbonyl and epoxides [14], and through these, graphene oxide acquires solubility, resulting in colloidal suspensions [15]. To recover the main characteristics of graphene, GO is subjected to various reduction treatments (RGO) [16][17]. However, RGO still contains defects due to the functional groups added during the oxidation process to the structure, which makes it difficult to recover the main properties of monolayer graphene. Nevertheless, the changes undergone in the structure of RGO endow solubility to the graphene layers. This acquires affinity with an aqueous medium, allowing the structure to be adapted and used together with other macromolecules. In this way GO can be used in the field of nanotechnology, for example in biomedical applications, such as the delivery of drugs [18][19] and environmental applications, such as the decontamination of pollutants in water [20][21]. Along with the functionalities of RGO and GO, some applications have also been developed in the electronics industry, such as sensors [22] and Field Effect Transistors [17][23].

On the other hand, LPEG was developed as an effective, fast and economical alternative to produce graphene on a large scale without introducing defects to the basal plane, resulting in inks or suspensions based on Few Layers Graphene (FLG). In 2008 *Fernandez Y. et al.* [9] obtained suspensions of few layers graphene with the assistance of solvents reaching large production of defects-free graphene. The study was carried out in various solvents, the most significant one has been N-Metyl-2-Pirrolidone (NMP) (Surface Tension= 40.9; Solubility Parameters: δ_D = 18, δ_P = 12.3 δ_H = 7.2) achieving suspensions of up to 0.01 mg/mL and the stability of suspension of about five months.

The parameters of the solvents should be a surface tension close to 40.79 mJ/m^2, and suitable Hansen solubility parameters [24].

Many solvents have been studied, especially those that meet the characteristics of surface tension and Hansen solubility parameters for suspensions of graphene. Some are Dimetylformamide (DMF)(Surface tension: 37.10 mJ/m^2; Hansen solubility parameters δ_D = 17.4, δ_P = 13.7 δ_H = 11.3), Dimethylacetamide (DMA) (Surface tension: 36.70 mJ/m^2; Hansen solubility parameters δ_D = 16.8, δ_P = 11.5 δ_H = 10.2), among others. However, the interaction between the solvent and graphene flakes could not be completely explained, because Hansen parameters also influence in the suspension [25], and it is doubtful to know whether the combination of dispersive, polar, and H-bonding interactions accurately describes the system at the molecular scale. One way to understand the solvent-graphene interaction could be by doing a comparison with NMP suspensions of carbon nanotubes, where it is claimed that the most important parameter is the dispersive component [24]. More details will be discussed in section 1.3.3. Concerning to the applications in LPEG there have been some potential applications in sensors [26], devices in transparent electrodes [27], and conductive composites [9].

1.1. Allotropes of Carbon

Carbon belongs to Group IV elements that are very active in producing many molecular compounds and crystalline solids. Carbon has six electrons, two electrons are found in the 1s orbital close to the nucleus, and four valence electrons in the valence shell, enabling it to bond to four other atoms, which tend to interact with each other to produce the various types of carbon allotropes [28]. In elemental form, the four valence electrons occupy the 2s and 2p orbitals, as illustrated in figure 1.1. When carbon atoms come together to form a crystal, one of the 2s electrons is excited to the 2p_z orbitals from energy gained from neighboring nuclei, which has the net effect of lowering the overall energy of the system. Interactions or bonding subsequently follow between the 2s and 2p orbitals of neighboring carbon atoms. [29]

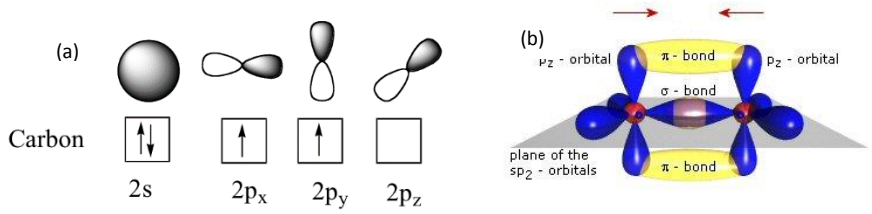

Figure 1.1 Arrangement of electrons and their correspondent spin (a) elemental carbon, (b) The 1s electron and two electrons of the p orbitals of the second shell interact covalently to form three sp^2 hybrid orbitals.

In chemistry, these interactions or overlap of atomic orbitals is generally called hybridization, and the junctions of orbitals that are formed are referred to as hybrid orbitals. The existence of numerous flavors of hybridization in carbon is the reason to form different allotropes.

Diamond

In diamond, Each carbon atom is covalently bonded to four other carbons in a tetrahedron, as is presented in figure 1.2(b); these tetrahedrons together form a three-dimensional network of six-membered carbon rings in the chair conformation, allowing for zero bond-angle strain. Therefore, diamond consists purely of sp^3 hybridized bonds, hence it possess highest hardness and thermal conductivity of any bulk material.

Graphite

Graphite is the most stable form of carbon; it has a layered planar structure. In each layer, the carbon atoms are arranged in a hexagonal lattice with separation of 0.142 nm, and the distance between planes (layers) is 0.335 nm, as is demonstrated in figure 1.2(a). Unlike diamond it is an electrical conductor, due to the sp^2 hybridizing, which has a delocalization of the π- bond electrons above and below the planes of the carbon atoms. High-purity graphite does not readily burn, even at elevated temperatures, for this reason, it is used in nuclear reactors [30] and for high-temperature crucibles for melting metals.

Fullerenes

Carbon nanomaterials make up another class of carbon allotropes. Fullerenes (also called buckyballs) are molecules of varying sizes composed entirely of carbon that take on the form of hollow spheres [31], ellipsoids, or tubes [32]. Buckyballs and buckytubes have been the subject of intense research, both because of their unique chemistry and for their technological applications, especially in materials science, electronics, and nanotechnology. Figure 1.2(c) represents the geometry of fullerene.

Carbon Nanotubes

Carbon nanotubes are cylindrical carbon molecules that exhibit extraordinary strength and unique electrical properties [33] and are efficient conductors of heat [34].

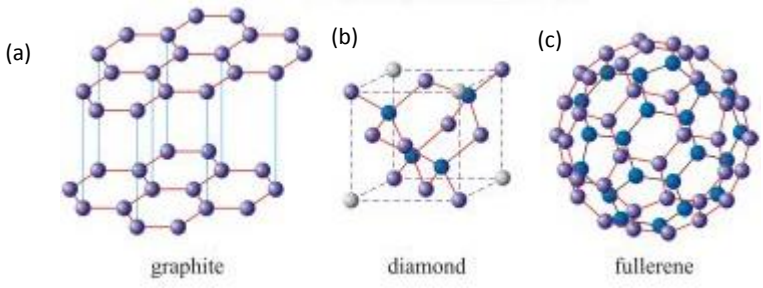

Figure 1.2 Allotropes of Carbon (a) Graphite; (b) Diamond; (c) Fullerene

1.2. Definition of Graphene

Graphene is a carbon allotrope, whose structure is a single planar sheet of sp^2 bonded carbon atoms that are densely packed in a honeycomb crystal lattice. Carbon-carbon bond length in graphene is ~0.142 nm, and these sheets stack to form graphite with an interplanar spacing of 0.335 nm [35]. The planar honeycomb structure of graphene has been observed by using different atomic microscopies and is show in figure 1.3.

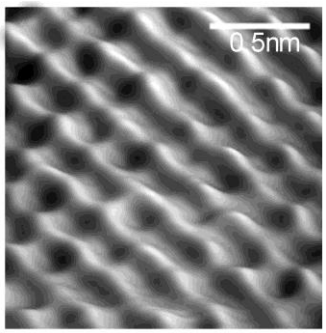

Figure 1.3 Carbon atoms and bonds in the honeycomb structure, image from STM microscopy. Ref. from [36]

Since the graphene was isolated in 2004 by Geim & Novoselov, graphene has marked a revolution in material science. Graphene is a semi-metal or zero-gap semiconductor, allowing it to display high electron mobility at room temperature, and others unique properties (see table 1.), as well as unbelievably thin thickness.

Property Name	Value	Reference
High Specific area	2630 $m^2 g^{-1}$	[35]
High values of mobility carriers	200000 $cm^2 V^{-1} s^{-1}$	[37]

Thermal conductivity	~5000 W/mK	
Fracture strength	125 GPa	[38]
Young's modulus	~ 1100 GPa	
high optical transmittance (with an absorption of ~2.3% towards visible light)	97.7 %	[39][40]

Table 1. The main discover properties of graphene material.

1.3. Production of Graphene

Graphene can be obtained by two different approaches. The Bottom-up strategy consists of assembling carbon atoms resulting from the decomposition of hydrocarbons on suitable surfaces (Chemical Vapor Deposition (CVD)) [41], or from the segregation of bulk carbon in SiC [4]. The other approach, called top-down, is suitable for the mass production of Graphene, and consists in exfoliating Graphite using mechanical [42] or chemical treatments [5] [16].

1.3.1. Chemical Oxidation of Graphite to obtain Graphene Oxide (GO)

One advantage of using graphite is its availability and low cost. GO can be produced by the oxidative treatment of graphite via one of these three methods; Brodie [43], Hummers [5], and Staudenmaier [44].

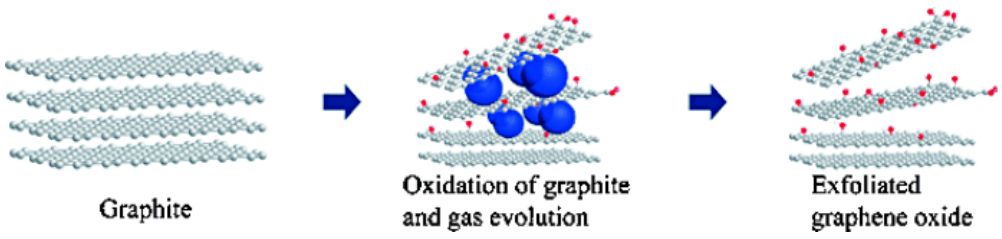

Figure 1.4 Schema of oxidation of graphite by using different methods, the following step to obtain graphene oxide is the exfoliation.

Brodie's method involves the addition of potassium chlorate (KClO3) to the slurry of graphite in fuming nitric acid. Staudenmaier improved Brodie's method by adding the chlorate in multiple aliquots over the course of the reaction instead of a single addition as

Brodie had done. This resulted in similar extent of oxidation to Brodie's multiple oxidation approach. Thereafter, Hummer and Offeman developed an alternative oxidation method by reacting graphite with a mixture of potassium permanganate ($KMnO_4$) and concentrated sulfuric acid (H_2SO_4), and achieved similar oxidation levels as well, but more rapidly. These three methods produce graphite oxide (GrO).

Once the material GrO has been obtained, a variety of thermal and mechanical methods can be used to exfoliate GrO to graphene oxide (GO), though sonication and/or stirring GrO in water are the most common. Thermal treatment can be used to produce expanded graphite [45], through applying a rapid microwave expansion to 700 W in a conventional microwave oven. The expansion treatment tries to improve the successive exfoliation step. In the sonication process, shear forces and cavitation [45], despite being much faster than mechanical stirring, has a great disadvantage in that it causes substantial damage to the graphene oxide platelets [12], *i.e.* the growth and collapse of micrometer-sized bubbles or voids in liquids due to pressure fluctuations, act on the bulk material and induce exfoliation. After exfoliation the solvent-graphene interaction needs to balance the inter-sheet attractive forces, these solvents would be water or polar organic media. When the sonication was produced, colloidal suspensions are obtained based on graphene oxide.

The formed GO has a basal plane decorated mainly with epoxide and hydroxyl groups, while its edges are decorated with carboxyl and carbonyl group (Figure 1.5). Currently, it does not existing a defined structure of Graphene Oxide (GO). Many researchers, such as Ruoff and co-workers [14][46], proposed different structures of GO.

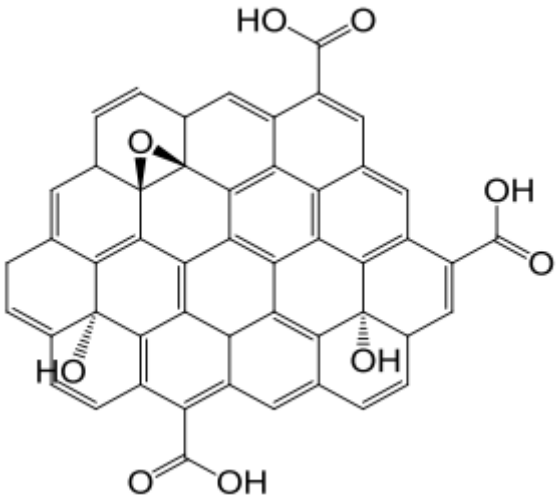

Figure 1.5 Chemically functional graphene, structure of GO with the functional groups.

One of the advantage of GO is undoubtedly that it is easily processable in liquid media such as water. GO is electrically insulating because of its disrupted sp^2 bonding networks [47]. GO is also a 2D form of carbon but with chemical moieties that render new functionalities while preserving some of the unique properties of the pristine material. The chemical exfoliation of graphite via oxidation leads to covalent functionalization, which dramatically alters the structure of graphene [46]. Therefore, it is not appropriate to refer to GO or reduced GO simply as graphene

since their properties are substantially different. GO can recover its electrical conductivity, by restoring its π-network by reduction [17][48], or thermal shock [45].

1.3.2.Exfoliated Graphene from Liquid Phase Exfoliation of Graphite (LPEG)

In order to produce graphene layers, many research groups have studied the simple exfoliation by sonication in suitable solvents and aqueous media. The liquid phase exfoliation, as it is showed in figure (1.6), typically involves three steps: i) dispersion of graphite in a solvent, ii) exfoliation, by using different types of sonication methods and iii) purification, through vacuum drying or filtration to recover the material.

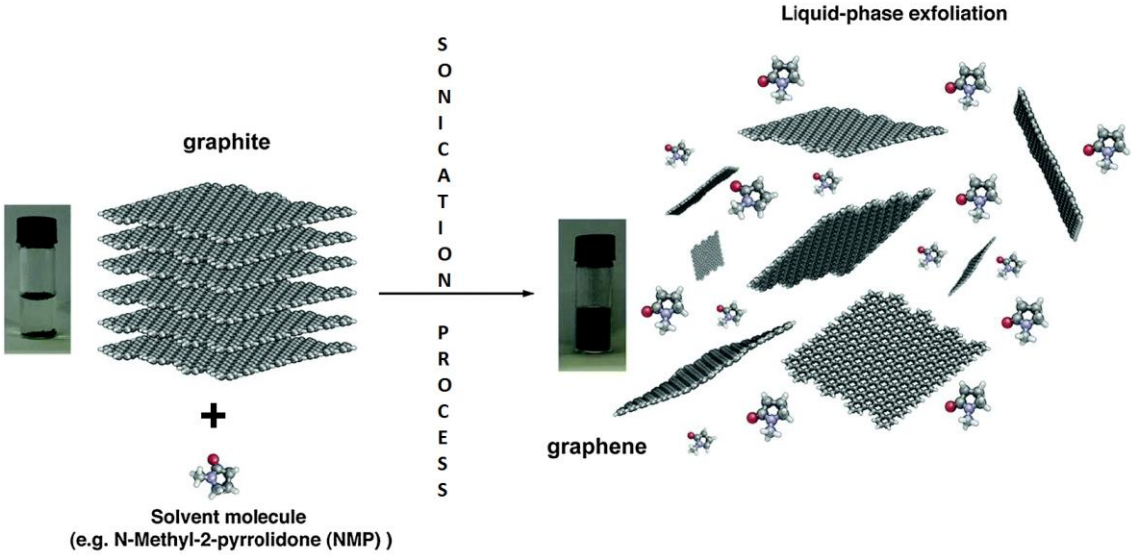

Figure 1.6 Exfoliation of graphite flakes by using a sonication method to produce graphene suspensions.

Solvents

In previous reports, *Y. Hernandez, et al. (2008)*, reported an easy method to obtain few graphene flakes applying a sonication method for some hours [9]. This procedure may be conducted thanks to the fact that the van der Waals attraction among adjacent layers is weak enough to let them slide on each other in the direction perpendicular to the c-axis. However, the attraction is strong enough to make complete exfoliation into individual layers challenging. In this sense, the interfacial tension plays a key role: it has been demonstrated that when the interfacial tension between solid and liquid is high, there is a poor dispersability of the solid in the liquid [49]. When talking about graphite, if the interfacial tension is high, the flakes tend to adhere to each other, hindering their dispersion in the liquid. It happens mainly for the property of the surface of a liquid that allows it to resist an external force, due to the cohesive nature of its molecules. [49] The best solvents for the dispersion of graphene and graphitic flakes have a $\Upsilon \sim 40 mJ/m^{-2}$, since

they minimize the interfacial tension between both. The solvents which have proved excellent match with the graphene suspensions are N-methyl-2-pyrrolidone (NMP – 40 mJm-2), N, N-dimethylformamide (DMF – 37.1 mJ m-2), and ortho-diclorobenzene (o-DCB – 37mJ m-2), as can see in figure 1.7.

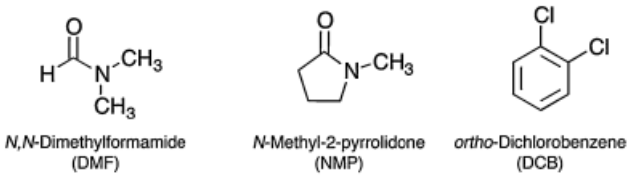

Figure 1.7 Common solvents used to exfoliate graphite into liquid phase; the chemical structure reveals different functional groups. (DOI: 10.1039/c3cs60217f)

A complete list of solvents tested as exfoliation media is given in reference [9].

Many of the solvents named have disadvantages, *e.g.* NMP is an eye irritant and may be toxic to the reproductive organs [50], and DMF may have toxic effect on various organs [51]. The main goal is to achieve good stability and more concentrated suspension, without hazards. Furthermore, high boiling points (NMP 203 ºC, o-DCB 181 ºC, DMF 154 ºC) limit their viability for real manipulation.

In order to achieve this scope, graphene suspensions have been produced in low boiling point solvents. However, before selecting the proper solvent to produce exfoliation is necessary to considering the Hansen Parameters. Hansen Parameters is a way of predicting if one material will dissolve in another and form a solution. The most important factor that must be taken into consideration when selecting the Hansen parameters, are that relative to the dispersability, polarity and cohesion H. For a good solvent to match with the surface of graphene the parameters must be in an interval of $\delta_D = 18\ (15-21)$ $(\text{MPa})^{1/2}$, $\delta_P = 9.3\ (3-17)$ $(\text{MPa})^{1/2}$, $\delta_H = 7.7\ (2-18)$ $(\text{MPa})^{1/2}$ [52]. When the production is based on low boiling point solvent, the dispersion quality is particularly sensitive to the dispersive Hansen Parameter. Successful dispersions are only achieved for solvents with 15 $\text{MPa}^{1/2} < \delta_D <$ 21 $\text{MPa}^{1/2}$ [53]. Furthermore, reasonable dispersions can be achieved for a much wider range of polar δ_P and H-bonding δ_H Hansen parameters (from 2-3 $\text{MPa}^{½}$ to 17-18 $\text{MPa}^{½}$ in each case) [53]. In 2010 *Coleman J. N. and co-workers* [52], produced suspensions in low boiling points with concentrations between 0.4 mg/mL and 0.5 mg/mL for chloroform and Isopropanol. The latter named displayed only flakes with less than 5 layers. One aspect to worth notice is that the dispersion in volatile solvents facilitates the deposition of graphene flakes onto substrates by the spraying method. While some aggregation is observed, the deposited flakes tend to be more numerous and thinner than the flakes deposited with high boiling point solvents.

Sonication

Since the first successful exfoliation of graphene in an organic solvent such as NMP in 2008, improvements in concentration of graphene dispersions have been achieved. By using drastically longer sonication times ~500 h [11], the concentration grows as time increased. While time varies from 0.05 to ~400 h, the produced concentrations for NMP reached values from 0.01 mg/mL to 1.2 mg/mL [11].

The exfoliation and dispersion processes need a certain amount of energy to be activated and usually this energy is provided from the outside by the means of sonication, whose effects are strongly dependent on solvent parameters, such as solvent viscosity, vapour pressure, and once again, surface tension. These type of solvents require much energy to induce cavitation and consequently release more energy [54]. Low-boiling solvents, with their high vapour-pressures and lower viscosities, release only less energy to graphite planes with worse exfoliation results [55]. Besides cavitation phenomena, particles are also subjected to shear stress forces, which linearly depend on solvent viscosity. However, the time consuming approach requires high energy. Prolonged sonication is not only energy-consuming, the size of the flakes are severely reduced. Sonication cuts vertical and horizontal exfoliated graphene flakes, which constitutes a critical problem for applications.

Raman spectra can provide information on the number and position of broken-conjugation areas in graphene, so-called graphene atomic - or point - defects, which can affect the electronic properties of graphene. Typically, the graphite sonication is considered as a non-destructive process; therefore defects are mainly located at the edges of the graphene flakes, and the basal plane is basically defect free [10].

Centrifugation

After sonication, the majority of the material is composed of thick graphite flakes, which can be removed by using differential strategies based on differential ultracentrifugation (sedimentation – based separation, SBS) [56] in a uniform medium or in a Density Gradient Medium (DGM) [57]. The SBS process separates particles on the basis of their sedimentation degree in response to centrifugal force acting on them [56].

The effect of centrifugation on the distribution is very strong, figure 1.8 (a), especially for short sonication times. For example, for sonication time of 2 min., even after mild centrifugation (15 min, 800rpm), proportion of large flakes with $L<6.5$ μm decreased dramatically to less than 1%, whereas when the suspension is not centrifuged, it contains 15% of large particles ($L > 11$ μm). This means that by applying mild centrifugation, large flakes and aggregates are completely removed, leaving a dark homogenous suspension

[58]. In conclusion, the sonication and centrifugation processes have noticeable effects on the mean flakes size; prolonged process leads to a suspension with reduced fraction of large particles.

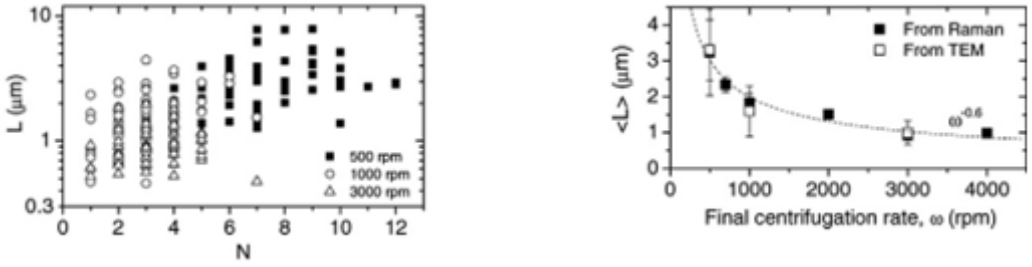

(a) (b)

Figure 1.8 (a) Plot represents the variation of number of layers between lateral sizes, depending of the centrifugation rate. (b) Mean flake estimated from the TEM analysis and the Raman spectra, dashed lines represent the empirical behavior. DOI: 10.1016/j.carbon.2011.09.001

1.4. Characterization Methods

The characterization of graphene is important to identify the better production procedures. Depending on the specific form of production, the more important properties to be determined are the lateral size, purity, thickness, other physical- chemical properties, and sheet resistance.

The most used experimental techniques are Scanning Electron Microscopy (SEM), Transmission Electron Microscopy (TEM), Atomic Force Microscopy (AFM), to verify the chemical structure Fast Fourier Infrared Spectroscopy (FTIR) and X-ray photoelectron spectroscopy (XPS), the last one sometimes used to study the electronic properties of graphene. In order to complete the study of electrical properties, the Flicker Noise measurements [59] and four point probes [60] are used.

1.4.1. Fourier Transformed Infrared Spectroscopy (FTIR)

In Fast Fourier Infrared Spectroscopy (FTIR) IR radiation passes through a sample, where the infrared radiation is absorbed and some of it is passes through (transmitted).

Infrared spectroscopy can result in the identification (qualitative analysis) of every different kind of material. In addition, the size of the peaks in the spectrum is a direct indication of the amount of material present. Through modern software algorithms, infrared absorption is an excellent tool for quantitative analysis.

Various studies conducted for graphene have shown the characteristic of Graphene Oxide by using FTIR, this is useful to identify the principal functional groups, see figure 1.9, due to the

chemical reaction that carried out for graphite and the successive changes in the basal plane [12][61]. The FTIR spectrum of graphene shows characteristic peaks, localized from 3050 to 3800, to belong at O-H stretching vibrations, these vibrations are relative to Hydroxyl and Carboxyl groups [62]. On the other hand, carbonyl groups appear at (1750 – 1850) cm^{-1}, to sp2 – hybridized, which correspond to C=C bonds are localized at (1500 – 1600) cm^{-1}; sometimes these vibrations have a weak infrared intensity. The last to analyze are the epoxy groups, which form the fingerprint of the material, the most prominent peaks are localized at (1230 – 1330) cm^{-1}. In general, the deep of the position becomes an estimate of the quantity of the functional groups over the basal plane in the structure.

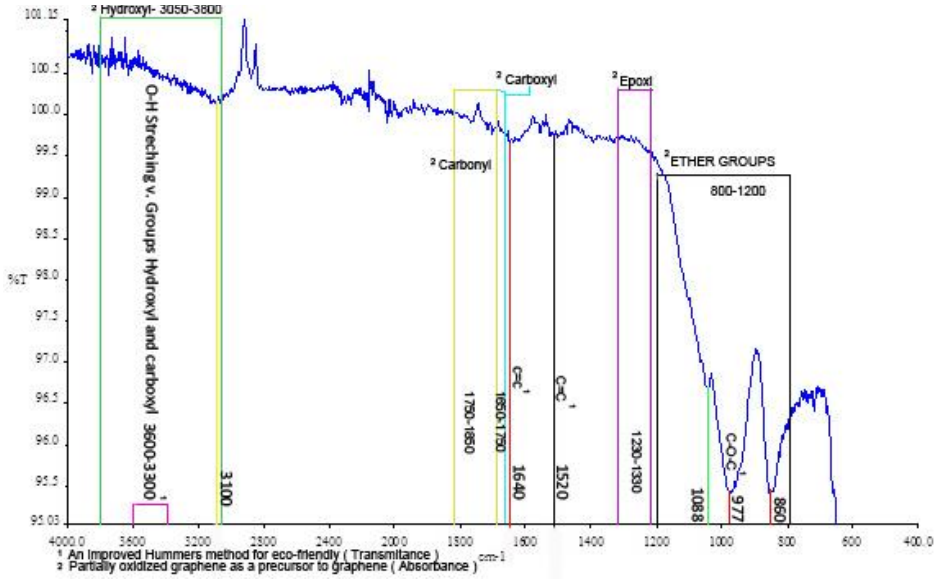

Figure 1.9 Represent a typical FTIR spectrum, here is represents the characteristic modes vibrational and intervals for each functional group for graphene oxide.

On the other hand, this technique is not frequently used to determine the chemical structure of graphene by CVD, epitaxial growth SiC, LPE, et al., because the main objective is to determine the existence of disorder, especially when others functional groups disrupt the structure.

1.4.2 UV-visible Spectroscopy (UV-vis)

The absorption on UV-vis corresponds to the excitation of outer electrons, as considerable as valence electrons, which can generally be found in one of three types of electron orbital:

1. Single, or σ, bonding electrons.
2. Double or triple bonds (π bonding orbitals)
3. Non-bonding orbitals (lone pair electrons)

Sigma bonding orbital tend to be lower in energy than π bonding orbitals, which in turn are lower in energy than non-bonding orbitals. When electromagnetic radiation of the correct

frequency is absorbed, a transition occurs from one of these orbitals to an empty orbital, usually an antibonding orbital, σ*, π* [63]. The possible electron jumps are shown in figure 1.10.

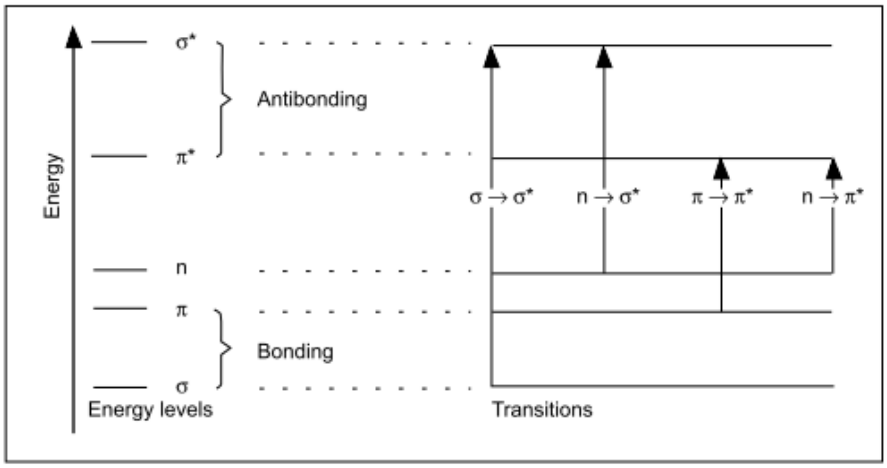

Figure 1.10 Electron transitions in ultraviolet/visible spectroscopy. Reference from: http://media.rsc.org/Modern%20chemical%20techniques/MCT4%20UV%20and%20visible%20spec.pdf

This technique is useful for graphene. In Graphene Oxide (GO), for example, the studies verify the level of oxidation. *Marcano et al* [6]., investigated diverse levels of oxidation of three production methods Hummers (HGO) [5], Hummers modified (HGO+) and Improved Hummers (IGO). The analysis UV-vis showed π – π* transitions (conjugation), therefore, less energy is necessary for the electronic transition, which results in a higher λ_{max}. IGO, HGO+ and HGO had very similar λ_{max} localized from 227 – 231 nm. This report is very similar and comparable with other reports, e.g. *G. Eda* [64] report that when π – π* transitions suffer a red-shifted, it indicates that is oxidized to a lesser degree. On the other hand, the spectra of graphene present other shoulder around $\sim 300 - 310\ nm$, this is attributed to $n - \pi^*$ transitions of the carboxyl groups (C=O bonds) [62] [6][64], the characteristic spectra is showed in figure 1.11.

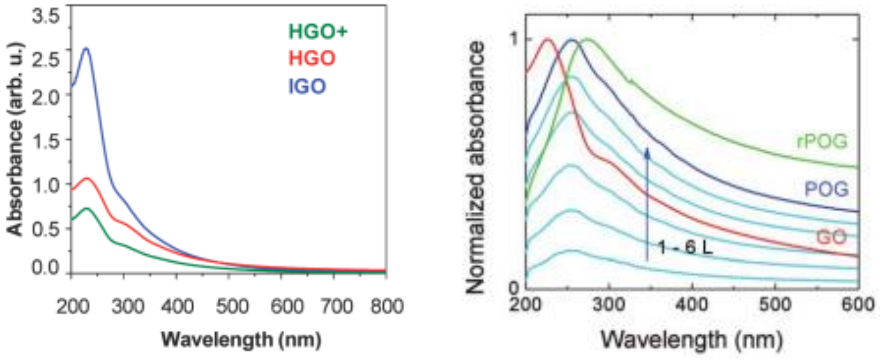

(a) (b)

Figure 1.11 Uv- vis spectrum belong to graphene oxide (GO). (a) Comparison between different methods of production graphene oxide, here is showing different levels of oxidation, from ref. [6] (b) Spectrum of Graphite Oxide, here is evident the red-shifted in Partial Oxide Graphene (POG) and Reduced Graphene Oxide (rGO), from ref. [64]

UV-visible analysis is used to verify the concentration of the graphene suspension by using the Lamber-Beer law [65]. Nguyen et al.,[66] reported a distinct absorption peak at 268 nm, which is related to the electronic π–π∗ transition of C=C bonds. The intensity of absorption spectra at 268 nm increases with the FLG concentration. In order to calculate the coefficient of absorption, the equation $A = \varepsilon LC$ was used, where A represents the absorption intensity (at 268 nm); L is represented as the distance that the light has travel through FLG dispersions and C is the concentration of FLG dispersions. The calculated absorption coefficient ε was ∼1371 L g^{-1} m^{-1}, figure 1.12 represent the summary of the experiment reported from ref. [66]. Similarly, the UV-visible spectrum is used to analyze the Carbon Quantum Dots (CQDs), when the solution is produced the characteristic peak is around 266 nm [67], therefore, to analyze graphene solutions or related is necessary verify the range wavelength and absorbance, to get a concentration and functional vibrations groups correctly.

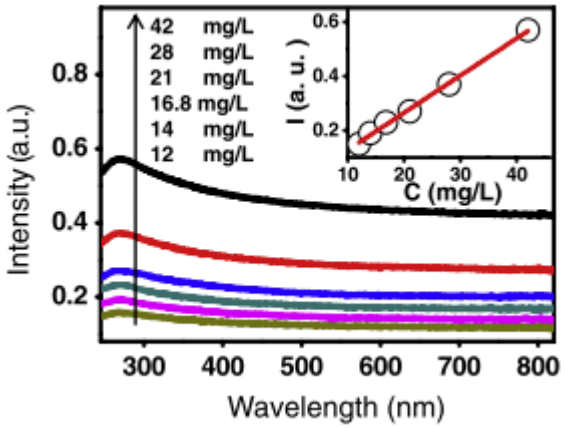

Figure 1.12 UV- visible spectra of few layers graphene, these represent different concentrations. From ref. [66]

1.4.3 Raman Spectroscopy

The most powerful and nondestructive tool to characterize graphitic materials and carbon nanostructures is Raman Spectroscopy. When a monochromatic light beam is incident on a material, a small portion of this beam is scattered in all directions. Understand the dispersions of the phonons in graphene are essential to interpret the Raman spectrum. To explain these dispersions it is necessary considering them as the result of collision processes between light and material molecules. There are two types of dispersions elastic dispersion (Rayleigh) and inelastic dispersion (Raman).

Raman Spectroscopy has always played an important role in the structural characterization of graphitic materials. The Raman signal variations observed for different numbers of graphene

layers, not only demonstrate changes in the electron bands, but also provide an easy and non-destructive means to determine single, bi-layer and few-layer graphene [29][68].

There are three important and characteristics Raman band in graphene, independently of the type of graphene that being analyzed. The first is called G band, it is associated with the doubly degenerate (TO and LO) phonon mode (E2g symmetry) at the Brillouin zone center [69]; many studies affirm that G-band is the only band coming from a normal first order Raman scattering process in graphene. The G Peak is due to the bond stretching of all pairs of sp^2 atoms in both rings and chains (A. Ferrari, 2006). The Raman shift reported to G peak in graphene and graphite bulk is localized at 1580 cm^{-1} measured at 514.5nm excitation (2.41 eV) [70]. An additional study was realized using a excitation source laser of 633 nm, in which the G band is localized around 1575 cm^{-1} [71]. Such a significant variation in G position and width may be attributed to electronic doping of the graphene by the substrates [72]. The intensity of G band increases almost linearly as the graphene thickness increases [73]. The Full Width at Half Maximum (FWHM) for G line varies within (18-21 cm^{-1}), for short sonication times, namely few minutes, nevertheless, the value of FWHM decrease to 12-16 cm^{-1} as the sonication time increasing (Alaferdov et al., 2014). The reduction of the FWHM for longer processing time probably indicates improved quality (less defects) of obtained flakes. FWHM tends to be around 12 – 14 cm^{-1} for thin flakes (3 – 15 nm) and 19 – 21 cm^{-1} for thicker flakes (more than 20 nm) [72]. In defect free graphene, the variation of FWHM of the G peak is due to doping. [71]

On the other hand, the G' and D-bands originate from a second-order process, involving two TO phonons near the K point for the G' band or one TO phonon and one defect in the case of the D-band. The G' band does not meet the Raman fundamental selection rules and has nothing in common with G peak; rather constitute approximately twice the D band frequency ($\omega_{G'} \sim 2\omega_D$), that is the reason for many authors refers it as 2D band. However, this two-phonon band is allowed in the second-order Raman spectra of graphenes without any kind of disorder or defects [69].

Both the D and 2D bands exhibit a dispersive behavior since their frequencies in the Raman spectra change as a function of the energy of the incident laser E_{laser}. The dispersive behavior in the frequency of D and 2D are originate from double resonance (DR) effect [69].

The D mode is due to breathing modes of sp^2 atoms in rings, namely A_{1g} breathing mode [70], and is a measure of the disorder in graphite planes due to defects incorporated into the graphitic structure. For perfect graphitic structure it a forbidden transition, but when the symmetry is broken in presence of disorder (e. g. a defect), the transitions are allowed. The D

band intensity decreases when increment of graphene thickness and is invisible for bulk graphite, demonstrating that defects are more easily introduced into thinner graphene sheets [73]. Hence in well-ordered (i.e. defect free) graphene and graphite, the D band is absent (Dresselhaus et al., 2005). In liquid phase exfoliation of graphene, the D band appears as a general characteristic due to the sonication energy, it brings damages in graphene sheets and create edge defects. The defects are attributed to edges instead of the structural disorder. Another important aspect widely studied is the I_D/I_G ratio, Chabot et al. [74] have reported a value of 0.25 for the process where graphene was obtained by Gum Arabic assisted physical sonication. Gayathri et al. [71] have informed of I_D/I_G ratio in the range of 0.2 – 04 in liquid phase exfoliation. Reina et al. [75] reported an I_D/I_G ratio 0.93, while Cheng et al. [76] reported a 0.05-0.3 ratio, both using Chemical Vapor Deposition. Different electrochemical methods for graphene synthesis give an I_D/I_G value in the range of 0.1 – 0.6 [77]. Regarding to Graphene Oxide (GO) is characteristic higher I_D/I_G ratios due to the high degree of oxidation [14]. Arapov et al. [78] reported values of I_D/I_G ratio about 7 – 8 , it correspond to graphene films prepared using oxidation.

The 2D band constitute an interesting aspect to distinguish graphite from few layers graphene and monolayer graphene, so the number of layers in the graphene sheet can be possibly determined from the intensity, shape and positions of the 2D band. The common practice to find the curves under the curve is fitting; generally the fit is realized using Lorentzian distribution. Compared with graphite, the difference lies in the fact that in graphite the 2D mode is composed of two elements, namely $2D_{1A}$ and $2D_{1B}$ (Yoon et al., 2008), generally about ¼ and ½ the G mode amplitude, respectively.

The 2D peak for single layer graphene is narrower and its intensity is around four time that of the G peak, it has a wavenumber localized at $\sim 2700\, cm^{-1}$, while the FWHM of peak correspond a value of $\sim 30\ cm^{-1}$ (Ferrari and Roberson, 2000; Ferrari et al., 2007).

For multilayer graphene, the 2D band can be fitted with multiple peaks due to the splitting of the electronic band structure [79]. Despite, for Single Layer Graphene (SLG) has an unique peak, when the study is conducting to Bilayer Graphene , the peak broadening into four components ($2D_{1B}$, $2D_{1A}$, $2D_{2A}$, $2D_{2B}$), it happens due to the Double Resonance process [68], a brief summary of the deconvolution peaks of 2D peak in bilayer graphene is shown in Table 2. The situation varies when the number of layers increases, from 3 layers up to 10 layers is easier distinguish few layers graphene thanks to $2D_{1A}$ and $2D_{1B}$ peaks, as incremented the number of graphene layers, $2D_{1A}$ reduces its intensity and suffers a blueshifted, hence if graphene layers are > 10

layers is difficult differentiate from bulk graphite and $2D_{1B}$ peak incremented its intensity, forming the characteristic peak of graphite localized at $\sim 2720\ cm^{-1}$. In table 3 are shown the relative peak positions at different graphene thickness [80]. The 2D band is red shifted for electron doping and blueshifted for hole doping, due to the charge transfer induced modification of the equilibrium lattice parameter [81]. Therefore Raman spectroscopy constitutes an effective technique to determine the doping type and dopant concentration in graphene. [71][80]

Incident Laser nm	Substrate	Sample Graphene	Number of layers	D Band cm^{-1}	G Band cm^{-1}	2D band cm^{-1}	Lorentzian peaks positions -2D				Reference
							$2D_{1B}$ cm^{-1}	$2D_{1A}$ cm^{-1}	$2D_{2A}$ cm^{-1}	$2D_{2B}$ cm^{-1}	
633	Si	Flakes	bilayer	1332	1579	2658	2617	2652	2676	2693	From [71]
		Flakes	bilayer	1332	1582	2656	2622	2657	2686	2709	
	Quartz	Flakes	bilayer	1328	1573	2660	2609	2640	2662	2682	
		Flakes	bilayer	1328	1573	2660	2621	2647	2670	2690	
488	Glass	Micro-mechanical cleavage	bilayer	....	1583	2696	2667	2684	2698	2735	From [80]

Table 2. Graphene samples, bilayer graphene in different substrate.

Sample Graphene	Number of layers	Lorentzian peaks positions -2D		Reference
		$2D_{2A}$ cm^{-1}	$2D_{2B}$ cm^{-1}	
Micro-mechanical cleavage	n=5	2728	2762	From [80]
	n=4	2702	2732	
	n=3	2697	2719	

Table 3. Graphene samples, Lorentzian peaks of deconvolution curves of few layer graphene in 2D peak, information from reference [80].

Regarding to the I_{2D}/I_G ratios has confirmed the presence of mono-, bi-, and multi-layer. The average thickness of the graphene sheets could be assigned based on the 2D band shape. The I_{2D}/I_G ratios of 3.31, 1.56, and 0.54 corresponded to the mono-, bi-, and multilayer graphene sheets, respectively [82].

Other important mode is D'-band caused for DR. The DR can also happen as intravalley process, i. e., connecting two points belonging to the same cone around the K or K' points, this gives rice to a weak disorder-induced feature which appears at~1620 cm^{-1} [71]. Other mode called G* peak at 2450 cm^{-1} [47], it has origin from a combination of the zone-boundary in-plane longitudinal acoustic phonon and the in-plane transverse optical phonon modes (Mafra et al., 2007). One important aspect of this mode is that represents the increase in the graphene layers, as layers increase, it suffer a red-shift from 2455 to 2445 cm-1, and the shape with different numbers of layers remain the same, except for single-layer graphene, where it can be

quite sharp [47]. Further, the appearance combination of D+D' phonons around $\sim 2950\ cm^{-1}$, also requires a defect for its activation [71].

1.4.4 Transmission Electron Microscopy (TEM)

A Transmission Electron Microscope (TEM) produces a high-resolution image of small samples in the order of micrometers or nanometers, black and white image from the interaction that takes place between prepared samples and energetic electrons in the vacuum chamber.

Depending on the thickness and the atomic number of atoms in the sample, the electrons are scattered under specific angles giving rise to the so called mass-thickness contrast [83]. The lighter areas of the image represent the places where a greater number of electrons were able to pass through the sample; in the darker areas sample, electrons are scattered or reflected by the dense areas of the object. All differences provide information on the structure, texture, shape and size of the sample.

To obtain a TEM analysis, samples need to have certain properties. They need to be sliced thin (0,2-0,3 nm) enough for electrons to pass through, a property known as electron transparency (Williams and Carter, 2009).

Further, TEMs are often equipped with analytical tools, such as detectors for energy-dispersive X-ray analysis (EDX) and electron energy loss spectroscopy (EELS) allowing for additional chemical analysis being carried out inside a TEM.

The emergence of aberration corrected electron microscopes makes it possible to examine samples that are sensitive to knock-on damage at a lower acceleration voltage where knock-on damage is significantly reduced while still retaining a very high resolution. These new generation electron microscopes allow for delocalization-free imaging and reach sub-Angstrom resolution.

Thank to availability of aberration correctors, atomic resolutions imaging of carbon nanostructures, including graphene and its defects, became accessible.

TEM imaging using bright-field phase contrast is highly sensitive on the focusing conditions. In contrast, images acquired with a high-angle annular dark field (HA-ADF) detector in a STEM are directly interpretable and are particularly useful for determining the number of graphene layers as the contrast intensity varies monotonically with sample thickness in thin samples (Gass et al., 2008; Li et al., 2008).

Coleman and co-workers [53], produced synthesis of few layers graphene and counted the numbers of graphene layers per flake by examining the edges of the flakes. The edges of the individual flakes are almost always distinguishable in TEM images of graphene multilayers. A minimum of 64 flakes per sample were analyzed; given as result an estimate of population produced with each solvent, the results are presented in figure 1.13.

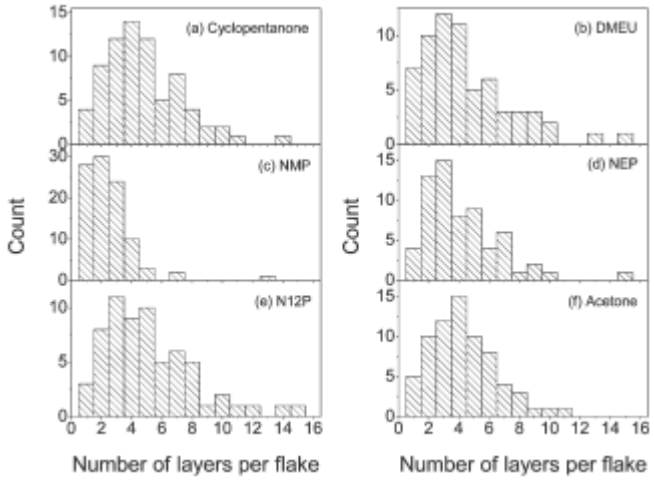

Figure 1.13 Histograms for numbers of layers per flakes from TEM, six solvents were summarized. From reference [53]

Since low-voltage aberration corrected TEM now enables researchers to study graphene with atomic resolution it also provides a platform to investigate structural defects.

1.4.5 Scanning Electron Microscopy (SEM)

Scanning Electron Microscopy provides high-resolution and long-depth-of-field images of the sample surface and near-surface, due to scanning with a focused beam. The electrons in SEM interact with atoms in the sample; these interactions contain information about surface topography and composition. SEM is one of the most widely used analytical tools due to the extremely detailed images it can quickly provide. Coupled to an auxiliary Energy Dispersive X-ray Spectroscopy (EDS) detector that acts as chemical analyzer, it provides a detail description of the components in the sample in percentage, weight and the relative atomic number.

In graphene field, the Scanning Electron microscopy helps in the determination of surface morphology and composition sample.

In Graphene Oxide (GO), the morphology can vary depending on the chemical treatment applied, (e.g. Hummers or Improved Hummers). In figure 1.14 is represented a samples of Graphite Oxide (GrO) after the Improved Hummers treatment of graphite flakes.

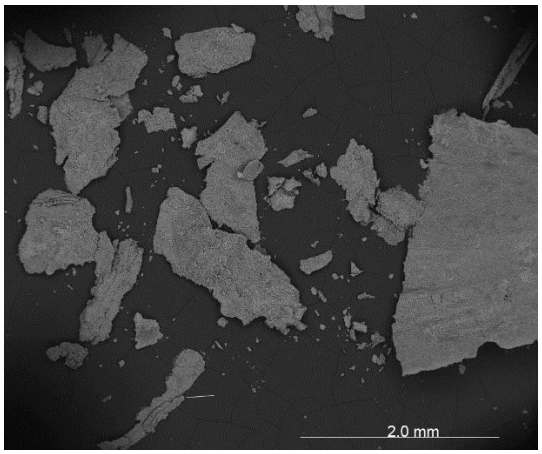

Figure 1.14 Graphite Oxide flakes after Improved Hummers treatment.

Another aspect in GO is the morphology, therefore is important differentiate. Firstly, it presented under form of small transparent flakes, sometimes isolated from each other, see figure 1.15.

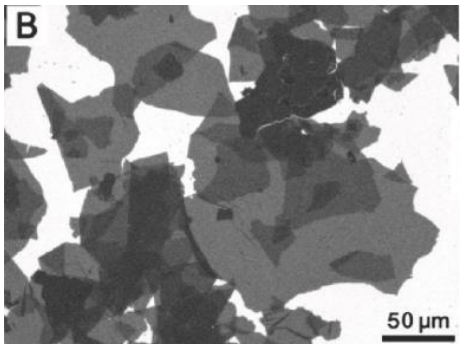

Figure 1.15 Flakes of graphene Oxide. From ref. [6]

1.5. Electrical Characterization

To evaluate the graphene material for nanoscale devices, the current versus Voltage (I-V) characterization is necessary; it may require the measurement of very small voltages due to the necessity of applying a very small current to the control power, or to reduce the Joule-heating effects. Therefore, low level voltage measurement techniques become important, not only for I-V characterization of devices, but also to resistance measurements of non-conductive materials and components. Several device properties and parameters can be deduced from the I-V characterization, as well as it is possible to understand the behavior of the graphene layer in presence of mobility charges.

Regarding to graphene materials, FLG devices have been tested at room temperature and the I-V characteristics were found to be linear. The devices could sustain extremely high current densities before they were destroyed at ≈ 1mA/µm, furthermore its nominal thickness (d≈ 1nm) has an equivalent value to ≥ 10^8 A/cm^2. Sometimes a small non-linearity is observed at high

currents, which could be due to the self-heating [84]. The Slope of the curve represents the resistance R by using the Ohm's law.

Additionally, the few layers graphene produced by arc discharge and dispersive in Dimethylformamide [85] has shown a classical linear I-V relationship, which it is indicative of semiconducting electrical conductivity, with an electrical conductivity of ~11 S/cm with 25 nm.

1.5.1. Four probe measurements – Sheet Resistance

The 4-probe sensing has developed to measure the resistivity of thin layer materials. The method is based upon a theorem which holds for a flat sample of arbitrary shape if the contacts are sufficiently small and located at the circumference of the sample.

In most cases 4-probe tests have been done on graphene materials arranged in devices, such as FETs or conductive electrodes. The main feature that can be obtained, corresponds to the resistance layer; this data is vitally important for flexible electronics and optoelectronics [86].

Graphene Oxide (GO) presents a sheet resistance (R_s) in the order of GΩ, specifically in ref. [87] reported to a sheet resistance of 4GΩ/□ for GO. However, when a reduction treatment is applied by using dimethylhidrazine, the sheet resistance decreased until it reached a value of 4MΩ/□. Graphitatization [88], hydrazine exposure and low temperature annealing, or high temperature vacuum annealing further decrease R_s down to 800 Ω/□ as presents ref. [89].

Regarding to dispersions of graphite-intercalated compounds and hybrid nanocomposites (GO mixed with CNTs) [90], were also attempted, with a minimum R_s=240 Ω/□. Graphene films produced by chemical synthesis currently show R_s=1.6 kΩ/□ as is shown in ref. [91].

On the other hand, Graphene Transparent Conductive Film (GTCF) [92] from LPE of graphite was fabricated by vacuum filtration followed by annealing, achieving R_s= 5 kΩ/□; the high R_s is most likely due to the small flakes size and lack of percolation [92]. The role of percolation in FLG suspensions is remarkable due to the size of flakes. When the size of flakes increase, the sheet resistance decrease from R_s= 6 kΩ/□ to R_s= 2 kΩ/□, see ref. [93].

1.6. Background of applications based graphene materials

In this chapter, the method to obtain and characterize GO, through oxidation of graphite are described.

Below is described a brief introduction to the developed applications. There are many applications related to graphene and graphene based materials. The functionalized material GO

has been widely used in the field of technology, due to the wide surface, GO has been tested as nano-carrier for nano-medical applications in the delivery drugs. On the other hand, the environmental remediation is other problem widely studied. For example GO has been used as material to remove pollutants in water.

1.6.1 Drug Adsorption in Bio-Medical application

Adsorption is defined as the property of a solid substance attracting and holding to its surface a gas, liquid, as well as a substance in solution or in suspension, and also condensation of a gas onto a surface.

Drug Adsorption in pharmacology is defined as the movement of drug into the bloodstream, which involves several phases. First, drug needs to be introduced via some route of administration (oral, topical-dermal, etc.) and in a specific dosage form such as a tablet, capsule, solution and so on.

1.6.1.1 Cancer drugs - DOXORUBICIN

Doxorubicin is an anthracycline antibiotic originally isolated from *Streptomyces peucetius var. caesius*. This amphipathic molecule possesses a water-insoluble aglycone (adriamycinone: $C_{21}H_{18}O_9$) and a water-soluble, basic, reducing amino-sugar moiety (daunosamine: $C_6H_{13}NO_3$). Figure 1.4.1 show the chemical structure of the molecule.

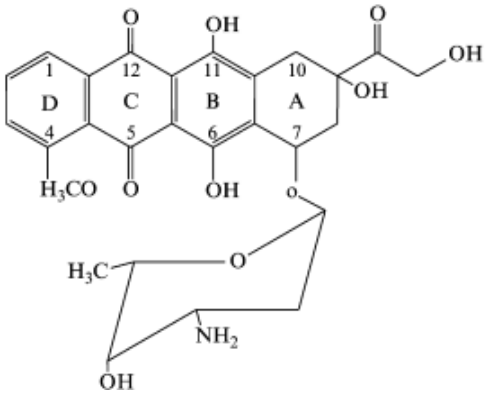

Figure 1.16 Chemical Structure of DOXORUBICIN

Doxorubicin has three significant prototrophic functions with associated pK_as: (i) the amino group in the sugar moiety (pK 1 ¼ 8.15), (ii) the phenolic group at C_{11} (pK_2=10.16), and (iii) the phenolic group at C_6 (pK 3= 13.2) (Bouma et al., 1986; Fiallo et al., 1998).

Doxorubicin is a chemotherapy drug used to treat many types of cancer. Well-defined as an anthracycline ring antibiotic, it is a highly effective anti-neoplastic agent against a wide range of human and animal solid tumors [94], and it is even used in leukemia chemotherapy [18].

Despite advances of this antitumor agent, it is hydrophobic and possesses inevitable, serious side effects such as nonspecific toxicity that limits the dose and use of the drug. To reduce the undesired effects without reducing drug potency, DOX is usually encapsulated into drug delivery vehicles that have the ability to protect the molecule of interest and selectively target specific compartments without adversely affecting the surrounding tissues [95]. The pH approach is import in drug delivery in cancer treatment especially in the presence of solid tumors. In fact, in this case the lysosome system in cells and solid tumors is acidic [96], and the extracellular area of most tumors is mildly acidic due to the increased production of lactic acid [97][98].

1.6.1.2 Nano-carriers in drug adsorption

Like many cancer drugs, DOX has notorious toxicity to humans and low efficiency by killing both cancerous cells and healthy cells. To address these concerns it is important to develop effective drug delivery systems, so that the toxic drugs are able to be delivered to cancerous cells directly and cause minimal damage to normal cells. Stimuli responsive materials are suitable vehicles to deliver drugs by responding to the tumor chemical–physical environment. The frequently external stimuli triggers are pH and redox.

The current materials used for the drug adsorption are sensitive materials which are promising in cancer therapy treatment. [99][100][101]

One interesting application is to use the NIR absorbance of CNTs to produce heat and kill cancer cells [102]. Properly functionalized CNTs are able to enter cells without toxicity, shuttling various biological molecular cargoes into cells [103]. Many investigations have shown that oxygen functional groups on carbon materials influence the adsorptive behavior [104].

In this context, Graphene Oxide has an important material, due to its layered structure and large surface area, which renders it suitable for intercalation or adsorption [105]. GO was used for the preparation of membranes and as a model system for membrane states [106] to test the loading of DOX onto GO surface.

1.6.2.Environmental application for removal of pollutants from water.

In developing and developed countries the wastes discharged from the textile, printing and tanning industries contain many dye stuffs; therefore it is necessary to improve materials, protocols and techniques for the removal of dyes from wastewater. Some dyes and their by-products may be carcinogens and toxics. 3, 6-Bis (dimethylamino) acridine, also known as

Acridine Orange ($C_{17}H_{19}N_3$) can be present in wastewater, because it is extensively used to impart color to different products.

1.6.2.1. Acridine Orange

Acridine orange is an organic compound. It is used as a nucleic acid-selective fluorescent cationic dye useful for cell cycle determination. It is considered a cell-permeant nucleic acid binding dye that emits green fluorescence when bound to dsDNA and red fluorescence when bound to DNA or RNA.

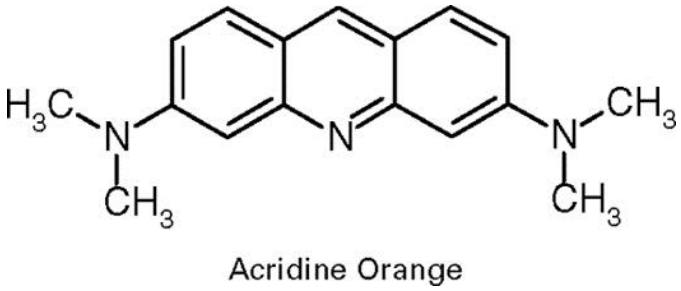

Acridine Orange

Figure 1.17 Chemical formulation of Acridine Orange

One of the most used dyes in the industry is Acridine orange (AO), which is a cationic dye that belongs to the acridine family; it is a dark orange to brownish solid, it exhibits bright orange color in aqueous solution and can appear in two prototropic forms AO and AOH^+ [107][108][109].

Acridine orange (AO) is a slightly cationic, lipophilic, weak base capable of permeating cell and organelle membrane structure. Although quite cell permeate in the neutral form, once protonated, these dyes tend to become trapped on the low pH side of the membrane barrier leading to their accumulation in acidic organelle structures. [107][110]

1.6.2.2. Carbon based materials & Acridine Orange in Waste Water

The more common processes used for the treatment of wastewater containing dyes have been coagulation, flocculation, biological and adsorption, among which the adsorption is found to be a cost-effective method [111][112]. Many investigations have been devoted to develop new adsorbents for the removal of dyes. Several studies have been done to test carbon materials such as activated carbon [113], carbon nanotubes [114], graphite oxide [115][116], graphene and graphene oxide [117][118]. Graphene oxide (GO) attracts highest interest due to the high surface and added functional groups [6][106]. However, few investigations have been reported about adsorption of AO on graphene oxide. Most of them reported a load of 95% pollutants onto GO [99].

CHAPTER 2

Physical Treatments

EXPERIMENTAL PART

Few Layers Graphene

Preparation and characterization

2. Physical Process – Few Layers Graphene

2.1. Preparation Method of Direct Exfoliation From Graphite

Graphene has been obtained in different ways, as mentioned in Section 1.3. The main objective is to preserve the characteristics of graphene as much as possible and to minimize the damage in the planar structure through some method on a large scale. The production of Liquid Phase Exfoliated Graphene (LPEG) was born as an alternative to mass manufacture, where through a given solvent or surfactant, the graphene layers acquire the possibility to remain in suspension for a long time, due to the surface tension or repulsion forces provided by some specific parameters of these chemical agents. It is necessary that external forces as cavitation (sonicator) [55] or shearing forces (homogenizer)[119] impinge on the surface of the material to overcome the Van der Waals forces present in graphite, achieving the exfoliation of material.

Many attempts to reach more stability and large concentration in the final suspensions were conducted by many research groups [120][52][121], as well as the commonly stabilizers used to produce suspensions of graphene as mentioned in section 1.3.3. The suspensions of graphene produced in liquid phase have been kept for up to five months with concentrations up to 0.01 mg/ml [9], whereas in higher concentrations up to~1.2 mg/ml [11] remaining stable at least one month. On the other hand, the material recover after the sonication could be re-dispersed achieving concentrations up to 63 mg/mL discriminating the subsequent centrifugation step [121]. The initial concentration, type of sonication, sonication temperature, sonication time, and centrifugation, are important to prepare a suspension based on few-layer graphene [58]. A suitable combination of these parameters makes the suspensions, also called graphene-based inks, suitable for industries such as electronics, sensors, transparent electrodes, and field effect transistors.

In this work, two ways to produce graphene-based inks have been experimented; (i) the exfoliation of graphite using a solvent mixture, and (ii) the FLG suspensions with the aid of Zeolite 4A (Z4A) to evaluate the performance. The characterization was carried out using different spectroscopies, regarding to the suspensions produced with the solvent mixture. The preliminary result shows that the suspended graphene layers cannot remain after the centrifugation process, so the stability is poor. Nevertheless, for the other type of suspensions produced with the aid of Z4A, the concentration improved 100% and the stability was reached within at least 5 months.

2.1.1. Chemicals and materials

Graphite flakes were purchased from Pingdu Huadong Graphite Co., Ltd (94.11% fixed carbon; 4.69%; size +50 mesh), the solvents utilized for the mixture were 1-Methyl-2-pyrrolidinone (NMP) (CAS number 872-50-4) and Dimethylsulphoxide (DMSO) (CAS number 67-68-5). Regard to the catalyst process, the Zeolite 4A (Molecular sieve 4A, powder, activated, ~325 mesh particle size CAS: 70955-01-0) was used, and tip sonicator UP 100H-Hilscher (100W, 30 kHz).

2.1.2. Preparation Method to produce Few Layer Graphene (FLG) by Liquid Phase Exfoliation of Graphite (LPEG)

2.1.2.1. Part A: Mixture of solvents to prepare FLG

In order to find a suitable mixture to improve the stability of FLG after the sonication process, two solvents were selected; the first one was NMP, being reported as the best solvent to disperse FLG and carbon nanotubes [121][42][24], and the second one was DMSO, reported as one of the solvents with medium capacity to disperse carbon-based materials [12][122]. The two types of solvents were used in different ratios following this order i) 3:1 NMP/DMSO; ii) 1:1 NMP/DMSO; iii) 1:3 NMP/DMSO.

i) 3:1 NMP/DMSO

Preparation of Volume 1 (Vol1)

The mixture was prepared with a volume of 100 ml. First, 25 ml of DMSO was added slowly to the 75 ml of NMP. This process produced an exothermic reaction; therefore it was carried out drop to drop under a fume hood.

ii) 1:1 NMP/DMSO

Preparation of Volume 2 (Vol2)

The mixture was prepared with a volume of 100 mL. First, in 50 ml of DMSO was added slowly 50 ml of NMP. This process produced an exothermic reaction; therefore it was carried out drop to drop under a fume hood. With regard to vol1 this produced a less exothermic reaction.

iii) 1:3 NMP/DMSO

Preparation of Volume 3 (Vol3)

The mixture was prepared with a Volume of 100 ml. First, in 25 ml of NMP was added slowly 75 ml of DMSO. This process produced a slight exothermic reaction than the Vol1; and the fume hood was used to avoid the toxic gases.

Experimental process

In order to evaluate the solvent mixtures, graphene in the three mixtures was sonicated using a tip sonicator, under the same conditions as follows: (i) 50 mg of graphite was put into a polypropylene test tube, (ii) then 10 ml of Vol*x* was added, (iii) and immediately the mixture was sonicated.

The experiment was conducted for exactly two hours. In the first hour, the mixture produced an exothermic reaction at the temperature reached 50 °C. At the end of the experiment, the temperature reached a value of 70 °C. The exothermic reaction could be produced due to the cavitation and the mix of two solvents [119]. After the sonication process, the suspension was centrifugated at 6000 rpm for 10 min, and the supernatant was collected in a portion of 80%, and then, it was put in a glass bottle to study the precipitation of each mixture.

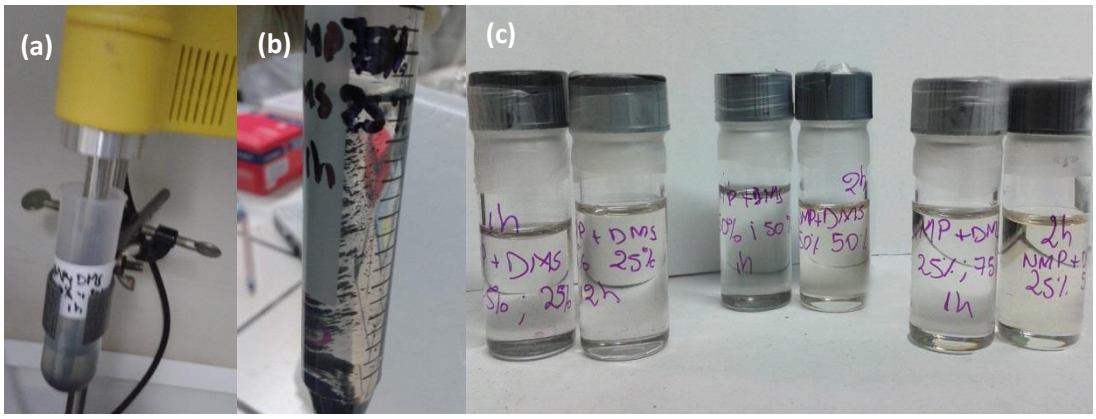

Figure 2.1 The experimental process. (a) Mixture in sonication process. (b) Suspension after centrifugation. (c) Supernatant solucion after the proccess; suspension in Vol1 (left); suspension in Vol 2 (center); suspension in vol 3 (right).

Immediately, after the centrifugation, the suspension precipitated as shown in figure 2.1(c) and as summarized in table 4.

N° Name	Solvent		Graphite			Sonication			Centrifugation	
	Mixture	Amount	Type	Amount (mg)	Type	Final Temp. (° C)	Parameters	Time (h)	Velocity (rpm)	time (min)
1Mix	NMP +DMSO (VOL1)	10 mL	flakes	50,1	tip	40	Cy:1.0 Am: 80%	1	6000	10
2Mix	NMP +DMSO (VOL1)	10 mL	flakes	50,1	tip	55	Cy:1.0 Am: 80%	2	6000	10

3Mix	NMP +DMSO (VOL2)	10 mL	flakes	50,1	tip	-42	Cy:1.0 Am: 80%	1	6000	10
4Mix	NMP +DMSO (VOL2)	10 mL	flakes	50,1	tip	-55	Cy:1.0 Am: 80%	2	6000	10
5Mix	NMP +DMSO (VOL3)	10 mL	flakes	50,4	tip	-45	Cy:1.0 Am: 80%	1	6000	10
6Mix	NMP +DMSO (VOL3)	10 mL	flakes	50,6	tip	-56	Cy:1.0 Am: 80%	2	6000	10

Table 4. Main parameters of suspensions produced with the mixture of solvents.

Experiments varying the speed of centrifugation

After the experiments presented in Table 1, it was decided to change the parameter of centrifugation to study the stability in the suspension and to increase the concentration. In this regard it was decided to start with the Vol1 mixture above described.

The first experiment was accomplished up until one hour (see table 2), then it was centrifuged at 6000 rpm. After that 3ml (1CF) was taken for the characterization. The residue was 7 ml, including the remaining solid. These 7 ml were placed under tip sonication for 1 h, and then, it was centrifuged at 3000 rpm. The supernatant solution (2CF) was taken in a volume of 3ml.

The residue after centrifugation at 3000 rpm was recovered in a volume of 4 ml. Before continuing the experiment; the residue at 3000 rpm was conducted to 40 °C and then, it was sonicated for an additional one hour. Immediately, the suspension was centrifuged at 1000 rpm, and the supernatant (3CF) was separated in a portion of 90% for the characterization.

For the last suspension, the residue was recovered in a portion of 0.7 mL, and then 5 mL of the solvent (Vol1) was added. After, the remaining mixture was sonicated for other hour. Afterwards, the suspension produced was centrifuged at 500 rpm, and the supernatant (4CF) was recovered in a volume of 3mL.

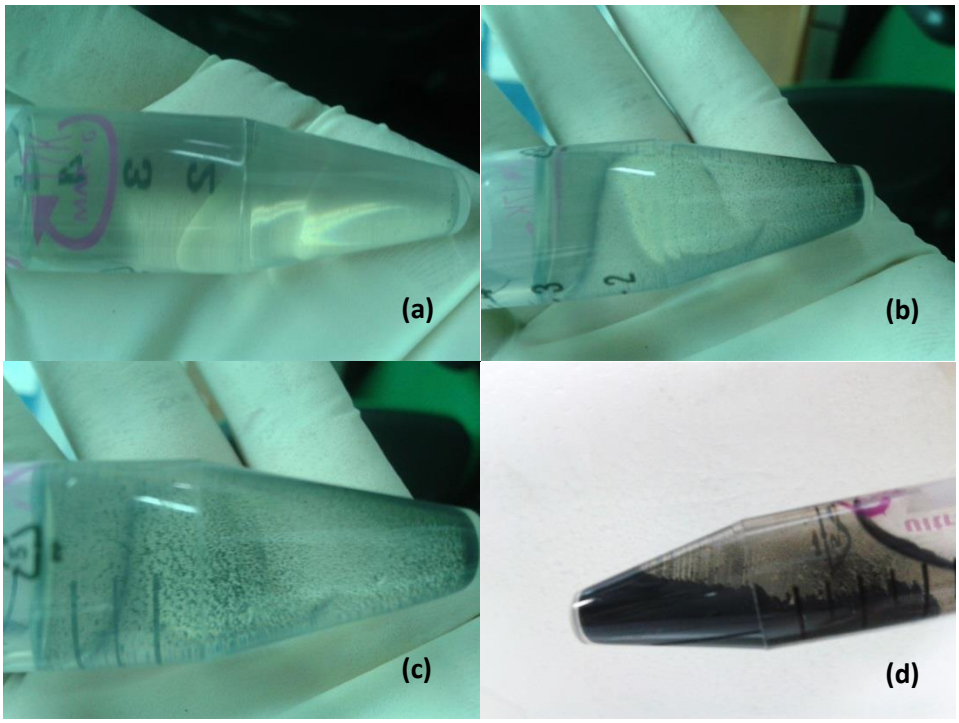

Figure 2.2 Supernatant suspensions recovered after centrifugation. (a) 1CF centrifuged at 6000rpm. (b) 2CF centrifuged at 3000 rpm. (c) 3CF centrifuged at 1000. (d) 4CF centrifuged at 500 rpm.

An important point to note in the experiment is the temperature. The temperature was increased almost 6 degrees every hour. When the temperature was raised, the solvent mixture began to degrade. This was stable until it reached 50 °C. Nevertheless, when this temperature is exceeded, a color change was noticeable in the suspension. Although attempts to control the temperature, it was not possible without the help of an external agent, such as an ice bath. In table 5 the main parameters are shown.

Name	Solvent		Graphite		Sonication				Centrifugation	
	Mixture	Amount (mL)	Type	Amount	Type	Final Temp (° C)	Parameters	time (h)	Velocity	time (min)
1CF	NMP+DMSO (VOL1)	10	flakes	50,1	tip	50	Cy:1.0 Am: 80%	1	6000	10
2CF	NMP+DMSO (VOL1)	7	flakes	residue after exfoliation process	tip	56	Cy:1.0 Am: 80%	2	3000	10
3CF	NMP+DMSO (VOL1)	4	solid	residue after exfoliation process	tip	58	Cy:1.0 Am: 80%	3	1000	10
4CF	NMP+DMSO (VOL1)	5	solid	residue after exfoliation process	tip	63	Cy:1.0 Am: 80%	4	500	10

Table 5. Parameters for the experiment varying speed centrifugation

2.1.2.2. Part B: Zeolite as catalyzer to prepare FLG

In order to improve the concentration of FLG suspension an external agent was added at the moment of sonication. Furthermore, to control the temperature, the bath sonicator model USC 300TH from VWR, with an ultrasonic power efficiency of 80 W, was used.

From the section above the degradation of the solvent mixture was detected, and it was caused by temperatures exceeding 50 °C. Therefore the bath sonicator will be used in this section. Furthermore, the centrifugation speed at 6000 rpm was very high, since the entire solid was precipitated out, consequently the variation in speed for the following experiments will be 1000 rpm. Meanwhile, to increase the concentration of FLG in the suspension, it was decided using a zeolite 4A together with graphite in the sonication process, as an agent of mechanical exfoliator.

The first experiment 1_BS (see Table 3) was conducted with the mixture of vol1. Graphite and zeolite (Z4A) were mixed first, and then 10 mL of Vol1 was added. The blend was then put in the sonicator bath for 3 hours to the first evaluation of degradation. During the three hours the temperature was maintained below 36 °C, afterwards the suspension was placed in the centrifuge at 1000 rpm of speed. The resultant suspension is plotted in figure 2.3 (a). However, the suspension was not able to maintain the stability, after 48 hours it was precipitated as figure 2.3 (b) presents. Despite the changes in parameters and the temperature maintained bellow 40 °C, the suspension did not have the capacity to remain dispersive. This fact could be related to the high surface tension created at the moment of mixture Vol1. When the surface tension is higher or lower than ~40 mJ/m^2, the suspension is precipitated [25].

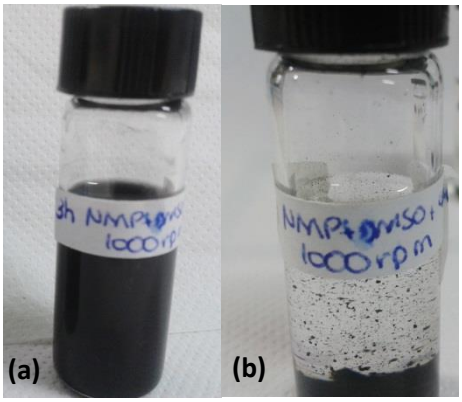

Figure 2.3 First suspension produced with bath sonicator 1_BS. (a) After the sonication process and centrifugation at 1000rpm. (b) Suspension 1_BS after 48 hours.

Besides the result of 1_BS, the experiment was conducted for 6 hours, and the temperature was maintenance up to 40 °C all of the time. After the sonication process, the blend was

centrifuged at 1000 rpm. After that, the supernatant solution was collected in a volume of 3ml. Afterwards the supernatant solution became clear and the solid was precipitated, as is depicted in figure 2.4 (a). Figure 2.4 (b) demonstrated the suspension after 48 hours, and the FLG was completely precipitated.

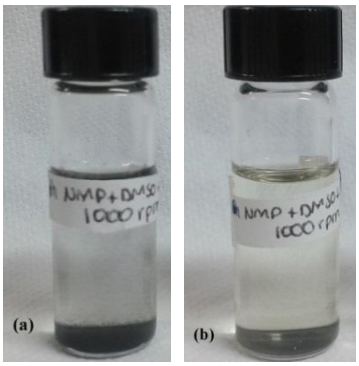

Figure 2.4 Suspension 2_BS conducted until up 6h. (a) After the centrifugation process. (b) After 48 h.

So far, the suspension has not been able to keep dispersed in the solvent mixture more than 48 hours. Nevertheless, there is an important point to note, in the first experiment (1_BS) by introducing the zeolite Z4A in the sonication, the dispersion could to maintain stable after centrifugation. Therefore, 3_BS was produced using NMP as a solvent base. Details of the production process are shown in Table 6.

The 3_BS experiment was conducted for 3 hours, always maintaining the temperature below 40 °C, after the time elapsed; the suspension was centrifuged at 1000 rpm for 10 min. It is worth to note that the suspension after centrifugation was stable. The supernatant solution in a volume of 3 mL was conserved in a glass bottle as shows figure 2.5 (a). The stability was good the time of stability was 65 days. In figure 2.5 (s) is depicted the suspension of FLG precipitated.

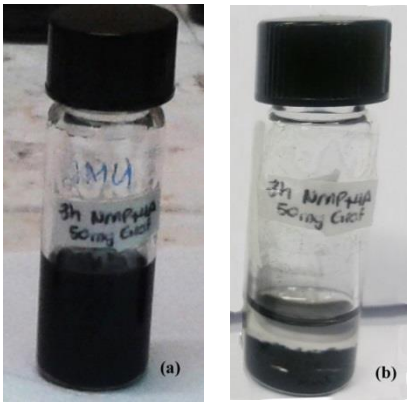

Figure 2.5 Suspension 3_BS solvent used NMP. (a) After centrifugation process. (b) After 65 days of rest.

ID	Name of experiment	Solvent		Graphite		Zeolite		Sonication				Centrifugation	
		Mixture	Amount (mL)	Type	Amount (mg)	Type	Amount (mg)	Type	Temp (°C)	Parameters	time (h)	Velocity (rpm)	time (min)
1_BS	3h_VOL1+Z4A_BS	NMP+DMSO (VOL1)	10	FLAKES	50,1	4A	50	BATH SONICATOR	36	80 W	3	1000	10
2_BS	6h_VOL1+Z4A_BS	NMP+DMSO (VOL1)	10	FLAKES	50,2	4A	50	BATH SONICATOR	40	80 W	6	1000	10
3_BS	3h_NMP+Z4A_BS	NMP	10	FLAKES	50,2	4A	50	BATH SONICATOR	36	80W	3	1000	10
4_F	6h_VOL1_F	NMP+DMSO (VOL1)	5	FLAKES	4000	....	...	MIXER	T.R.	75% Cap.	6	1000	10
5_F	3h_NMP_F	NMP	12	FLAKES	2000	...	...	MIXER	T.R.	75% Cap.	3	1000	10
6_F	6h_NMP_F	NMP	12	FLAKES	2000	...	...	MIXER	T.R.	75% Cap.	6	1000	10
7_F	6h_NMP+Z4A_F	NMP	15	FLAKES	2000	4A	2000	MIXER	T.R.	75% Cap.	6	1000	10

Table 6. Parameters of experiments using Zeolite 4A, as well as Bath Sonicator and Mixer.

Until now it has been 65 days of a suspension with stability. In order to increase the stability and concentration, the initial parameters of the quantity of graphite and sonication process were changed (see table 6). To start the experiment a Silver Capuccino Maker Deluxe was used. All experiments were performed with the mixer at 10000 rpm (75% speed rotation).

In the initial stage, 4 grams of Graphite and 5 ml of Vol.1 were mixed and placed in the mixer for 6 hours. At the end of exfoliation, the blend (4_F) was centrifuged at 6000 rpm. The suspension (4_F) could not maintain its stability, therefore it maintained the initial characteristics tested with the tip and the sonicator bath; in this case the temperature of the experiment did not exceed 27 °C, the result suspension is depicted in figure 2.6 (a). To confirm the previous analysis, at first glance, the solvent mixture by themselves was ineffective to stabilize FLG graphene.

In the second step, 2g of graphite were exfoliated in the mixer using NMP as solvent stabilizer for 3 hours. However, after three hours the exfoliation of (5_F) was not obtained as expected. Therefore, the experiment was allowed to continue up to 6 hours. The temperature did not exceed 26 °C. When 6 hours passed, the mixture (6_F) was removed and centrifuged at 1000 rpm for 10 min. After that, a gray suspension was observed, and is shown in figure 2.6 (b). More details of experiment are presented in table 3.

In the third attempt, 2g of graphite and 2g Z4A were exfoliated in the presence of NMP (see table 3, 7_F). After 3 hours, there was evidence of good exfoliation, and during the experiment the temperature was 25 °C. However, in order to compare the result of exfoliation between suspensions, the experiment was allowed to complete 6 hours. Then it was centrifuged at 1000 rpm for 10 min and placed in a glass bottle to the characterization. The result of suspension (7_F) is plotted in figure 2.6 (c).

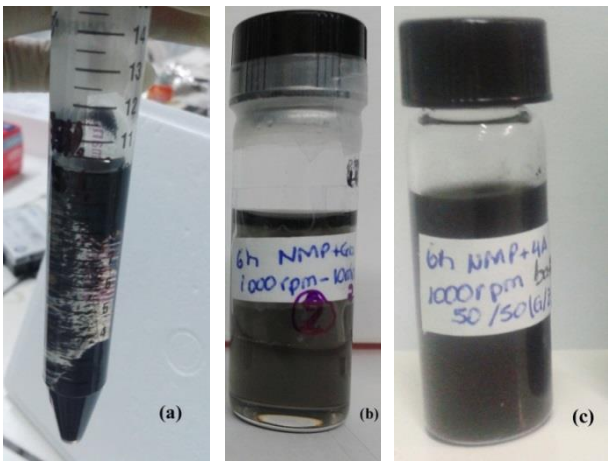

Figure 2.6 Suspensions carried out with mixer at 75% of total capacity. (a) Suspension 4_F produced with Vol1. (b) Suspension 5_F produced with NMP. (c) Suspension 6_F produced with Z4A and NMP.

The 5 _F sample was stable for 7 days with 50% of precipitation. In the following 17 days the solid was completely precipitated. Regarding to the suspension 6_F after 20 days almost 80% was precipitated. After several attempts to preserve the stability, the suspension 7_F after 200 days is still suspended, and just presents the 10% of precipitation.

Apparently, the exfoliation of graphite with the assistance of Z4A affects the stability of the suspension, as already noted in 3_BS (after 65 days was precipitated) and currently the 7_F suspension exhibits a good stability and exfoliation, therefore the introduction of the zeolite crystals not only enhances the exfoliation process, acting as a catalyzer, but also helps preserve the stability when the suspension be produce at room temperature.

2.2. Characterization of Few Layers Graphene by Physical Methods

The FLG suspensions were prepared as described above, the morphology of FLG surface samples was studied by using a Field-Emission Scanning Electron Microscopy (FESEM) model Quanta Feg 400 F7 (FEI), with accelerating voltage in the range of 5 to 10 kV. Furthermore, the Transmission Electron Microscopy (TEM) was carried out by Jem-1400 (JEOL/EO) with accelerating voltage of 80Kv and magnification up to 120000. Raman micro spectroscopy was done with a Horiba Jobin model 400, using a 50x objective lens and 532 nm excitation light. The UV-visible spectrum was performed by UV-Visible spectrophotometer UV- 160A Shimadzu, with a quartz cell of 1mm optic path.

2.2.1. Mixture of solvents to prepare Few Layers Graphene

2.2.1.1. UV- visible analysis

In order to complete the study of stability, UV-visible spectroscopy was performed. Analyses were made within an hour of each of the suspensions produced to check out whether the graphene layers had kept dispersed in the suspension, despite the transparency of suspension. The UV-visible spectrum was performed by UV-Visible spectrophotometer UV- 160A Shimadzu, with a quartz cell of 1mm optic path, and a baseline using the same mixture.

3:1 NMP/DMSO MIXTURE

The spectrum in figure 2.7 belongs to suspension 1Mix (see table 4).The UV-vis analysis show a prominent peak at 269 nm., it belong to π–π^* transitions, which represent the C-C bonds [71], and the absorbance value is 0.861. Apparently, a few quantity of graphene material is suspended in the supernatant mixture. However, the deformation appears at ~330 nm., in then n–π^* transitions [65], which correspond to the delocalized electrons of the solution.

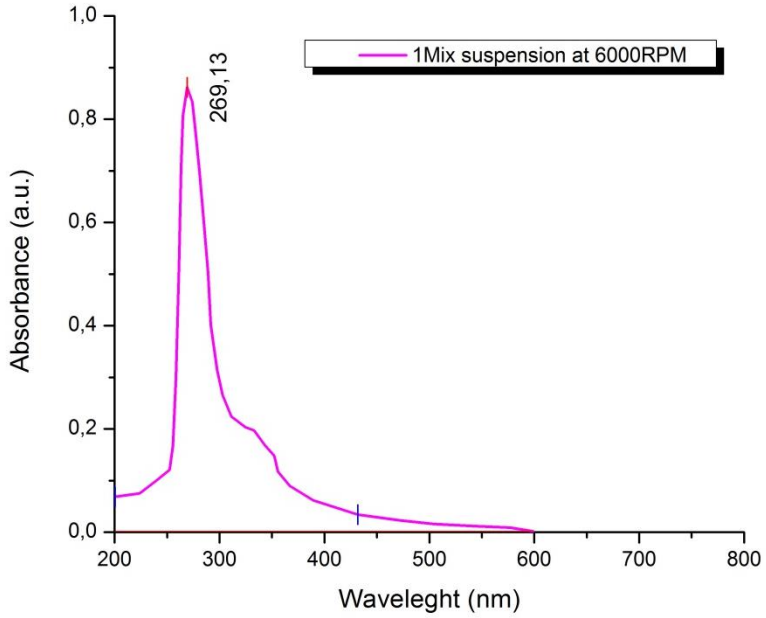

Figure 2.7.UV-visible analyses of sample 1h NMP+DMSO (75:25), it was analyzed in a range of 200 nm to 800nm by using quartz cells

1:1 NMP/DMSO MIXTURE

The Spectrum in figure 2.8 belongs to the suspension 3Mix (see table 4). The main prominent peak is localized at 271 nm, almost at the same range of the previous suspension, and also in this instance the peak belongs to C=C bonds which correspond to π – π* transitions [66]. Apparently in this time, the suspension remains more concentrated than the first one 4Mix. Nevertheless it also shows a protuberance at ~335 nm, which is related to n–π* transitions, which could probably indicate the association between FLG remains and the mixture through C=O bonds.

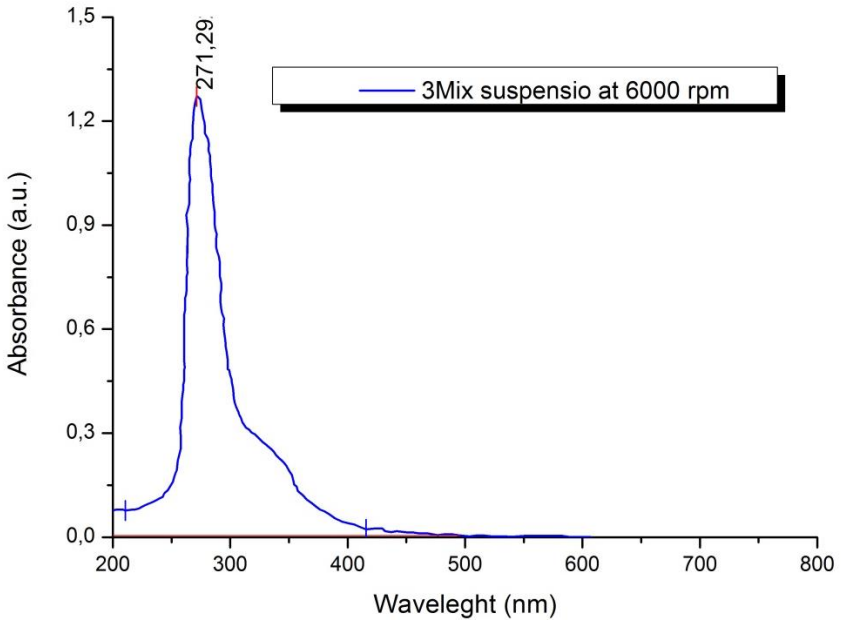

Figure 2.8.UV-visible analyses of sample 1h NMP+DMSO (1:1) in a range of 200 nm to 800nm by using quartz cells.

1:3 NMP/DMSO MIXTURE

Figure 2.9 shows the spectrum of suspension 5Mix. The most prominent peak is localized at 274 nm, which belongs to n–π* transitions. Even though the peak is prominent, more than the previous two, it is difficult to ascertain if the suspension retains suspended graphene layers due to the transparency.

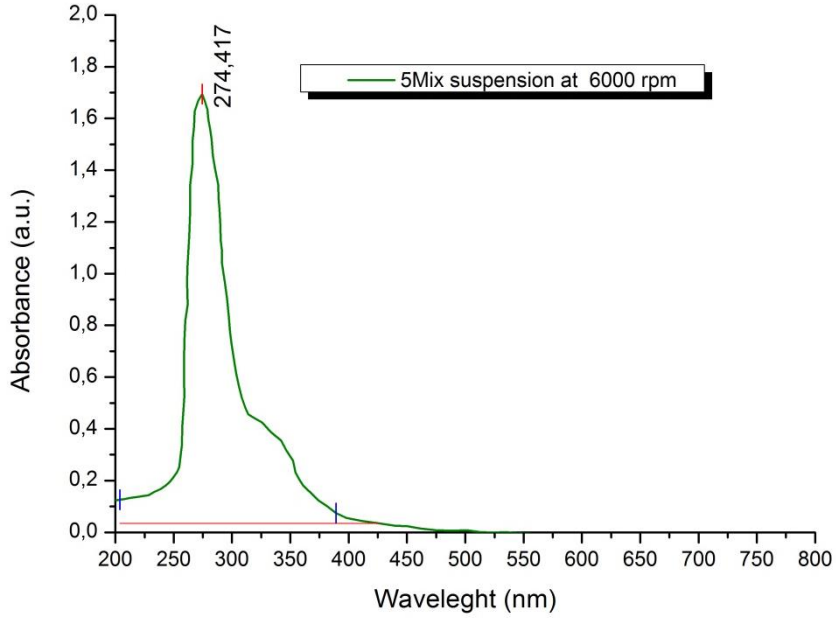

Figure 2.9.UV-visible analyses of sample 1h NMP+DMSO (1:3) in a range of 200 nm to 800nm by using quartz cells.

Experiments varying the speed of centrifugation

Fig. 2.10 depicts the spectra of all the experiments carried out with varying speed of centrifugation. The first suspension had a peak at 269 nm, and absorbance of 0.86 a.u. A dramatic change was observed in the suspension 2CF (see figure 3.4) where the prominent peak is localized at 286 nm, which could belong to the characteristic peak of NMP [123]. Apparently the suspension has been precipitated, and only the original molecules of solvent in greater proportion remain suspended. When the experiment of 2CF was conducted for another additional hour to produce 3CF, another change was evident; the main peak studied has shifted to a higher position of 4 nm. The degradation of the mixture in the suspension 3CF was obvious, and the colour of supernatant was change to slight grey-yellow. Finally, the suspension was sonicated for additional one hour at the same conditions (see table 2, chapter 2), and centrifuged at 500 rpm. When the Uv-visible analysis was carried out, the spectrum showed a blue-shift of 13 nm. An important observation related to this experiment was in the colour of suspension that was yellow-black. Clearly it showed that by varying the speed of centrifugation, greater amount of layers in suspension was achieved. Since the results showed a small improvement in stability by varying the centrifugation, it is possible that the suspension contains layers of graphene.

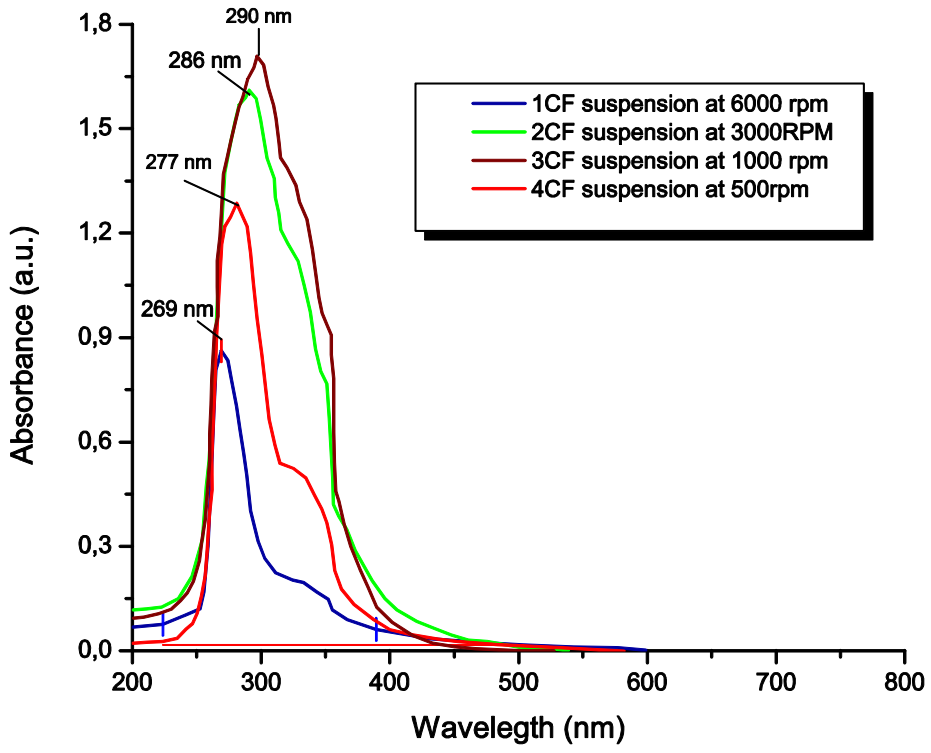

Figure 2.10.UV-visible analysis of experiment varying speed of centrifugation, all samples was analyzed in a range of 200 nm to 800nm by using quartz cells.

It is important to note that UV-visible analysis refers to different functional groups located in close domains, making it difficult to distinguish the FLG. To confirm proper exfoliation product the Raman spectroscopy will be used.

2.2.1.2. Raman Spectroscopy

In order to verify the production and quality of FLG suspensions, the Raman Spectroscopy was carried out in a Horiba Jobin model 400, using a 532 nm laser as excitation source. Raman spectroscopy was performed on a glass substrate; it was not easy to identify the presence of layers of graphene. After intense search small bright layers were seen under the optical microscope, from which the following results were obtained for each mixture. The Raman spectrum of 1Mix suspension presented in figure 2.11 (a) has two characteristic peaks. The peak located at 1573 cm^{-1}, which is known as the G band, is related to the degenerate zone-center LO and iTO phonons mode[69][68]. These phonons represent an active Raman mode. Furthermore, the second peak belongs to 2D band and is localized at 2709 cm^{-1}. The 2D band is an overtone of D mode, and correspond to double resonance (DR) effect [69][79]. The inset in figure 2.11 (b) shows the fitting done in 2D peak, which was fitted using three Lorentzian functions. The maximum values of each curve are shown in Table 7. Apparently, after the fitting of the curve, it reveals that FLG was present in the suspension 1Mix. However the intensity of the peak located at 2713 cm^{-1} is higher than the other two located at 2666 cm^{-1} and 2692 cm^{-1} respectively. According to other studies [80][72], the peak of the Lorentzian function localized at 2666 cm^{-1} should be higher (because the thickness of the graphene layers have decreased) [124], in order to obtain graphene layers of acceptable quality. Regarding to the defects in the structure, the D band at 1344 cm^{-1} is almost imperceptible, which confirms that the exfoliation treatment do not cause strong damage to the the material [79].

The Raman results of the suspension produced with Vol2 is plotted in figure 2.11(c). The spectrum shows a narrow G peak at 1564 cm^{-1}, the downshifted of G peak could be related to nonintentionally doped of graphene layer [70]. The 2D peak is localized at 2688 cm^{-1}, the fitting of 2D peak was completed by three Lorentzian functions (see table 7.), from where the first curve has a main peak at 2666 cm^{-1}; it is higher than the others two generates curves. This fact, changes the shape of the 2D peak which could mean the presence of thin graphene layers [125].

The suspension produced with Vol3 presents the Raman spectrum plotted in figure 2.11 (e). Whereas the spectra presented above have ordered graphitic structures, this spectrum shows a slight disruption, exhibiting a noisy spectrum. The main differences are the increased intensity of the D peak, which could be reated to the amorphization of the structure [70], and the widening

of the G peak. As regards the 2D peak, it was more difficult to do the fit, due to the noise in the spectrum. The main intense curve is localized in the range of 2683 cm^{-1}. However, it is difficult to verify if it corresponds to a bilayer graphene, due to the noise in the spectrum, and in addition to the quantity of layers in this suspension was almost imperceptible.

Lastly, the figure 2.12 shows a comparison between the original graphite spectrum and the exfoliated graphite suspension with the solvent mixture. The inset is more evident of the variation in shape of 2D peak, as well as the crystallinity of structure present in peak G for 1Mix (figure 2.12(b)) and 3Mix (figure 2.12(c)), whereas the 5Mix presents a structural disorder rather than the crystalline structure.

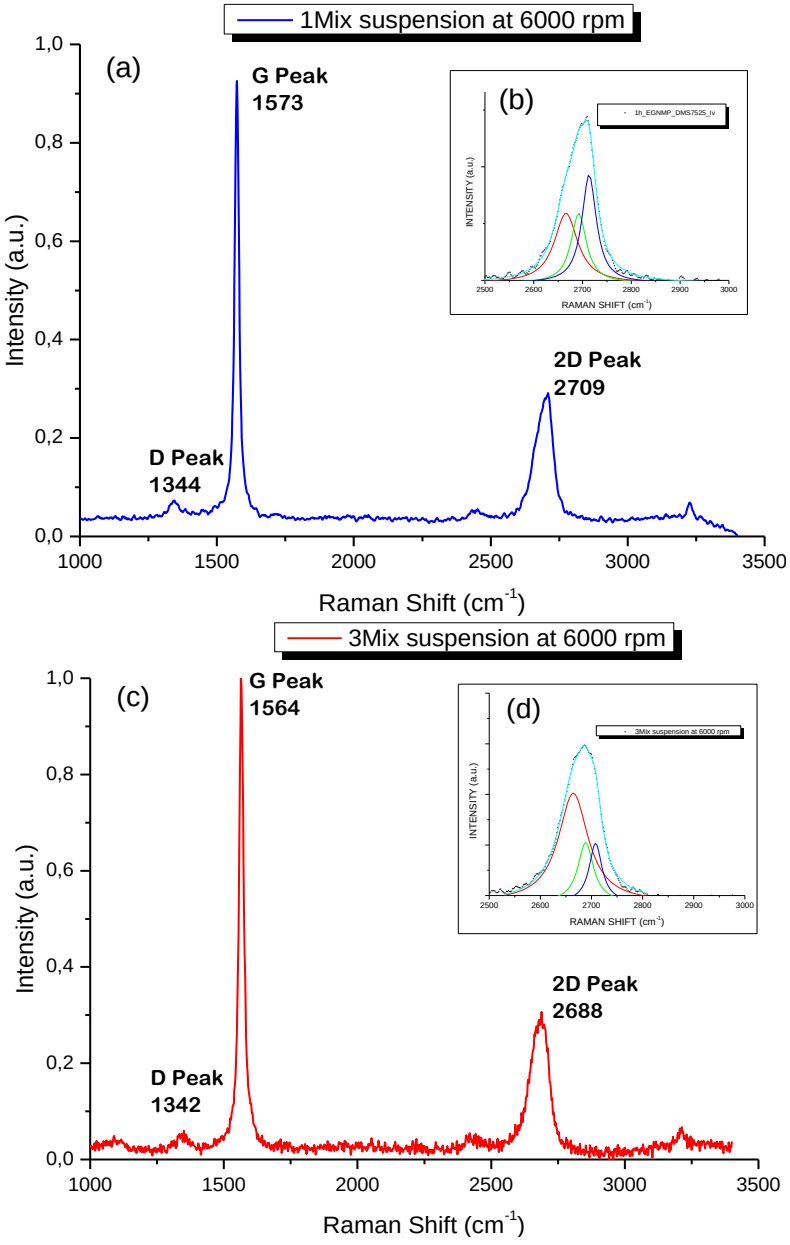

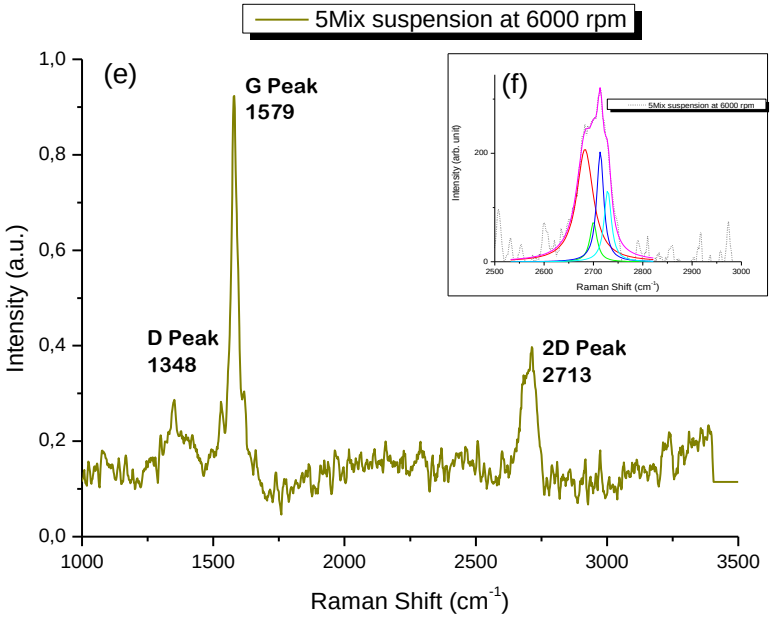

Figure 2.11 Raman spectra of suspensions produced with different mixtures. (a) Suspension 1Mix (3:1 NMP/DMSO). (b) Fitting of 2D band of 1Mix spectrum. (c) Suspension 3Mix (1:1 NMP/DMSO). (d) Fitting of 2D band of 3Mix suspension. (e) Suspension 5Mix (1:3 NMP/DMSO). (f) Fitting of 2D band of 5Mix. All the suspensions were sonicated by tip sonicator for one hour and centrifuged at 6000 rpm for 10 min. (see table 1, chapter 2).

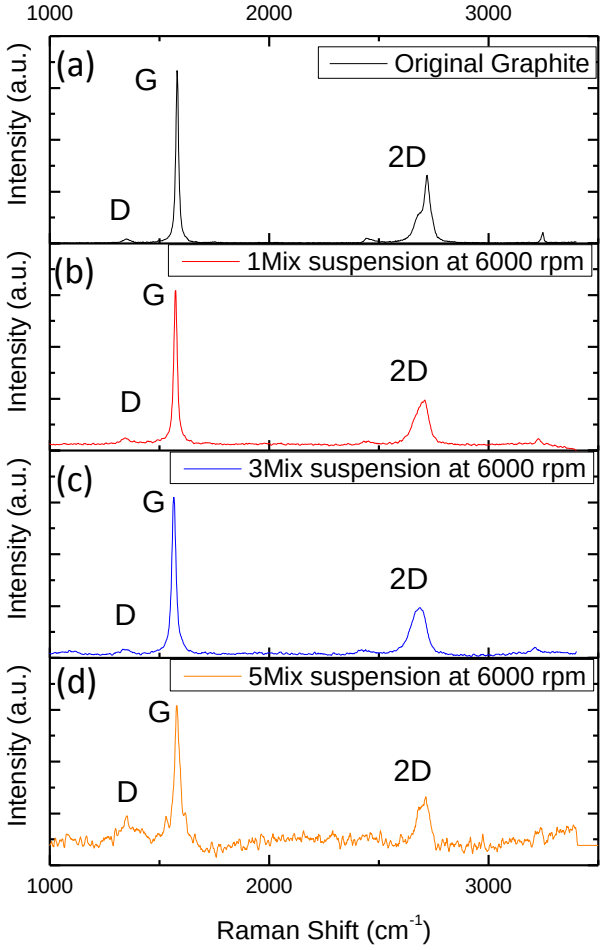

Figure 2.12 Comparison of Raman spectra of suspensions produced with different mixtures.

Name	2D band (cm^{-1})	Raman Shift (cm^{-1})
Original Graphite	2719	2677
		2720
1 Mix suspension	2709	2666
		2692
		2714
3 Mix suspension	2688	2664
		2689
		2708
4 Mix suspension	2713	2683
		2700
		2714
		2729

Table 7. Fitting of 2D peak for Raman Spectra.

Concerning the speed of centrifugation, the Raman spectra show the change from 1CF suspension (Figure 2.13 (a)) up to 4CF suspension (figure 2.13 (d)). The main goal was to evaluate the remaining solid after centrifugation. At first glance there are differences in the structure of particles, for example in figure 2.13(d) the spectrum is unclear, specifically for the 2D peak. However, figure 2.13(c) presents an acceptable spectrum especially for the evaluation of the 2D peak. For the localization and the shape of the peak, and taking into account that as the centrifugation decreases in velocity, more FLG remain suspended [25][58], it was decided to continue the experiment at 1000 rpm in order to reach more suspended FLG.

An important aspect that can be evaluated through this experiment is the temperature. As the temperature increases the mixture of solvents degrades, this fact could also influence the noise in the spectrum. However, as the speed of centrifugation decreases, it helps in the suspension concentration, even if the degradation of mixture of solvent is present.

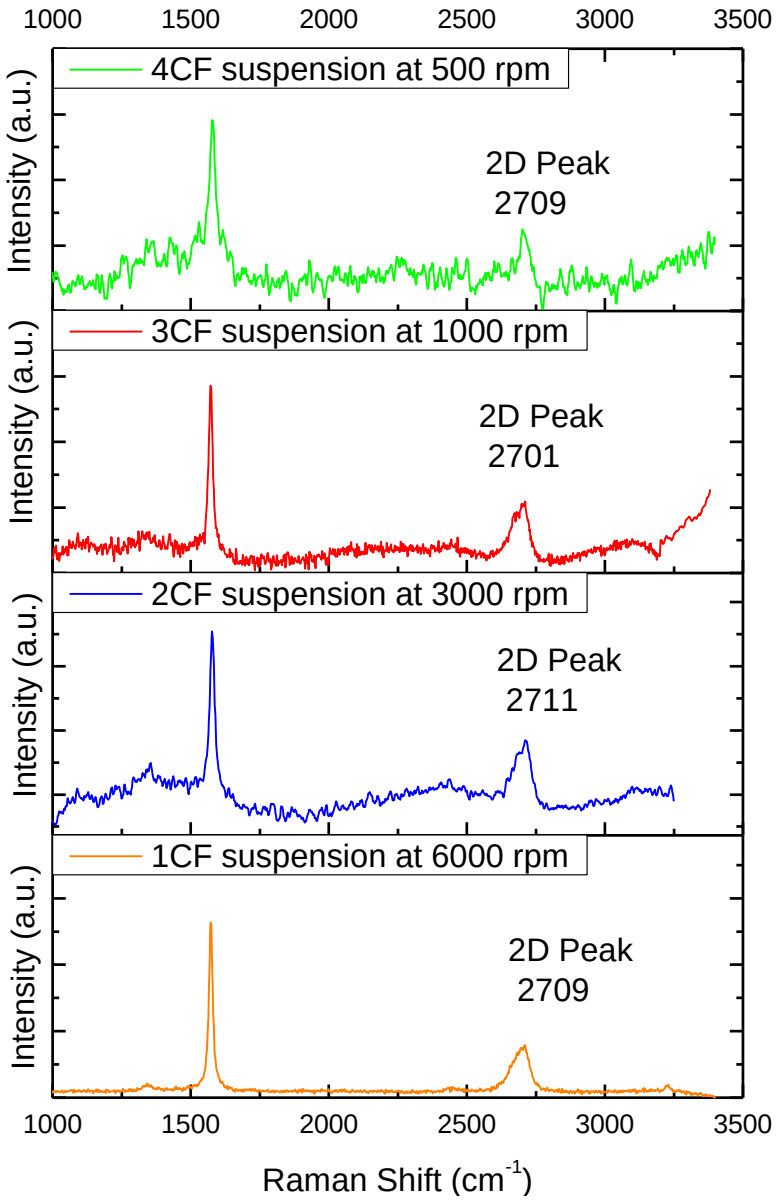

Figure 2.13 Raman spectra of variation of speed of centrifugation. (a) 1CF suspension produced with Vol1 and centrifugation at 6000 rpm. (b) 2CF suspension at 3000 rpm exfoliated with vol1. (c) 3CF suspension at 1000 rpm with vol1. (c) 4CF suspension centrifuged at 500 rpm.

2.2.2 Zeolite as catalyzer to produce Few Layer Graphene

Regarding to the production of Few Layers Graphene (FLG), the Field Emission Scanning Electron (SEM) Microscope was used with an accelerating voltage of 5 to 10 keV, and magnification up to 100000x. Furthermore, the Transmission Electron Microscopy model JEM-1400, with accelerating voltage of 80 keV, frame size 3296 x 2472, and magnification up to 150000x was used.

2.2.2.1 Scanning Electron Microscopy (SEM)

The study of the morphology of samples 3_BS and 7_F (section 2.1.2.2) was done on the solid resulting from centrifugation. Concerning to 3_BS, broken crystals of zeolite were presented due to the sonication process, as well as transparent flakes of graphene in great amount (figure 2.14(a)).In figure 2.14(b), it is evident that the remaining pieces of zeolite are covering the graphite layers that could not be exfoliated. This fact could be understood as follows; the crystals of zeolite and the thicker layers of graphite are heavier than FLG, so that they first precipitate, leaving a supernatant solution composed of thinner layers of graphene. An important aspect is that the residual crystals continue separated from graphene layers after the sonication due to the observation of the largest transparent and folded FLG (figure 2.14(c)). Lastly, a few slim flakes similar to nanoribbons can be seen in figure 2.14(d).

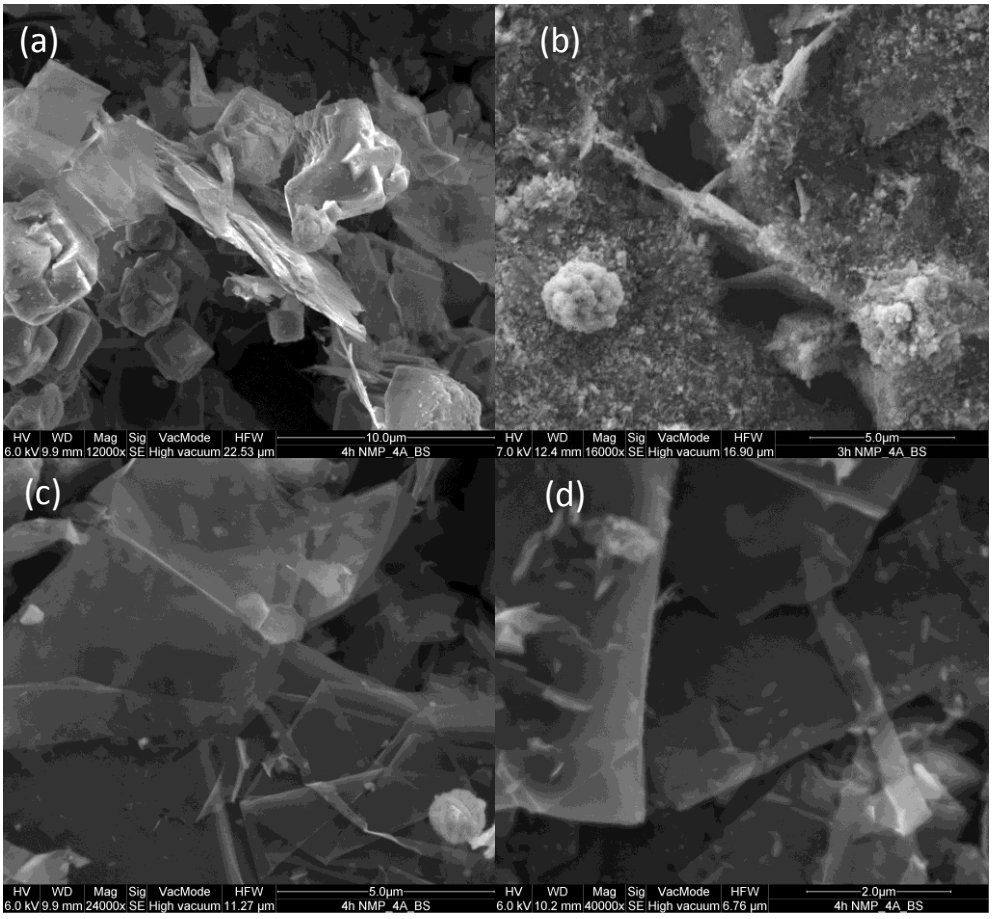

Figure 2.14 SEM microscopy of 3_BS suspension. (a) FLG with zeolite 4A after the centrifugation. (b) FLG in the remaining solid. (c) Large and folded transparent flakes of FLG (d) Exfoliation process has produce also large and slim flakes similar to Nano ribbons.

Regards to the morphology of suspension 7_F, the main difference detected was in the form of zeolite residual crystals, which are present in figure 2.15(a) and these seem clean without damage. This means that there are differences in the way FLG is produced, depending on the

exfoliation process. In suspension 3_BS, the crystals of zeolite seem strongly broken and participated in the exfoliation process. The crystals of zeolite in 7_F appear cleaner and preserve the initial structure, producing rather a mechanical exfoliation with the help of the mixer, see figure 2.15(b). The FLG in 7_F was observed in greater amount and seems larger than in 3_BS, see figure 2.15(c). Furthermore, in 7_F the FLG appear cleaner without small pieces of zeolite, see figure 2.15(d).

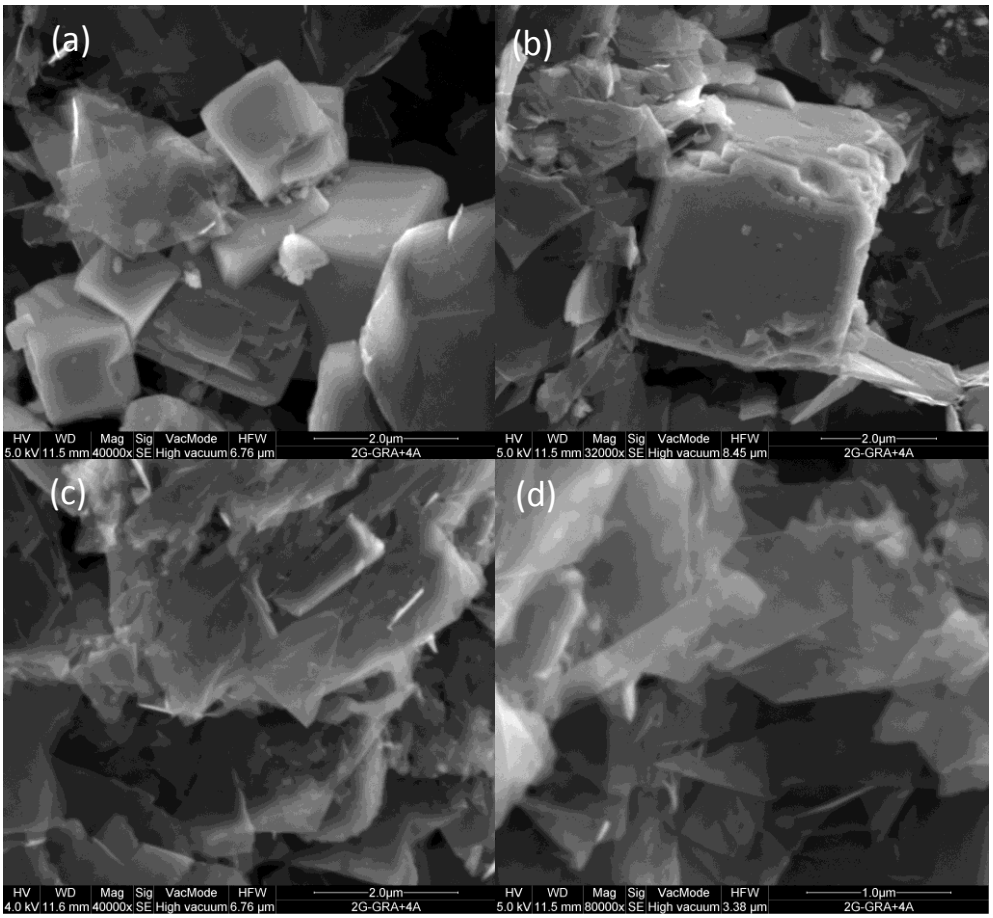

Figure 2.15 SEM microscopy of 7_F suspension. (a) Crystals of zeolite 4A after the centrifugation. (b) Residual zeolite after sonication process. (c) Large and folded transparent flakes of FLG (d) Transparent FLG in great amount.

2.2.2.2 Transmission Electron Microscopy (TEM)

The TEM microscopy was carried out on the supernatant solution for the 3_BS and 7_F suspensions. The suspension 3_BS presents transparent and folded layers, displayed in figure 2.16(a). Figure 2.16(b) depicts FLG, and the inset at 10nm corresponds to the diffraction pattern. This reveals that the graphitic domains were moved from the original position due to the sonication process. The corresponding four set of spots can be attributed to a graphene layer with a specific orientation [29]. Furthermore, the diffraction pattern demonstrates the crystallinity in the structure despite the moved domains. Figure 2.16(c) shows one FLG, where

the edges can be easily counted and it corresponds to flake of approximately five layers. The diffraction pattern done in the edge of the layer reveals a crystalline multilayer graphene [9]. This could be related to the exfoliation process, where the physical process by itself is not enough to exfoliate the graphite until it reaches a single layer in just three hours. In figure 2.16(d), a folded FLG presents a diffraction pattern that corresponds to a flake in the order of three layers. This can be verified in the set of the points present in the diffraction pattern at the top.

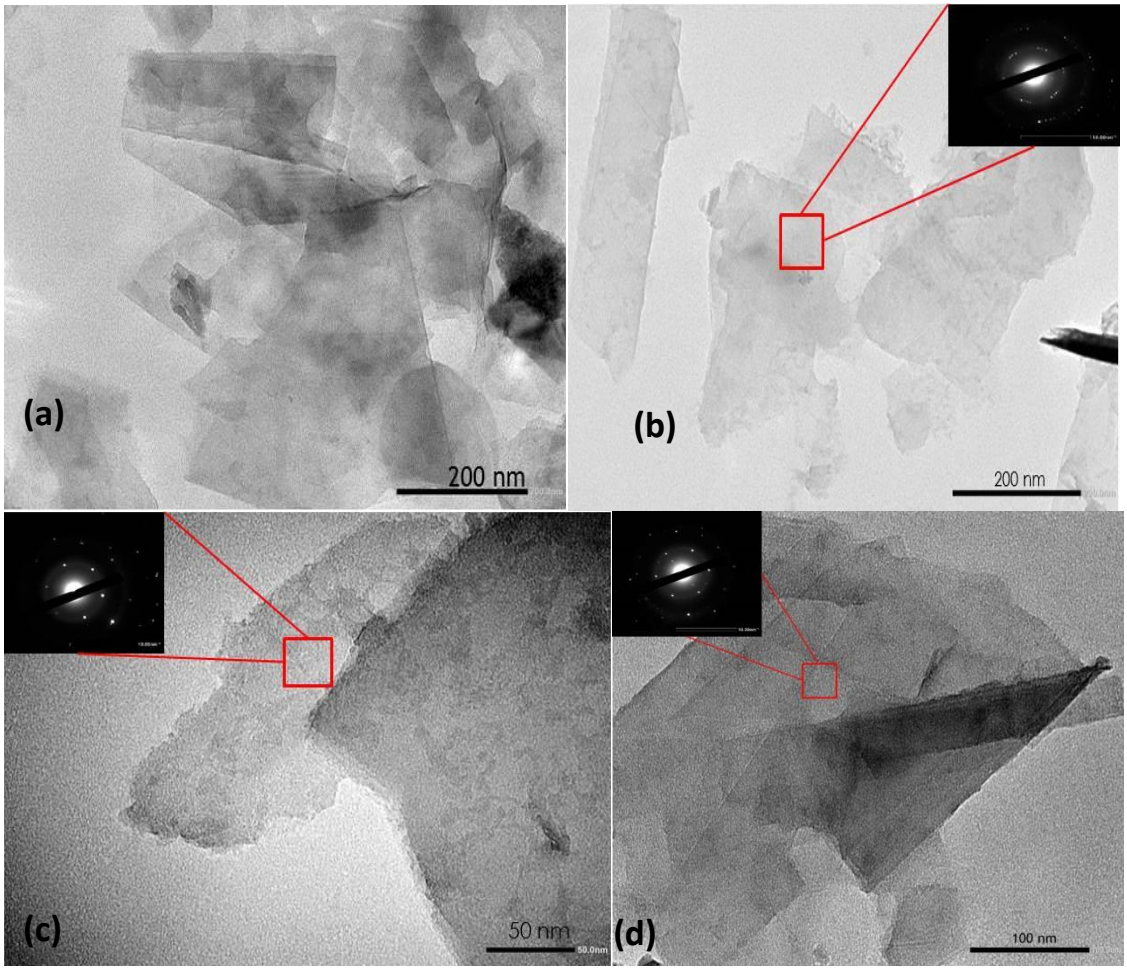

Figure 2.16 SEM microscopy of 3_BS suspension. (a) Transparent and folded few layers graphene. (b) Transparent FLG with diffraction pattern at the top in the image. The Diffraction are in the range of 10 nm and present four set of spots. (c) Flake of four layers graphene, pattern diffraction corresponding to a multilayer graphene flakes. (d) Folded flake of three layers graphene.

Regarding to suspension 7_F the TEM images are displayed in figure 2.17. The suspension presented thicker than thinner layers as in the 3_BS suspension. Additionally, at the top of figure 2.17(a) is plotted the Diffraction Pattern corresponding to the FLG flake in suspension 7_F. The three set of spots constitute a multilayer graphene with different orientations [29]. Figure 2.17(b) presents a large thick FLG, and the Diffraction Pattern reveals a crystal multilayer

graphene that is well oriented. Overall in the suspension 7_F FLG was observed, e.g. in figure 2.17(c) is a zoom of the edges of the previous image. Despite the fact of the thicker flakes it is remarkable that the exfoliation works, many of the graphitic domains founded were thin crystals of graphite and FLG.

.

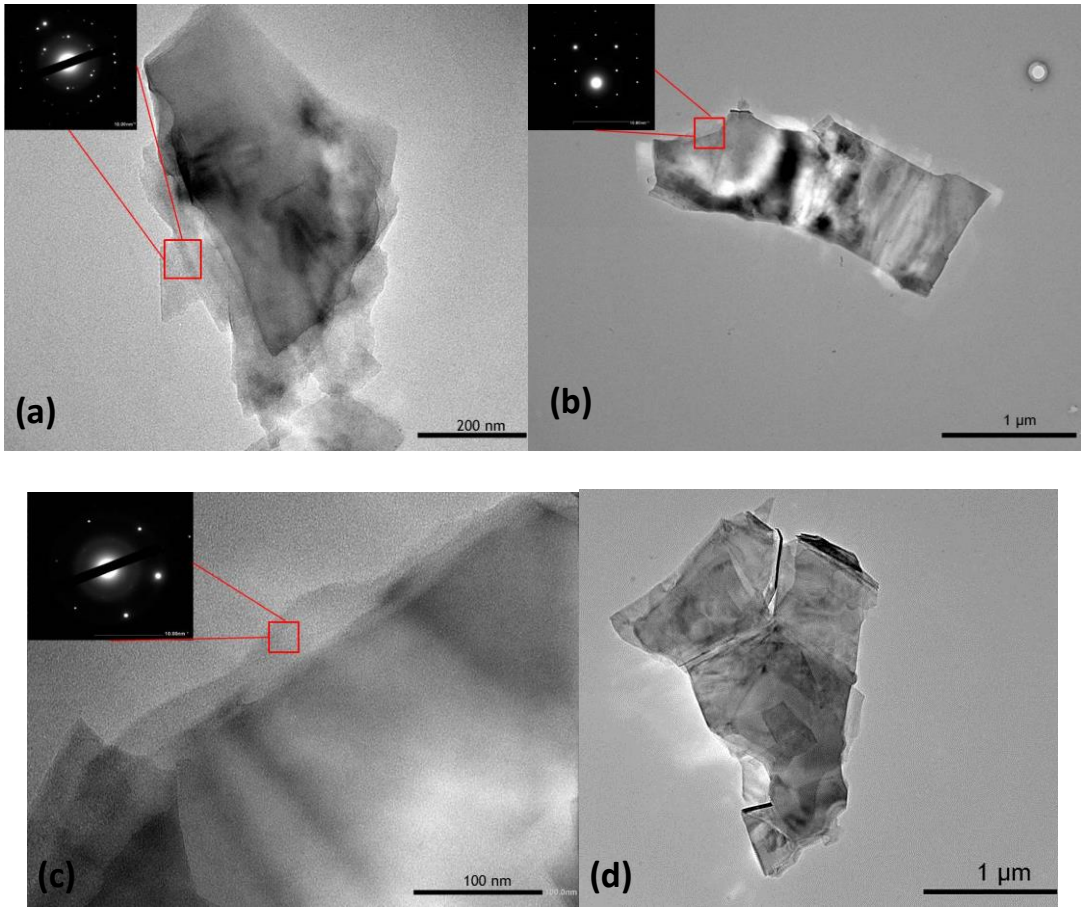

Figure 2.17 SEM microscopy of 7_F suspension. (a) Thicker FLG with a Diffraction Pattern of a set of four spots, it seems as an overlapping of various exfoliated flakes. (b) FLG with a measure approximate of 2 µm. Diffraction Pattern confirms the crystallinity in the structure. (c) A zoom of image b, especially in the borders, Diffraction Pattern shows as the FLG are composed of five layers. (d) Thicker exfoliated FLG which seems almost transparent.

2.2.2.3 Raman Spectroscopy

The Raman spectroscopy was conducted by using a glass substrate and drop-casting technique for both suspensions. Figure 2.18(a) shows the graphite spectrum that displays the main peaks. The first one corresponds to the G peak localized at 1579 cm^{-1}. The G peak is due to the bond stretching of all pairs of sp^2 atoms in both rings and chains [70]. The second one corresponds to the 2D peak at 2719 cm^{-1} and originates from a two phonon double resonance Raman process

[69][70]. Concerning to the D peak is almost unnoticeable at 1346 cm^{-1}. The ratio of I_D/I_G is 0.06 whereas the ratio for I_{2D}/I_G=0.39.

With respect to the suspension 3_BS depicted in figure 2.18(b), there are three main peaks present in the Raman spectrum. The first peak is the D peak at 1340 cm^{-1}, and it represents the disorder in the structure, related to the breathing mode of the sp^2 carbons atoms and is activated by the existence of defects such as edges, functional groups, or structural disorders [68].. The second peak is the G peak localized at 1566 cm^{-1}, and this is shown in figure 2.18(a). The G peak preserves the narrow structure, indicating that after the centrifugation any damage was introduced in the in-plane structure (C=C bonds). The last peak is the 2D peak localized at 2694 cm^{-1}. The interesting fact is the change in the wavenumber and the shape of the 2D peak, which was analyzed by a fitting procedure. The fitting was conducted using the Origin software, and through two Lorenztian functions the fitting was complete. Table 8 presents the results and wavenumbers for each function. Based on this fact, the curve localized at 2681 cm^{-1} increased its intensity, which changed the shape in the 2D peak. Many studies conducted by *Ferrari et al.* [68][125] reveal that through the shape of the 2D peak it is possible to verify the number of layers in FLG. Therefore in this study, the 3_BS suspension reveals a 2D peak shape that corresponds to a thickness of 2 to 5 layers. Additionally, the ratio I_D/I_G slightly increased and this might be due to the decrement in size of the FLG after sonication, but this increment is more related to the edges of the flakes in the 3_BS suspension rather than its structural defects [25][126].

Lastly, the spectrum of 7_F suspension is shown in figure 2.18(c) and it contains three main peaks. The first peak corresponds to D peak at 1342 cm^{-1}, and it could be related to the energy dispersion caused by the edges of exfoliated flakes, rather than the structural disorder that was induced. The G peak localized at 1571 cm^{-1} preserves a narrow shape after the exfoliation process. Regarding to the 2D peak, the shape varies slightly from the 2D of 3_BS. Nevertheless, it can be still fitted using two Lorentzian functions located at 2678 and 2709 cm^{-1}, whose parameters are shown in table 8. When the comparison of these two functions is performed with respect to the graphite spectrum, it is remarkable to see a change in wavenumber, as well as changes in intensity for each suspension produced. Through this analysis it is evident that in 7_F suspension are present FLG in the range of 5 to 10 layers [70].

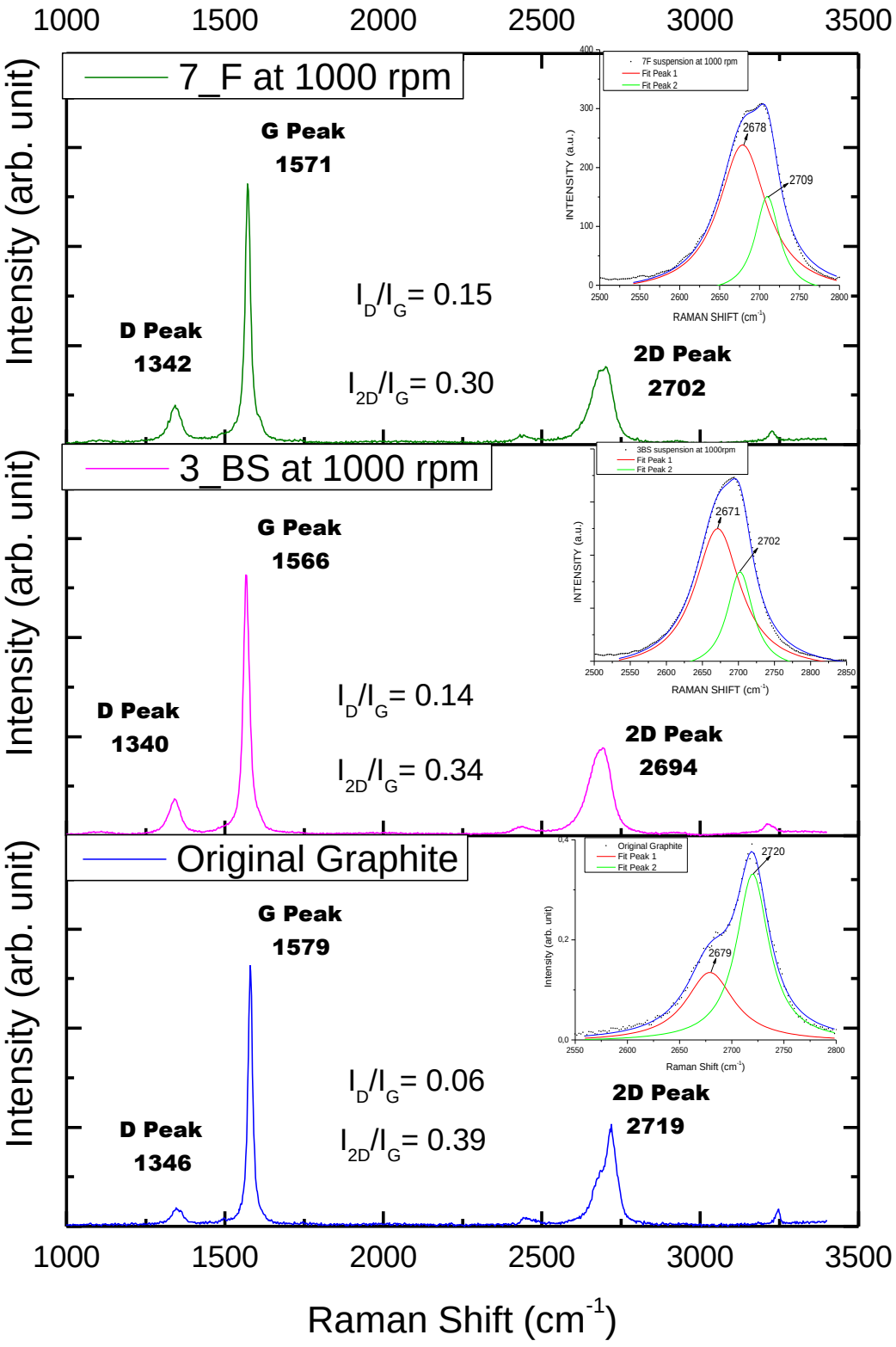

Figure 2.18 Raman spectra of suspension based FLG. (a) Graphite Raman spectrum. (b) The 3_BS suspension with the main Raman peaks, the inset shows the fitting carried out over the 2D peak. (c) The 7_F suspension, three main peaks are present which correspond to the main Raman modes. The inset shows the fitting by using two Lorentzian functions.

Name	$2D_1$ Peak cm^{-1}	Intensity arb. Unit	$2D_2$ Peak cm^{-1}	Intensity arb. Unit
Graphite	2679	0.13	2720	0.34
3_BS	2671	0.28	2702	0.19
7_F	2678	0.25	2709	0.17

Table 5. Result of fitting of 2D peak for each suspension and graphite.

2.2.3 Electrical Characterization of Few Layers Graphene (FLG) by Liquid Phase Exfoliation (LPE)

The introduction of graphene-based inks into specific electronic applications, such as conductive films and Field Effect Transistors (FETs), has motivated to experimentally study the behavior of electric 2D resistivity (ρ2D) and Charge Neutrality Point (CNP) under specific variations of Electric and Magnetic Fields [127][60][128]. Most of these studies have been addressed on Single Layer Graphene (SLG), Bilayer Graphene (BLG) and Few Layer Graphene (FLG) prepared by CVD [71][129], as well as samples prepared by micromechanical exfoliation, resulting in structures in the micrometers or nanometers scale [130][8]. With the introduction of FLG-based inks, it is important to study the behavior of macrostructure films devices made of interconnected individual FLG slices, randomly ordered or self-assembled [131].

As mentioned in section 2.1.2.2, two suspensions based on FLG have been prepared in order to test perform Electrical Characterization (EC) of the self-assembled films produced with the 3_BS and 7_F suspensions. Since the electric response to temperature changes is important for evaluating possible application areas of 2D materials, EC studies as a function of temperature are also presented and discussed.

2.2.3.1 Preparation of Samples – Experimental Part

In order to measure the electric properties, FLG self-assembled flakes samples were formed by the drop-casting technique. Firstly, 2μL of each suspension were deposited over an Al_2O_3 substrate with Au (thickness of ~1.3 μm) Interdigitated Electrodes (IDE). Then, the substrate was dried at 100 °C in a conventional oven for 10 min. This procedure was repeated twice for each suspension and substrate respectively (see table 9). Figure 2.19(a) shows the Al_2O_3-IDE after the deposition of FLG-based inks with the channel of the sample holder in black. This channel (black) presents a width of ~150 μm and then is larger compared to the average length of FLG's obtained (~3 μm). The total area of the channel is ~1.39mm^2. FLG self-assembled flakes samples were electrically characterized using a Source-Measure Unit (SMU) Keithley-2410C. The current-

voltage (I-V) characterization consisted of five cycles of voltage exploration, in the range V= [-1, 1].

The results were averaged for each sample and computed in order to obtain the 2D film resistivity (*ρ2D*) according to the conventional expression:

$$\rho_{2D} = \frac{\rho_{3D}}{t} = \frac{\Delta V}{\Delta I} \cdot \frac{W}{L} \quad [\Omega] \qquad (1)$$

Where ρ_{3D} is the three-dimensional resistivity, t is the thickness of the film, *ΔV* is the single variation of applied voltage, *ΔI* is the variation of measured current, while width (*W*) and length (*L*) are determined by the path between IDE1 and IDE2, as it is showed in figure 2.19(a) in black.

With regard to thermal characterization, the temperature of FLG self-assembled samples was increased every 15 °C in the range *T*= [30, 130] °C. At every interval, 2D resistivity was measured by the same procedure used in equation (1). Afterwards, in order to test thermal stability and eventual evaporation of solvent without stimulating oxidation process in the samples, these were kept up to 150°C during 3 hours without a controlled atmosphere. Then, samples were left to cool by natural heat dissipation and the thermal-electric characterization was conducted again to verify if changes had happened. To develop this thermal-electric characterization, the instrumentation reported in [132], [133] was used.

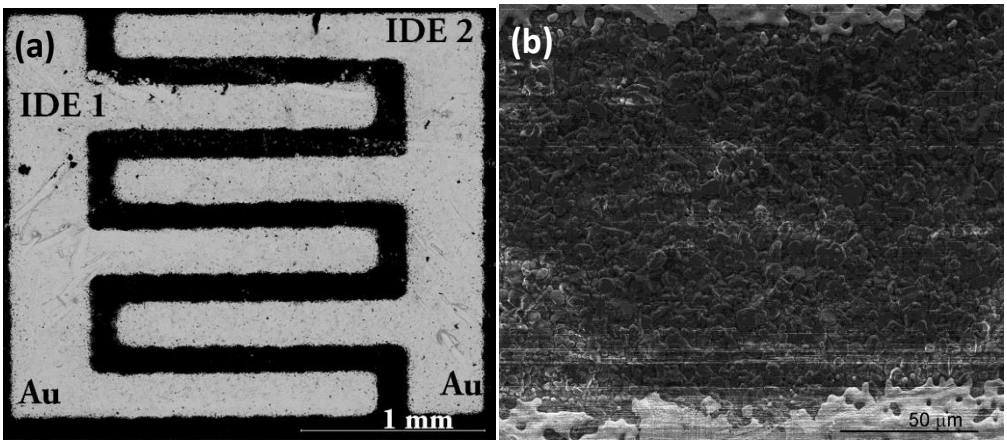

Figure 2.19. (a) SEM morphology of Al_2O_3 – Au electrodes (IDE), thickness of Au ~1.3 µm. In black is represented the path between each electrode. (b) Path between the electrodes, after depositions of FLG inks

Denomination		3_BS	7_F
Deposition on Substrate	Amount / µL	2	2
	# Times	2	2
Temp. Dry / °C	Temp. /°C	100	100
	Time /min	10	10

Table 9. Summary of deposition times for each Al_2O_3

2.2.3.2 Electric characterization

Results obtained for FLG inks are plotted in Figure 2.20, which were normalized to their maximum film resistivity (ρ_{CNPn} with n as the sample number). It is evident the presence of a Charge Neutrality Point (CNP) around the zero Volts bias condition. CNP occurs when the surface charge enters in an equilibrium state for positive and negative charges [134], [135].

As mentioned in section 2.2.2.1 and section 2.2.2.2, samples are composed of several transparent FLG, which at the moment of deposition become randomly-interconnected; FLG-based inks fill the freeway between IDE electrodes. The resistivity decreases while the applied voltage *V* increases. In determining the above described resistive behavior, it is not possible to distinguish the role played by the individual FLG, the contacts between FLG's, and the Au contacts to the FLG film. However, one can hypothesize that a contribution to the decrement of resistivity while the applied voltage *V* increases (see Figure 2.20), regardless of the sign of polarization, could be related to a possible decrement of the distance between interconnected FLG flakes induced by the magnitude of bias increment. In fact, the flakes are attracted to each other by Van der Waals forces, forming non-linear Ohmic contacts [136]. The same kind of measurements and data treatment was performed over a commercial resistor (SMD 2805, 49KΩ), see figure 2.20 (blue-linked dots). As expected, the resistance is constant regardless of the applied voltage. In conclusion, 7_F suspension had the smallest ρ_{CNP} value with ~188 kOhm, while the 3_BS suspension had a ρ_{CNP} value of ~7MOhm.

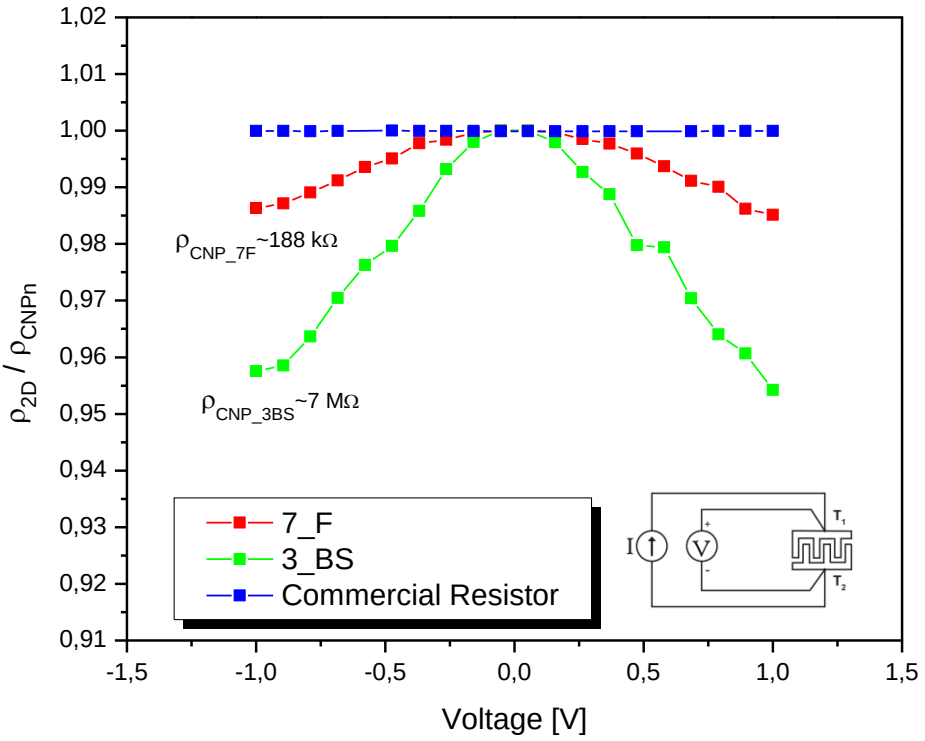

Figure 2.20 2D film resistivity (ρ2D) normalized for the resistivity on Charge Neutrality Point (ρCNPn) for every sample. Also, the normalized resistivity of a commercial resistor is reported for comparison.

2.2.3.3 Thermal-Electric Characterization Measurements

After the electrical characterization of the samples, the temperature was increased. Figure 2.21(a) and (b) present the measurements performed before and after annealing process, respectively.

Measurements demonstrate that resistivity decreases with increasing temperature. However, a non-linear dependence on temperature can be observed. It is worth noting that high current densities could lead to self-heating of sample films and, by consequence, the decreasing of resistivity started a positive feedback. Also, it is evident that the annealing improved the 2D conductivity of the samples. In fact, all FLG samples undergo a resistivity reduction, but particularly, the 3_BS reduced its resistivity by a factor of 1.75. Another important aspect to highlight is that new resistivity values were maintained over time, which could be due to evaporation of the solvent favoring the interconnection of the FLG flakes. Nevertheless, 7_F sample remains the better conductive film reported in this work, even if its resistivity was reduced only by a factor of ~1.3 after annealing.

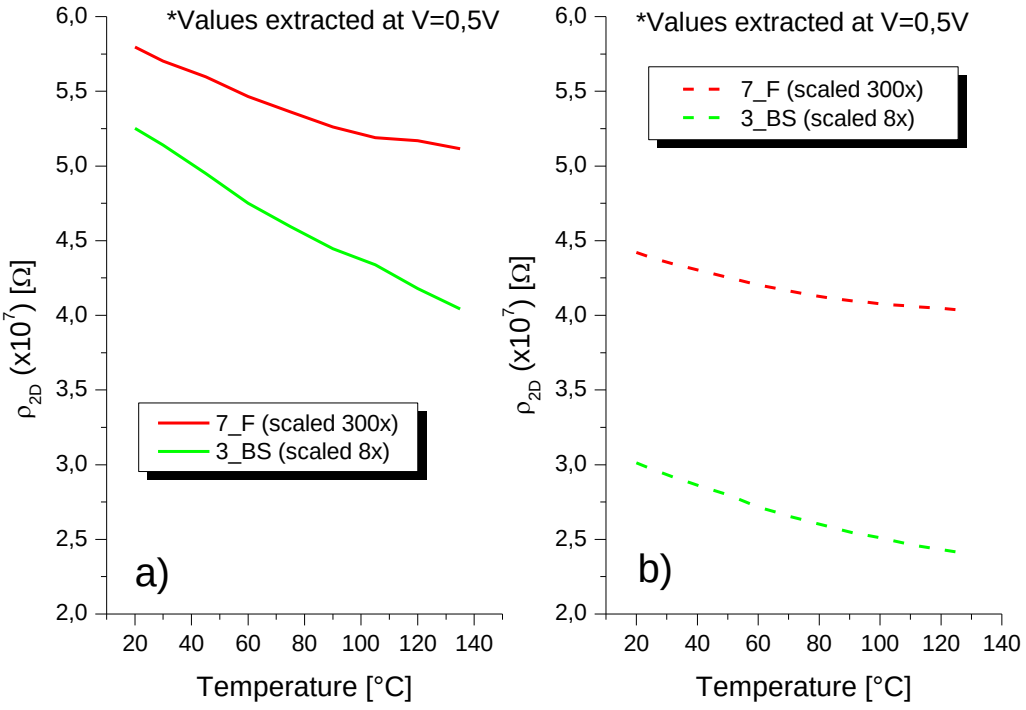

Figure 2.21 Measurements of 2D resistivity ((ρ_{2D}) as a function of temperature. a) Before annealing. b) After annealing at *T*=150 °C without control atmosphere.

2.3 Conclusions

The mixture of the solvents is ineffective in the exfoliation of graphite by sonication. The blend remains dark within the first hour, however afterwards the centrifugation reveals a supernatant solution completely clear and transparent, i.e. the solid is precipitated. On the other hand, an interesting parameter to evaluate is the temperature, because if it exceeds 50 °C, the blend begins to change the color from transparent to yellow.

The production of FLG was improved by adding the zeolite 4A in the phase of exfoliation. The stability of suspensions was evaluated by taking account the days before precipitation, and it is worth to note that the improvement in stability by adding the Z4A and the control of temperature was noticeable. A comparison between suspensions reveals that 3_BS suspension precipitated after 65 days. On the contrary, the suspension 7_B after 200 days keeps being suspended. In this case the zeolite not only acts as a catalyst but also as a stabilizer.

UV-vis absorption reveals that in the supernatant solution of the mixture of solvents few graphenic domains remain suspended after the centrifugation. The Raman spectrum revealed few thin ordered flakes produced after the sonication process. However, these could not be well studied due to the transparency and the small residual quantity in the supernatant. The speed of centrifugation was varied, and more suspended flakes were achieved. Nevertheless, when the temperature increases it harms the production of FLG with the solvent mixture, therefore it is important to control the temperature that does not exceeding 40 °C. However, the mixture of solvents was not capable to maintain the suspended FLG for more than 2 days.

SEM microscopy show that the crystals of zeolite and FLG do not bind after the sonication process. In 3_BS suspension the crystals of zeolite are broken and it is possible that small pieces of residual crystals decorate the FLG. On the other hand, the change of the exfoliator in the exfoliation process avoids any damage to the zeolite crystals, which lead to cleaner FLG. TEM microscopy confirms the very short thickness of FLG in 3_BS, while, 7_F suspension shows thicker FLG.

Through the fitting of 2D peak in the Raman spectrum by using the Lorentzian functions, it was possible to verify the number of layers in the suspensions. In 3_BS, FLG have a range of 2 to 5 layers, which are similar to previous reports [124][125]. On the other hand, 7_F suspension also displays an ordered structure after the exfoliation process with a number of layers in the 5 to 10 layers range. Finally, the ratio of I_D/I_G demonstrates that after the exfoliation process no damage occurred in the in-plane structure.

The Electrical Characterization (EC) was conducted over the 3_BS and 7_F suspensions. The Charge Neutrality Point (CNP) corresponds to the maximum film resistivity, which was present for 3_BS around 7 MΩ, whereas for 7_F was 188 kΩ. Regarding the electrical behavior of FLG inks, a hypothesis has been proposed, that a contribution to the decrement of resistivity while the applied voltage *V* increases, could be related to a possible decrement of the distance between interconnected FLG flakes induced by the magnitude of bias increment.

Concerning the thermal-electric measurements, the resistivity in the samples decreases after the annealing treatment. For 3_BS ink based FLG the resistivity decrease by a factor of 1.75, whereas for 7_F the resistivity was reduced by a factor of 1.3

CHAPTER 3

Chemical Method

Experimental Part

Graphene Oxide

Preparation and characterization

3. Chemical Process - Graphene Oxide

3.1. Preparation of Graphene Oxide

Hummer's method has been used for nearly 30 years by several research groups to produce graphite oxide[61][137], there are other groups who have made small changes to this method. Successively, most of the modifications made by other groups in Hummer's method were carried out in order to achieve a higher degree of oxidation, and/or to reduce the toxic gases (NO_2, N_2O_4, ClO_2, etc.) during the course of the reaction. It is not easy to propose a general model for the structure of GO, since the type of functional groups and their distribution are determined by variations in the oxidation method.

In this work, the synthesis of graphene oxide was performed according to traditional Hummer's method [5] and improved Hummer's method reported by *D. Marcano* [6]. We used the last method in order to avoid some toxic gases [64][14][138]. The main objective of this experiment was to obtain a functionalized material, whose properties can be used in technological applications, and at the same time a material it might able to recover partially or totally the properties of graphene by applying an appropriate reduction method.

3.1.1. Chemicals and Reagents

Graphite flakes were purchased from Pingdu Huadong Graphite Co., Ltd (94.11% fixed carbon; 4.69% ash continent; 81% size +50 mesh) were utilized as precursor without pretreatment. In order to oxidize Graphite, Sulfuric Acid (H_2SO_4) with CAS Number: 7664-93-9, Orthophosphoric Acid (H_3PO_4) with CAS Number: 7664-38-2 and Permanganate Potassium ($KMnO_4$) were used. Finally to produce colloidal suspensions, tip sonicator UP 100H-Hilscher (100W, 30 kHz), with cycle 0.8 and amplitude 90 % was used.

(a)

3.1. (a) Graphite used with +50 mesh dimension

3.1.2.Preparation Method of Graphene Oxide (GO)

Firstly, we prepared a mix of H_2SO_4/H_3PO_4 in a ratio of 240:26.8 mL (9:1). During mixing, an exothermic reaction occurred, that was controlled by an ice bath. In a three coding flask of 500 mL, 1g of graphite was added into 6 g of $KMnO_4$, then, a magnetic stirrer was inserted into the flask to improve the homogeneity of the reaction. To start the oxidation treatment, H_2SO_4/H_3PO_4 was added slowly to avoid exothermic reactions, an ice bath was used, figure 3.2(a), after few minutes the mixture was mixed under magnetic stirring.

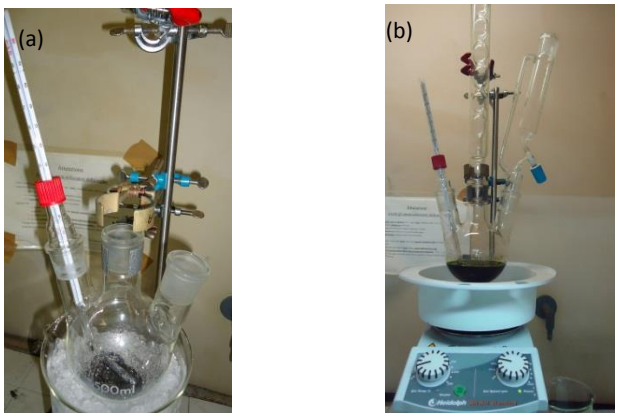

Figure 3.2 production of graphene Oxide (a) Initial moment to produce suspension, ice bath to prevent the exceded temperatures; (b) all reagents mixed under magnetic stirring.

The mixture was stirred for 12 h, during this time the temperature was monitored and mainained at ~50° C. Figure 3.2 (b) shows the suspension afterfew minutes of stirring. After that, ice (133.33 mL) was slowly introduced into the solution and 1 mL of Hydrogen Peroxide was added. When the addition of hydrogen peroxide occurred, immediately a rapid increase of temperature in the solution was measured, reaching up to 90° C in 5 min. The temperature was then lowered at 50° C and it was maintained in this condition for 20 min as showed in figure 3.3. Finally, before the filtration, the acidity of the solution was reduced by using phosphate buffer several times, until reach pH 4.5. The resultant material was washed with distilled water and centrifuged at 6000 rpm several times.

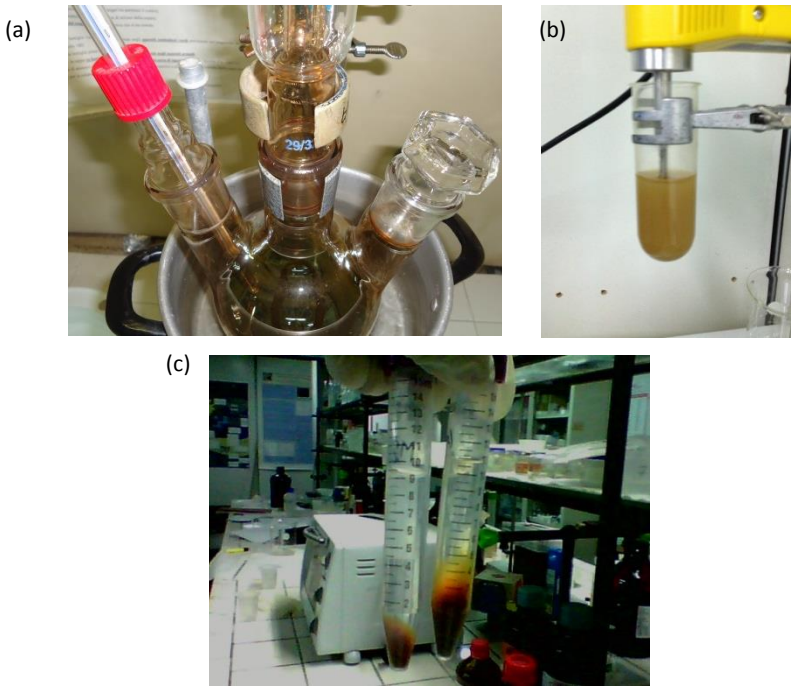

Figure 3.3 Suspension of graphite Oxide (a) Later twelve hours of mechanical agitation (b) Sonication carried for short times; (c)Colloidal Graphene Oxide suspensions obtained.

The remaining material was used to carry out the sonication process into distilled water three times by using a tip sonicator for 45 min, this resulted in a colloidal homogeneous suspension, as demonstrated in figure 3.3 (b) and (c).

Finally, the colloidal suspension obtained was dried at room temperature for around a month. The result of the product has produced little and thin flakes of graphene oxide. The total weight of the material obtained was 1.53 g.

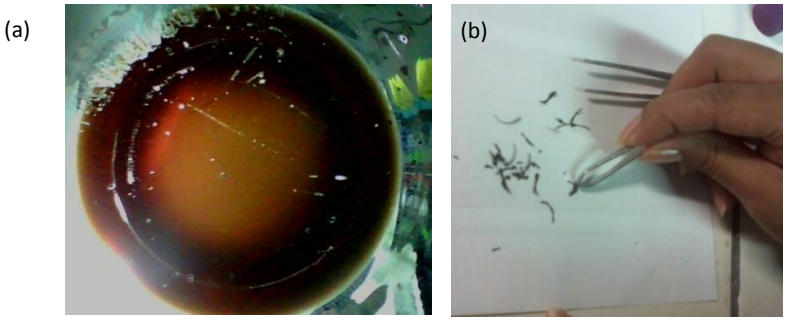

Figure 3.4 Obtained Material dry flakes of graphene Oxide.

3.2. Characterization of Materials obtained by Chemical treatment

3.2.1.SEM Microscopy

The equipment that was used is the Field Emission Scanning Electron Microscopy (FESEM) model Quanta Feg 400 F7 (FEI) with magnification up to 200000x, and the accelerating voltage was 10-20 Kv. In order to study the surface, the samples were metalized with copper, due to the low conductivity present in the Graphene Oxide (GO).

For initial graphite, SEM microscopy analyses evidences that the material presents a variable dimension of the carbon flakes, and an average of diameter of about 500 μm, as shown in figure 3.5 (a).

Figure 3.5(b) shows the initial graphite, the surface is smooth with a little attachment, due to the natural mixing of flakes.

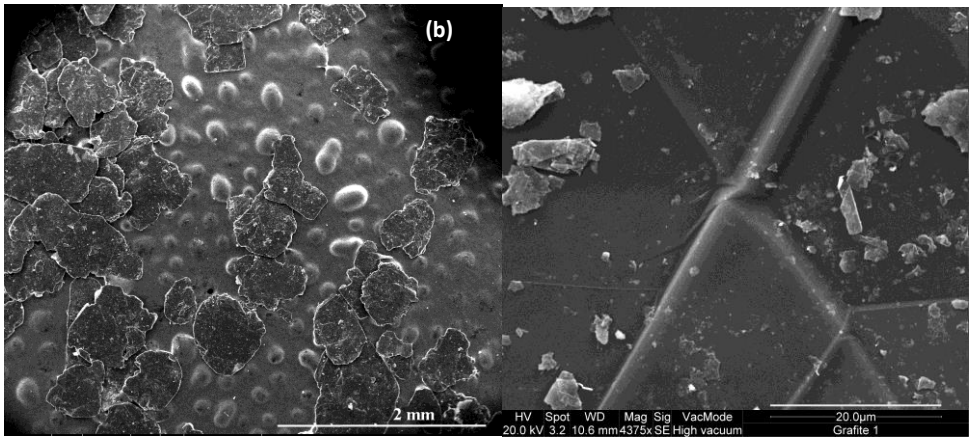

Figure 3.5 SEM microscopy of initial graphite.

The Electron Dispersion X-ray (EDS) spectroscopy in figure 3.6 shows the presence of little traces of impurities, resulting probably from the preparation procedure of the graphite flakes in the chinese factory (table 10).

(a)

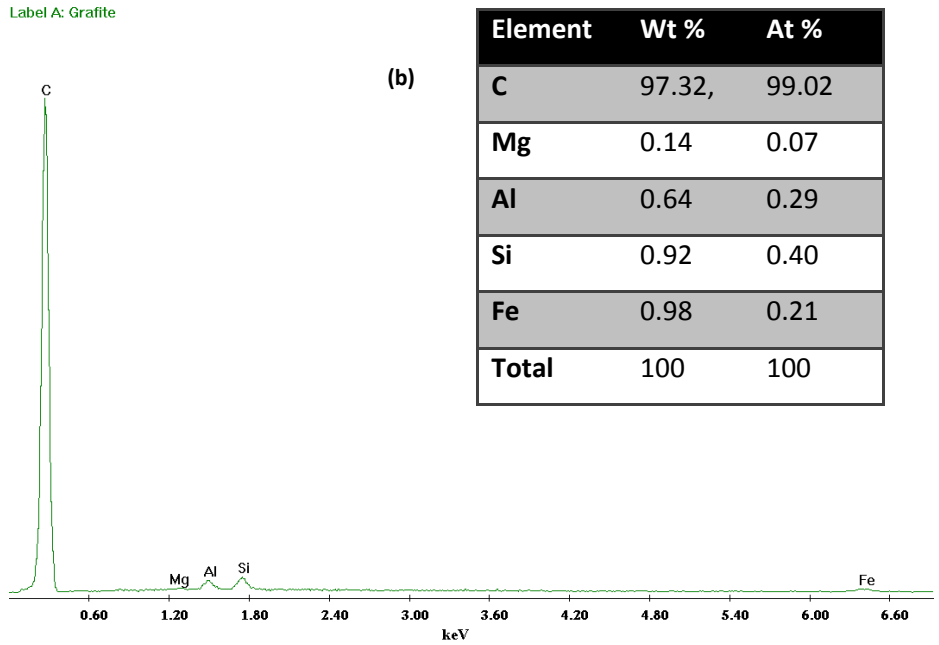

(b)

Element	Wt %	At %
C	97.32,	99.02
Mg	0.14	0.07
Al	0.64	0.29
Si	0.92	0.40
Fe	0.98	0.21
Total	100	100

Figure 3.6 (a) EDS analysis over graphite sample. (b) EDS results belong to the initial graphite.

After the oxidation treatment, a portion of graphite oxide was dried for 1 hour in the oven at 50 °C. After that, the material was recovered, and its SEM image is shown in figure 3.7 (a). The surface was dramatically modified; and a little aggregate appeared through the surface. Additionally, there were changes in the color of the flakes to dark-brown. These means that the treatment applied was effective and the oxidation of graphite was reached, perfectly in concordance with the literature [6][14][139].

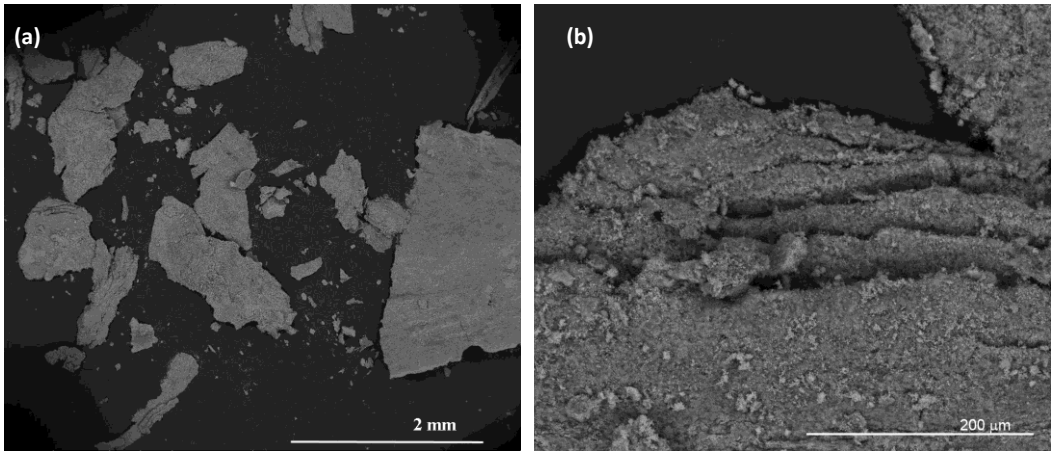

Figure 3.7 SEM images of Graphite Oxide after the chemical treatment taken with different magnifications.

The EDS spectrum, shown in fig. 3.8 (a), confirms the presence of oxygen (66.12 % carbon, 27.83% oxygen), together with other elements whose percentages are shown in fig. 3.8 (b) , resulting from the synthesis procedure.

(a)

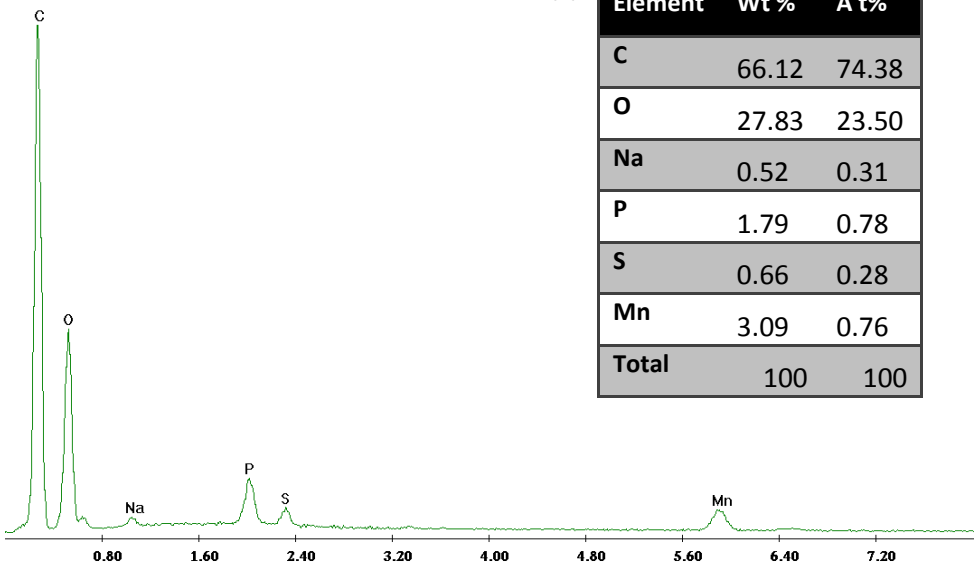

(b)

Element	Wt %	A t%
C	66.12	74.38
O	27.83	23.50
Na	0.52	0.31
P	1.79	0.78
S	0.66	0.28
Mn	3.09	0.76
Total	100	100

Figure 3.8 EDS results of Graphite Oxide (a) Graphic report for Graphite Oxide, ratio atoms which form the structure (b) Summary table with the percentage weight of atoms present in the sample.

Finally, a yellow colloidal suspension was obtained, by sonication, see figure 3.9(a). The morphology of initial graphite oxide was changed completely; when the material was left to dry it changed the colour to brown powder. Furthermore, figure 3.9(b) shows that the appearance of the solid material has changed. In the results there have been a few little flakes, where the particles have an average measure of < 1µm as presented in table 10.

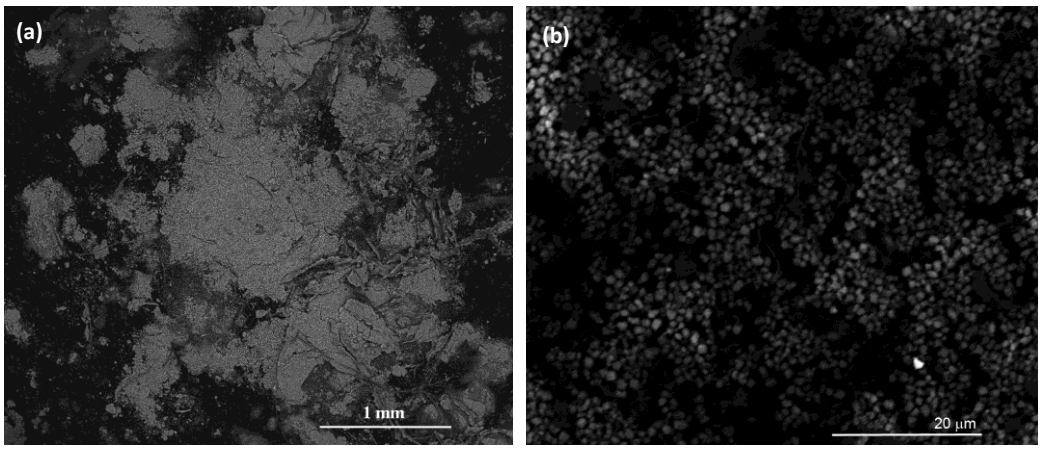

Figure 3.9 (a) Powder of graphite oxide (b) the morphology after sonication process.

(a)

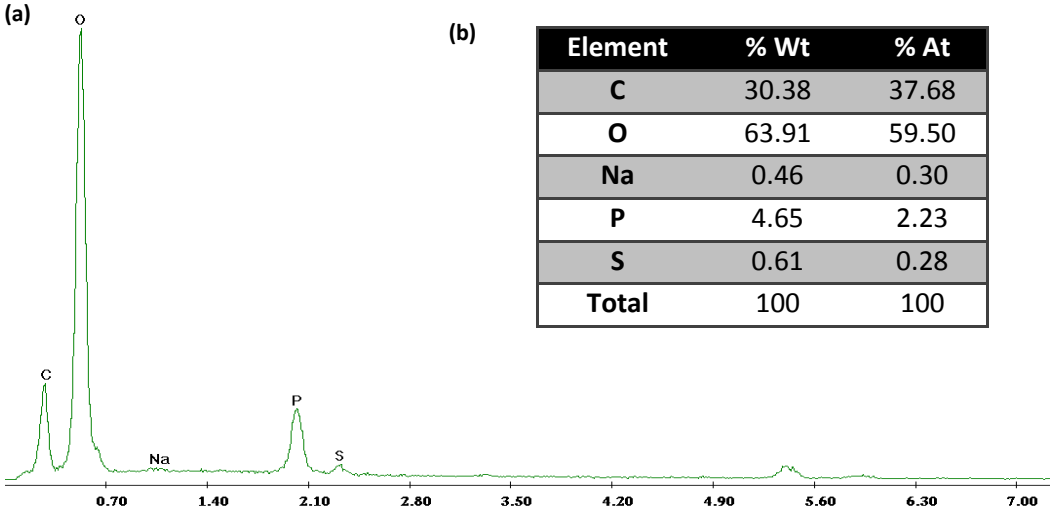

(b)

Element	% Wt	% At
C	30.38	37.68
O	63.91	59.50
Na	0.46	0.30
P	4.65	2.23
S	0.61	0.28
Total	100	100

Figure 3.10 EDS results of GO dry colloidal suspension (a) Graphic report for GO, ratio atoms which form the structure (b) Summary table with the percentage weight of atoms present in the sample.

The EDS characterization in the colloidal suspension reveals a high percent of oxygen atoms due to the chemical treatment, which means that a high level of oxidation was reached through the applied treatment, probably due to the decrease in size after sonication.

Table 10. Total average on twelve samples of Graphene Oxide

N° of measure	Original Graphite (µm)	S 1 GO (nm)	S 2 GO (nm)	S 3 GO (nm)	S 4 GO (nm)	S 5 GO (nm)	S 6 GO (nm)	S 7 GO (nm)	S 8 GO (nm)	S 9 GO (nm)	S 10 GO (nm)	S 11 GO (nm)	S 12 GO (nm)
1	520	73	54	63	168	168	108	102	121	135	91	105	83
2	574	111	79	59	143	116	101	114	117	122	89	82	127
3	347	79	116	49	131	131	94	101	128	191	99	79	74
4	385	65	123	90	282	217	125	87	130	162	109	92	97
5	576	90	152	75	169	262	98		127	209	92		75
6	498	90		79		169	126		150	150			88
7	443			92			118			75			
8	574						118			117			
9	263			70			126			128			
10	429												
Total Average	461	85	105	72	179	177	113	101	129	143	96	90	91

3.2.2.Raman Spectroscopy

Raman Spectra were acquired by Renishaw Spectrometer using a 100x objective with an incident red laser (633 nm). The excitation laser was focused over the dry powder, figure 3.10(a) presents the intensity of the two principal bands of GO, the first one around $1350\ cm^{-1}$ that represent the D peak [6][64] and the second one is the G peak, which is associated with the doubly degenerate (iTO and LO) phonon mode (E2g symmetry) at the Brillouin zone center [69]. In the spectrum in figure 3.10(a), the G peak is broadened and shifted to $1594\ cm^{-1}$ with respect to graphite and both G peak and D peak have almost the same intensity. This fact confirms the lattice distortion induced due the chemical treatment. On the other hand, the second order of D, called 2D peak cannot be observed, these originates from two phonon double resonance, in the Raman process [79]. The fact that 2D peak disappeared confirming that the treatment has been successful. The presence of D' peak remains around $\sim 1620\ cm^{-1}$ that is generally visible in defect graphene [71], in this case it is almost imperceptible. Apparently, in the moment of the broadening, G and D' peaks overlap at the same time due to high disorder in the structure, as represented in figure 3.10(b).

Regarding to the spectrum in figure 3.10 (a), it is important to recognize the Full Width Half Medium (FWHM) of G peak, the value of FWHM for G peak is 64. In the literature, the normal value of FWHM for G peak is from 18 to 20 [82]. G peak is related to sp^2 domains, is possible that it changes to sp^3 domains [70]. The ratio of intensity I_D/I_G is 0.95, which corresponds to a high level of oxidation. [14]

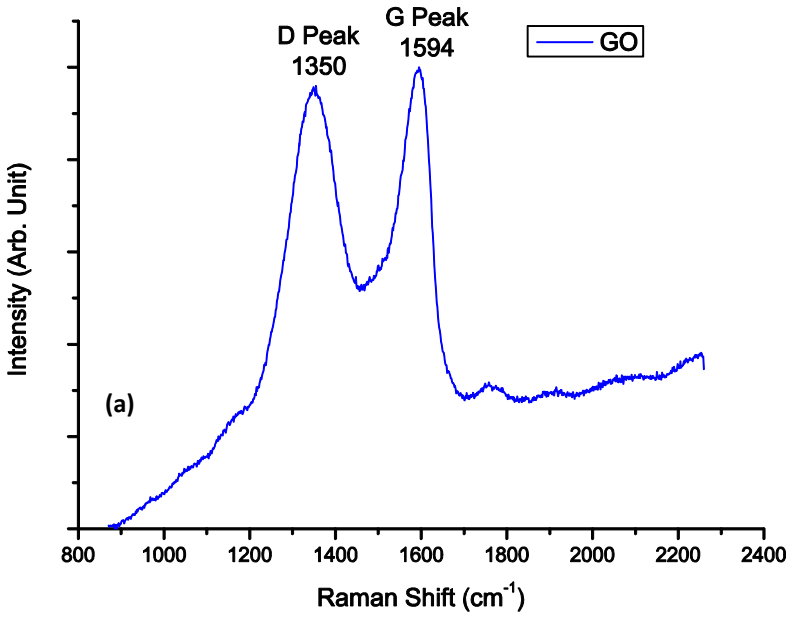

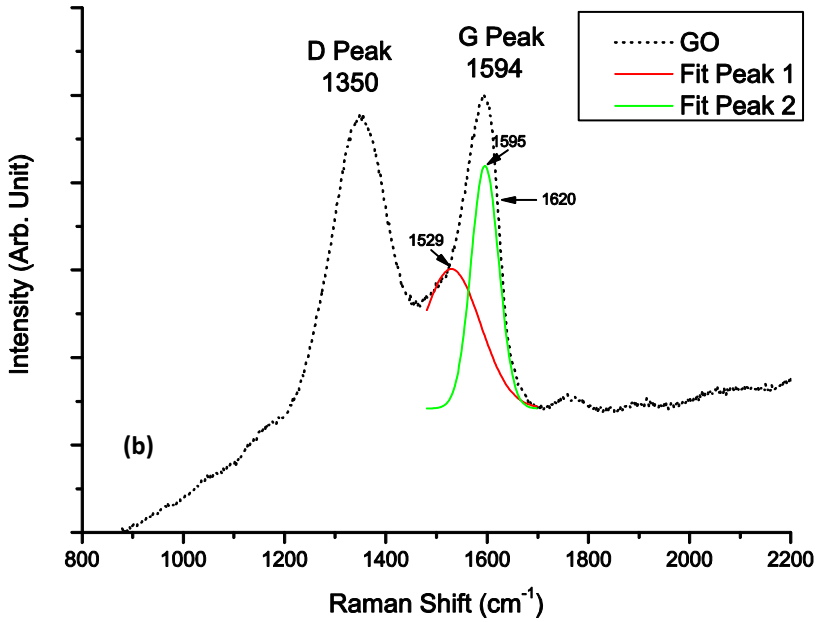

Figure 3.10 Raman Spectrum of obtained GO. (a) Principal bands after sonication process. (b) Fitting of G band in Raman spectrum.

3.2.3.Ultra violet visible Analysis (Uv-vis)

The UV-visible spectrum was performed by UV-Visible spectrophotometer UV- 160A Shimadzu, with a quartz cell of 1mm optic path, GO was in aqueous solution. The spectrum in fig. 3.11 suggests the presence of an ordered structure with great retention of carbons rings in the basal planes. In fact, the absorption peak at 224 nm can be attributed to $\pi \rightarrow \pi^*$ transitions of C=C bonds, corresponding to the aromatics groups [62]. In addition, a small protuberance centered about 362 nm is observed, which corresponds to C=O bonds in the domain of the carbonyl groups. The spectrum indicates nearly the same characteristic peaks of graphene oxide previously reported in the literature [6][64][12][140].

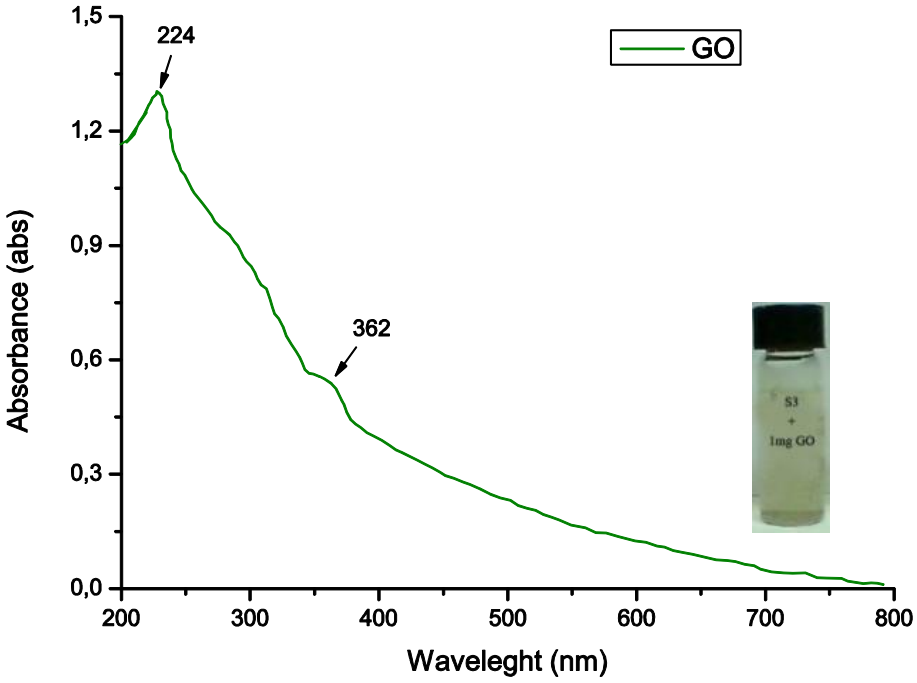

Figure 3.11 Uv-visible spectrum of colloidal suspension of Graphene Oxide (GO)

3.2.4.Fourier Transformed Infrared Spectroscopy (FTIR)

Fourier Transform Infrared Spectroscopy was carried out in Spectrophotometer model Perkin Elmer Spectrum 100, with a scanning range from 400 cm^{-1} to 4000 cm^{-1}, in mode FTIR-ATR. For the analysis, GO were dispersed in KBr disks.

FTIR-ATR spectrum of GO is reported in figure 3.12. The inset presents the following functional groups of GO: O–H bonds (stretching vibrations 3087 cm^{-1}), C-H bonds (stretching vibrations 2932 cm^{-1}), C=O bonds (stretching vibrations from 1730 cm^{-1} to 1456 cm^{-1}). Additionally, the peak observed at 1630 cm^{-1}, may correspond to the deformation of the hydroxyl (-OH) groups in the presence of water [141]. The functional groups which have hydrophilic oxygen-containing characteristics, produce GO sheets with a good dispersability in aqueous medium [62]. The epoxide characteristic bands are localizing in the range from 970 cm^{-1} to 850 cm^{-1}. The epoxide groups are responsible of the formation of covalent bonds with oxygen atoms, which overcome the attraction generated by Van der Waals forces and facilitate the separation between layers.

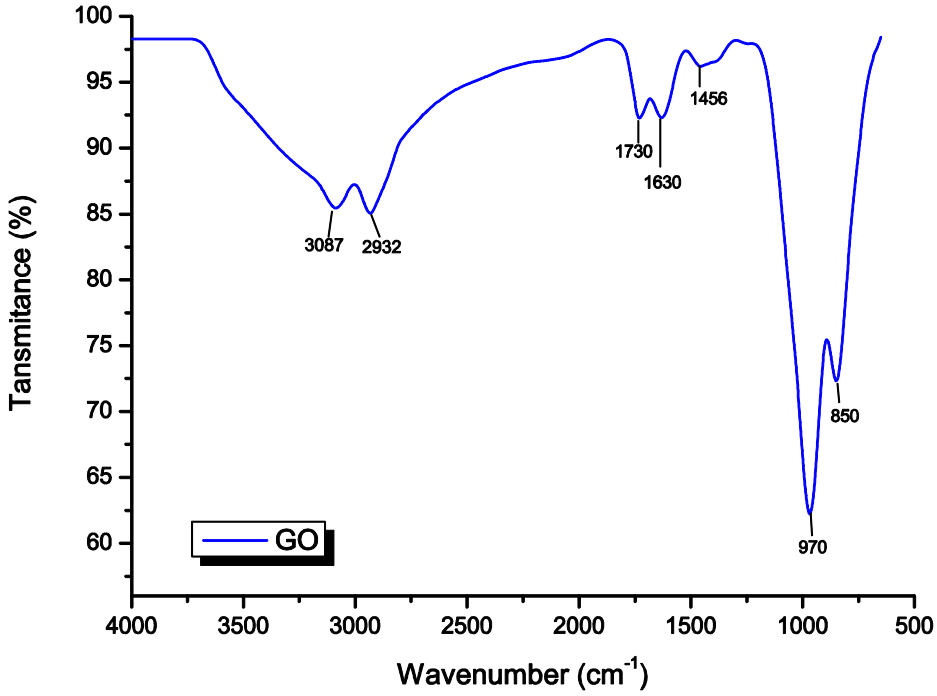

Figure 3.12 FTIR – presented the characteristics of principal functional groups

The obtained results suggest that the final product prepared by oxidation treatment contains the following functional groups: hydroxyl, carboxylic and epoxide, in accordance with previous reports [96][95].

3.3. Conclusions

Graphite oxide was produced by using oxidizing agents such as H_2SO_4, H_3PO_4, and $KMnO_4$, in a suitable combination. After several washes and the sonication, the colloidal suspensions were recovered through the centrifugation. The colloidal suspensions were characterized to verify the existence of Graphene Oxide. In order to weight the obtained material, the colloidal suspensions were dried in a vessel, and at the end of the process, the final product weighed 1.93 mg in powder form, which can be easily re-suspended in an aqueous medium by mild sonication.

Surface morphology studies showed the production of few-layers graphene oxide with the lateral size in the range of micrometers/nanometers. Raman spectroscopy showed that the graphite structure is distorted. The D peak increases in intensity showing that a disruption in the structure had happened. It is worth to note that the shape of the G peak changes after the oxidation treatment, becoming wider and upshifting, which confirms the lattice distortion.

Concerning the UV-vis analysis, the main peak reported for the GO colloidal suspensions was localized at 224 nm, that represent the C=C bonds presents in the solution. Furthermore, another peak was localized at 362 nm, that correspond to C=O bonds. The two main peaks

confirmed the presence of new functional groups decorating the graphene structure. Furthermore, FTIR spectroscopy indicates presence of functional groups such as hydroxyl, carboxyl, ether and epoxides.

CHAPTER 4

Applications with Graphene Oxide

DRUG DELIVERY

4. Bio-Medical application: Drug Adsorption

Currently, it is not surprising that graphene has generated a great interest in nanomedicine and biomedical applications [94][99]. The graphene have a planar structure (which offers an excellent capability to immobilize a large number of substances, including metals, drugs, and biomolecules, and it can be easy functionalized constituting an excellent material for drug delivery cancer.

One of the most critical diseases in the world is cancer; generally, the malignancy of tumors is detected only at advanced stages. Unfortunately, the great problem using chemical anticancer species is that the administration of drugs can be toxic to healthy cells in chemotherapeutic approach. In this context, various attempts have been made to explore the targeted drug delivery [142][96], as well as to detect cancer cells at an early stage [2]. Currently, the loading drug is critical in drug carrier research; therefore it is necessary to improve the stacking efficiency. On the other hand, site-directed drug targeting is very important for improving the drug efficiency and decreasing side effects.

In order to evaluate the potential use of GO in drug delivery applications, it was crucial to test the loading capacity through adsorption of Doxorubicin hydrochloride (DOX); this drug is very famous in the cancer treatment [102][18]. DOX was generously provided by Pfizer Italia S.r.l. (Italia), Figure 4.1.

(a)

(b)

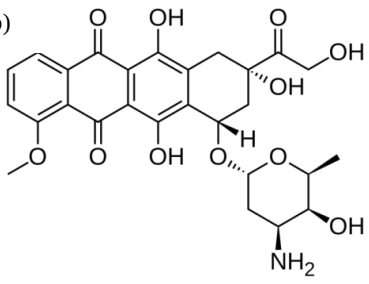

DOX

Figure 4.1 Doxorubicin Hydrochloride in solution with original concentration of 50 mg/mL. (b) Molecular structure of DOX

In chapter 3 has described the process to obtain GO and its characterization. Figure 4.2(a) shows the chemical structure of GO.

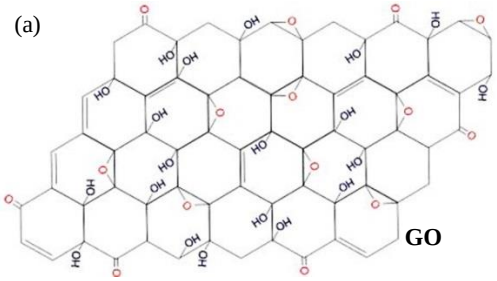

Figure 4.2 Graphic representation of molecular structure. (a) Molecular structure of GO[105];

4.1. Adsorption Process of DOX on GO

The study of the adsorption process of DOX on GO was performed by using the experimental depletion method. In particular, DOX aqueous solutions in various concentrations with two different pH values (7.7 and 3) were prepared. The initial buffered DOX concentrations used in this work are equal to: 20 µg/mL, 50 µg/mL, 100 µg/mL, 200 µg/mL.

To perform the adsorption process, 2 mL of DOX were put in contact with 1 mg of GO powder, and then these were placed under agitation at different times, by using a vortex mixer (VWR, 58816-123) in dark conditions. The loading capacity was studied in different pH media and in order to compare the results obtained, the original solution was used as target. The data were compared with previous reports [3][6] for similar materials.

The determination of Point of Zero Charge (PZC) was performed in aqueous suspension using a mixture containing GO 1 % wt, in order to determine the acidity of GO and evaluate the type of interaction present in this process. Obtained value was pH 4.35 after two hours, whereas, the final value reached (equilibrium value) was pH 5.16 after twenty-four hours.

4.2. Characterization of DOX on GO

The reagents and products were analyzed by ultraviolet spectrophotometer model UV- 160A Shimadzu, as well as series of different concentrations of DOX (20 µg/mL, 50 µg/mL, 100 µg/mL, 200 µg/mL) at pH 7.7, and DOX (10 µg/mL, 100 µg/mL, 200 µg/mL) at pH 3 were used to obtain the calibration curves with $\lambda_{máx}$= 489 nm as the excitation wavelength.

For all experiments, the remaining supernatant solution after incubation time was leave to stand for ~15 min, and then, the residual concentration was measured using a corresponding DOX standard as a target to create a comparison; the following equation describes the process:

$$Q_{fin} = C_{fin} \times V_{fin} \quad (1)$$

where Q_{fin} represented the amount of DOX that has not been adsorbed after the time of contact considered; the variable C_{fin} represents the initial concentration and V_{fin} was the volume used. After the incubation time and resting for ~15min, the amount of drug loading has been determined using the following equation:

$$x = \frac{Q_{in} - Q_{fin}}{mgGO} \quad (2)$$

where *x* symbolizes the amount of DOX that has been immobilized per microgram of GO; the Q_{in} is the variable that represents the DOX initial amount in micrograms; the Q_{fin} is the value of amount described in the eq.1.

In order to obtain the percentage of adsorption, the amount of loaded DOX onto GO (*x*) must be divided for the initial amount of DOX (x_{in}), as follows:

$$\%ad = \frac{(x*100)}{x_{in}} \quad (3)$$

In order to estimate the chemical structure of the materials, the FTIR-ATR spectroscopy has been conducted by using a spectrophotometer model Perkin Elmer Spectrum 100 in the scan range from 450 cm^{-1} to 4000 cm^{-1}, using the reflection mode. The DOX, GO and DOX-GO materials were dispersed in KBr, and used compressed pellet method for the analyses.

Additionally, to study the surface morphology SEM microscopy observations were performed, by using a Field Emission Scanning Electron Microscopy (FESEM) model Quanta Feg 400 F7 (FEI), with magnification up to 200000x and the accelerating voltage from 10 to 20 kV. Finally, to obtain the chemical composition and chemical ratio of atoms in the prepared materials an Energy Dispersive X-ray Analyzer (EDS) was used.

4.3. Results and discussion of DOX on GO

4.3.1.UV- visible analyses

(a) 

(b) 

Figure 4.3 Increment of adsorption process at different pH (a) Test of DOX-GO at pH 3 in a concentration of 50 µg/mL, (b) test of DOX-GO at pH 7.7 in a concentration of 100 µg/mL.

The obtained supernatant solutions at different incubation times and pH values are showed in figure 4.3. It is evident that in both cases the adsorption process was successful.

Figure 4.4(a) shows the UV-visible spectra, performed at pH 7.7, for three solutions GO, DOX and DOX-GO respectively. The DOX curve presents two characteristic peaks: the first one localized at 240 nm, which is produced for the aromatic groups (C=C bonds), the second one at 487 nm, corresponding to characteristic peak of DOX drug [7][6][8].

In order to analyze the interaction between the drug and the inorganic material, the curve of DOX-GO was observed, resulting in one of the red shifting towards 282 nm, in which this wavelength corresponds to the n→π* transitions of C=N bonds. This fact could be an attribute to the interactions between of DOX amine groups and GO carboxyl groups. Additionally, it can be observed that the characteristic band centered at 487 nm, which respect to the standard spectrum of DOX not presenting a band shift, after 24h of contact reveals a dramatic decrease of absorbance intensity confirming the obtained process adsorption on the GO.

Furthermore, figure 4.4(b) reports the similar spectra of GO, DOX and DOX-GO obtained at pH 3 and it reveals a visible band shift relative to DOX-GO. In fact, the spectrum obtained for native DOX sample shows two peaks, one at 236 nm (which corresponds to π→π* transitions of aromatic groups), and the second one at 485 nm. The spectrum of DOX-GO exhibits two peaks, one at 288 nm in the domain n→π* transitions of C=N bonds. It can be observed a different drug behavior with respect to the neutral solution: the ratio of the characteristic peaks is varied probably due to the different coordination of proton to the chemical functional terminal groups.

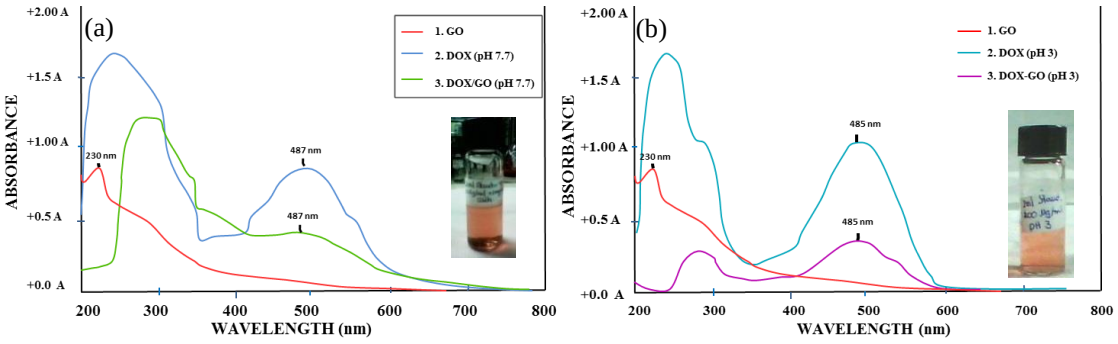

Figure 4.4 UV-visible a) GO in aqueous solution, DOX at pH 7,7 and DOX loaded with, b) GO in aqueous solutions, DOX at pH 3 and DOX loaded with GO, both results carried out at 24 h under agitation.

4.3.2.FTIR - Spectroscopy

In order to obtain further information of chemical structure in the nano-hybrid, the FTIR-ATR analysis was used. Figure 4.5 shows the spectrum of three molecular species, making a comparison among the original materials and the final product obtained. The figure 4.5(a) presents the principle functional chemical groups of Doxorubicin, as O–H stretching vibrations at 3425 cm^{-1}, C-H stretching vibrations at 2931 cm^{-1}, N–H stretching vibrations at 1622 cm^{-1}, C=C stretching vibrations at 1416 cm^{-1}, C–H stretching medium-weak in the range from 1273 cm^{-1} to 1092 cm^{-1}, N–H deformation bonds at 796 cm^{-1}; according to the data previous reported [3][6][8][9][10].

Figure 4.5(c), presents the DOX–GO spectrum and it shows visible differences with respect to the precursor species. Especially, it is possible to observe the O-H bands corresponding to hydroxyl groups, which are centered at 3368 cm^{-1} and 3100 cm^{-1}, respectively. The bands shown below (figure 4.5(c)) present a shift to lower position of the initial DOX. Futhermore, it presents a band about at 3087 cm^{-1}, which suffered a small red shifted with respect to the similar GO vibrational band. These experimental evidences confirm the chemical interactions between the adsorbent and the drug.

In addition, figure 4.5(a) and 4.5(b) show two peaks, one at 2931 cm^{-1} and other at 2932 cm^{-1}, both belonging to C-H bonds corresponding to Quinone portion [8]. It can be observed that the band suffered a red shifted during the interaction. Likewise the band relative to C=O bonds is centered at 1730 cm^{-1}, and it experiences a blue shifted in comparison to the product result (GO). Figure 4.5(b) display a band at 1630 cm^{-1}, whereas, figure 4.5(a) presents a peak at 1622 cm^{-1}. It can be observed that after the molecular interaction, both disappeared shifting to higher position resulting to a new band, this is represented in figure 4.5(c) corresponding to N-H groups [3] centered at wavenumber equal to 1654 cm^{-1}. It is possible to rationalized this behavior thinking that an interactions will occurs in the adsorption process, due to the new hydrogen bonding [6].

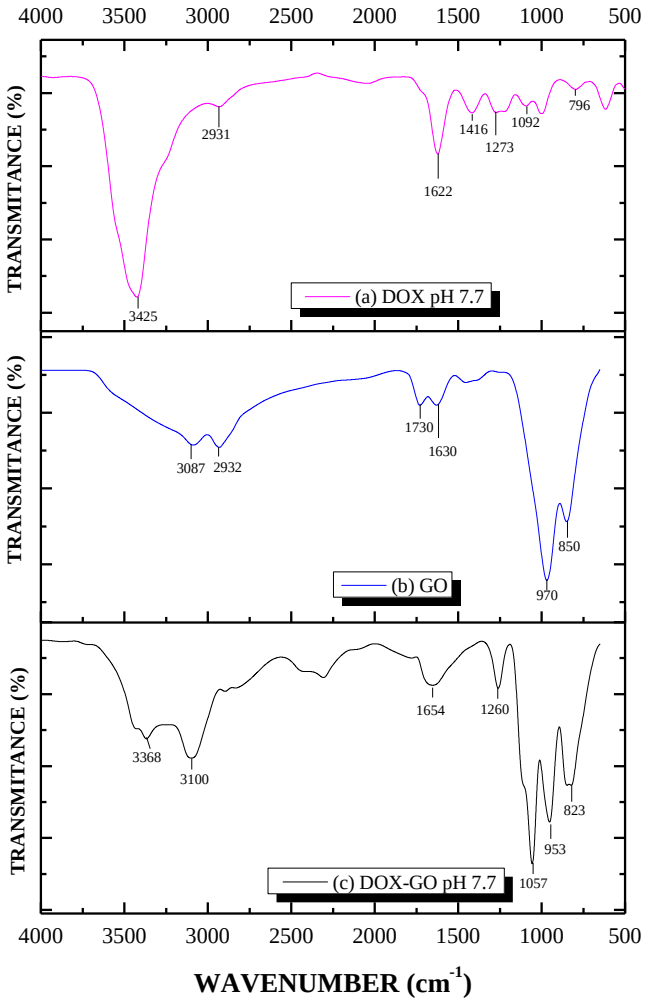

Figure 4.5 FTIR-ATR (a) the spectra of free DOX at concentration of 200 µg/mL in neutral ambient, (b) the original spectra of GO in aqueous solution and finally (c) the resultant product DOX-GO in neutral ambient at pH 7.7

In order to complete the study, in figure 4.6 is presented the different FTIR analyses for the nano-hybrid from 4 h to 24 h, each inset shows the loading of DOX onto GO step by step for a concentration of 200 µg/mL in neutral conditions (pH 7.7).

Figure 4.6 presents the spectra of residual GO after the time of contact with a concentration of 200 µg/mL at pH 7.7 as medium. The nano-hybrid DOX-GO was obtained by decantation of supernatant, following the product was left to dry at room temperature for 15 days. In figure 4.6 (a) is present the spectrum of product DOX-GO after 4h of interaction, where the O-H groups have wavenumbers at 3451 cm^{-1} and 3248 cm^{-1}, resulting in the first reaction in the GO material. To respect the carboxyl groups, the initial wavenumber was localized at 1730 cm^{-1} in GO, when the interacctions are produced, this wavenumber suffers a red shift towards 1758 cm^{-1}, in table 11 is summarized the principal functional groups.

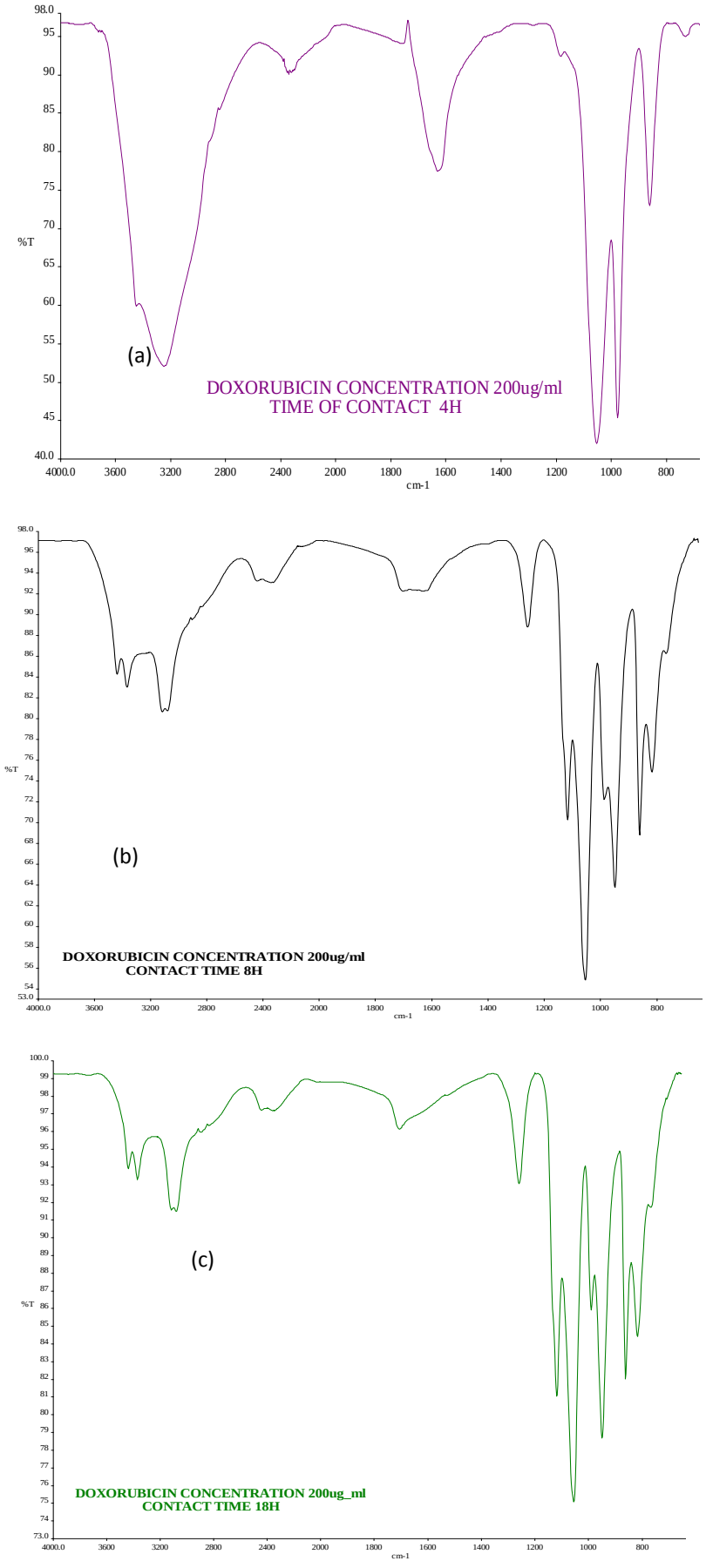

Figure 4.6 Adsorption process in a concentration of 200 µg/mL pH 7,7 (a) 4h; (b) 8h; (c) 18h.

Following with the study, figure 4.6 (b) presents the DOX-GO after 8h of interaction: it is evident the dramatic change in the structure, where the vibrational O-H groups creat another band at 3118 cm^{-1}, while the carboxyl groups showing just one peak at 1698 cm^{-1}. Since the structure of GO has aromatic groups at 1630 cm^{-1}, it is possible that the reaction with the DOX molecule discriminates the presence of C=C due to the loading. In table 2 is presented the principal functional groups of DOX-GO after 8h of interaction.

The analysis was conducted until 18 h of interaction and in figure 4.6 (c) is showed the relative spectrum of DOX-GO. Regarding to the functional groups formed, the main change is reported in the vibrational band of hydroxyls groups, which present a shift of 38 cm^{-1} confirming the continuos interactions between DOX and GO after 18h. In the contrary, the C=O bonds present a band centered at 1706 cm^{-1} with a shift of 8 cm^{-1} with respect to the spectrum in figure 4.6 (b).

Table 13 reports the main vibrational bands observed.

CONFRONT OF DOX WITH GO CONTACT TIME 4h at pH 7,7				
Name of Functional Group	**Functional Group**	**Characteristic Absortions (cm^{-1})**	**Type of vibrations**	**Importance for the study**
Alcohol	O-H	3451,59	Stretching Strong	HIGH
		3248,52		
Carbonyl	C=O	1758,94	Stretching Strong	HIGH
Alkene	C=C	1630,77	Stretching Variable	HIGH
Amine	C-H	1183,92	stretching Medium weak	HIGH
Ether	C-O	1054,41	Stretching Strong	MEDIUM
Alkene	=C-H	978,45	Bending Strong	LOW
		862,72		
		733,94		
Alkyl Halide	C-Cl	673,96	Stretching Strong	LOW
		662,95		

Table 11. Principal functional groups present in DOX-GO at 4h of interaction (pH 7.7)

DOX-GO TIME OF CONTACT 8h at Ph 7,7				
Name of Functional Group	**Functional Group**	**Characteristic Absortions (cm^{-1})**	**Type of vibrations**	**Importance for the study**
Alcohol	O-H	3440,84	stretching strong	HIGH

		3371,83		
Carboxylics Acid	O-H	3118,8	stretching very broad	HIGH
Nitriles	C≡N	2344,93	stretching strong	LOW
Carbonyl	C=O	1698,92	stretching strong	HIGH
Amine	C-H	1259,88	stretching medium	HIGH
Amine	C-H	1118,7	stretching medium	MEDIUM
Ether	C-O	1054,54	stretching strong	MEDIUM
Alkene	=C-H	987,72	Bending Strong	LOW
		949,63		

Table 12. Principal functional groups present in DOX-GO at 8h of interaction (pH 7.7)

DOX-GO TIME OF CONTACT 18h at Ph 7,7				
Name of Functional Group	**Functional Group**	**Characteristic Absortions (cm^{-1})**	**Type of vibrations**	**Importance for the study**
Alcohol	O-H	3440,93	stretching strong	HIGH
		3372,93		
Carboxylics Acid	O-H	3080,91	stretching very broad	HIGH
Nitriles	C≡N	2344,97	stretching strong	LOW
Carbonyl	C=O	1772,93	stretching strong	HIGH
Alkene	C=C	1645,89	stretching variable	HIGH
Amine	C-H	1258,87	stretching medium	HIGH
Amine	C-H	1116,7	stretching medium	MEDIUM
Ether	C-O	1052,56	stretching strong	MEDIUM
Alkene	=C-H	987,7	Bending Strong	LOW
		948,64		
Alkene	=C-H	987,7	Bending Strong	LOW
		948,64		
		861,67		
		816,71		

Table 13. Principal functional groups present in DOX-GO at 18h of interaction (pH 7.7)

The FTIR-ATR spectra of samples were used in acidic conditions; these are reported in figure 4.6. The spectrum of DOX–GO, figure 4.6(c) exhibits an interesting behavior in comparison with GO adsorbed (range from 3087 cm^{-1} to 2932 cm^{-1}). In this range it presents a blue shifted, forming one band at 3073 cm^{-1}, corresponding to O-H groups. Furthermore, the vibrational band centered at 1600 cm^{-1}, can be attribute to the interactions between C=C bonds of GO and N–H bonds of DOX. Figure 4.6 presents a medium and large band at 1096 cm^{-1} due to the stretching bands of the C=O groups [95]. The analysis of this spectrum confirms the effective loading of DOX on GO.

All the experimental results demonstrated the effective adsorption on GO, due to the interactions among the hydroxyl groups of GO and the amine groups of DOX. This behavior suggests a strong π–π stacking interaction between sheets of GO and DOX [140][141]. Similar studies reported the adsorption of DOX on single-walled carbon nanotube [102][146], where the loading capacity (31.2 %)is lower than the GO prepared in this work (90.5 %).

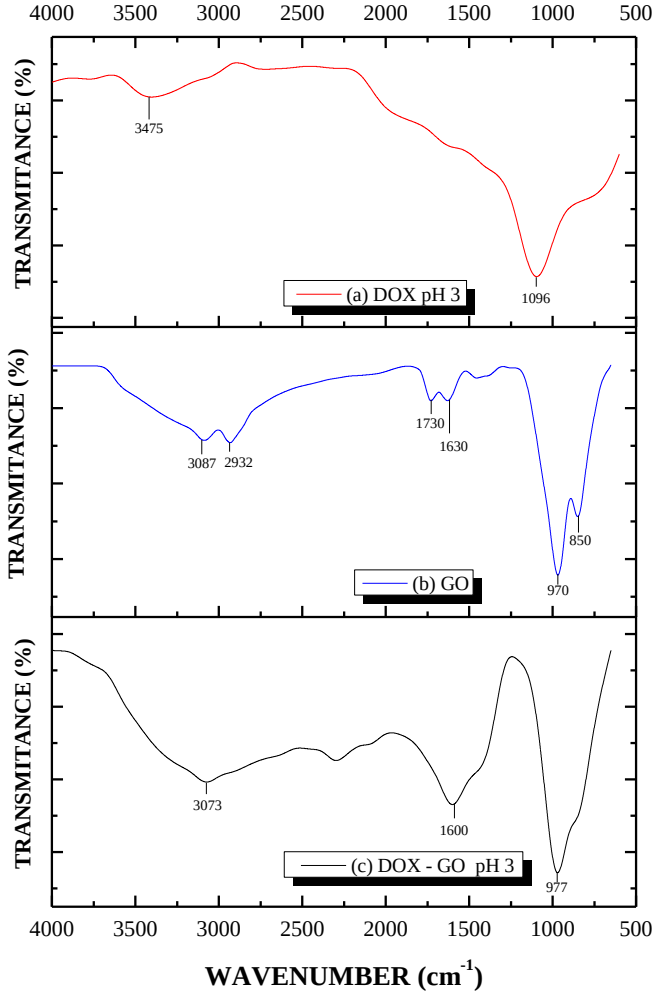

Figure 4.6 FTIR-ATR obtained of dried KBr solid solution (a) DOX solution with a concentration of 200 µg/mL in acid ambient at pH 3, (b) GO spectra and (c) DOX-GO showing the nano-hybrid later 24 h of contact between both products.

4.3.3. Adsorption Process

Figure 4.7 depicts the percentage of adsorption of DOX on GO. In particular the adsorption values obtained for all concentrations at pH 7.7 are plotted in figure 4.7(a). The process was slower at pH 7.7.

Figure 4.7(b) shows the adsorption values related to concentrations at pH 3. In acidic conditions, the incubation time completed 24 hours, so the kinetic of adsorption is quicker considering the dynamic of adsorption. Figure 4.7(c) presents a comparison between the maximum percentages of adsorption as time varies; these results confirm the theory exposed on the adsorption capacity.

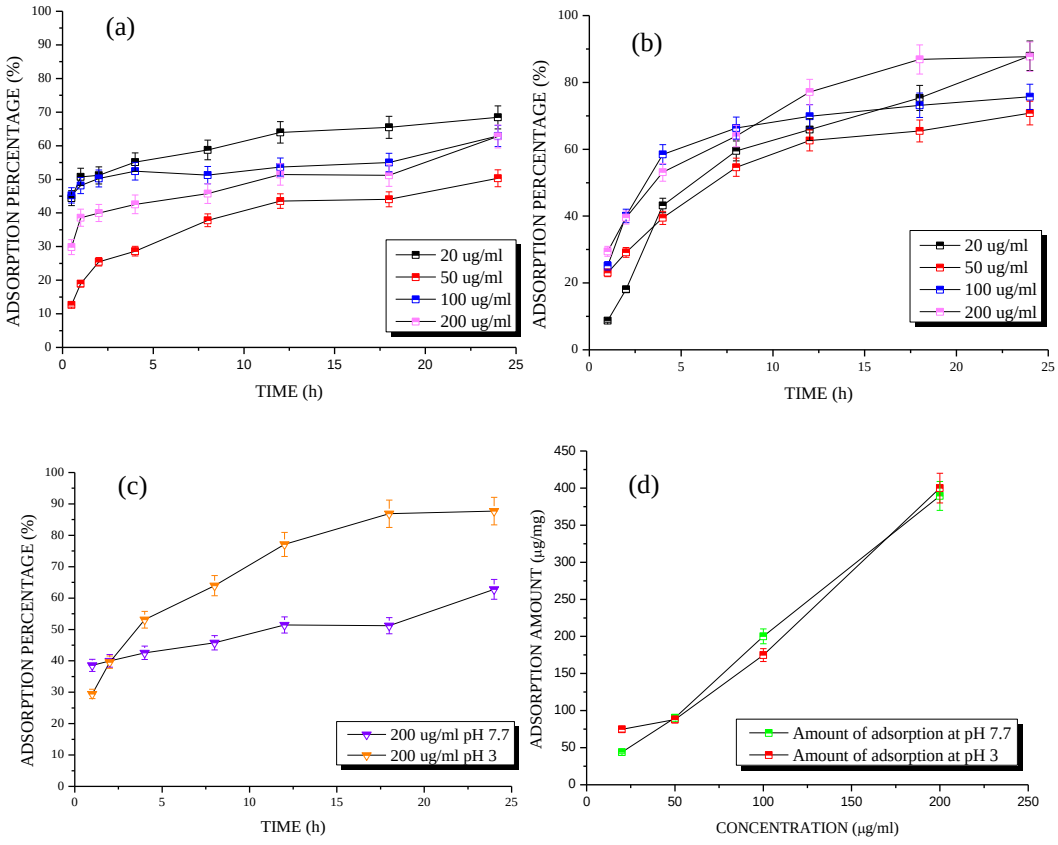

Figure 4.7 Curves of DOX adsorption onto GO at room temperature by using different contact times: (a) Adsorption percent of DOX at pH 7.7 by different times and concentrations; (b) Adsorption percent of DOX at pH 3 to different times and concentrations under dark shaking; (c) Highest percentage of DOX adsorption obtained at different pH for 200 µg/mL initial concentration; (d) Highest amount of DOX loaded onto GO at different initial pH and concentrations solutions.

The analysis of the adsorption of DOX on GO varying the drug concentrations at different pH, evidences that the kinetic of adsorption is faster to 20 μg/mL than the other solutions used.

In particular, the loading capacity grows up depending on pH. It reaches a maximum value at 24 hours of ~90 % at pH 3 under dark agitation. This behavior in acidic conditions can be described by four kinds of hydrogen bonds occur between the –OH groups of GO and the –OH groups of DOX, and between the -COOH groups of GO and the –NH2 groups of DOX [140][141][95].

The performance of GO observed in acidic conditionsshowed different kind of hydrogen bonding interactions involved. In fact, in this pH condition the $–NH_2$ groups of DOX are protonated and cannot participate forming hydrogen bonds then only two types of hydrogen interactions are possible (between –COOH of GO and –OH of DOX , as well between–OH of GO and –OH of DOX[141]).

It is evident that, even if the number of hydrogen bonding interactions decrease under acidic conditions [142], the loading capacity of DOX is faster than neutral conditions. Therefore, it can be makes a proposal: the interactions between the sheets of GO and chemical groups of DOX is π –π stacking. Regarding the maximum loading capacity of DOX on GO, Figure 6.7(d) reports a maximum quantity of 400 μg/mg, it was obtained for the higher concentration at 200 μg/mL.

This work reveals very promising results in the preparation of inorganic biomaterials carbon-containing and it constitutes the first approach in the complex evaluation for the optimization of novel adsorbent for drug delivery systems.

4.4. Conclusions

DOX adsorption performance on GO was investigated by using the depletion method varying the incubation time, drug concentration and the pH values. The adsorbent amount achieved was 400 μg/mg in the highest concentration. The adsorption percentage of the drug on GO was observed to be higher (equal to 90 %) due to the different hydrogen-bonds produced among –OH, –COOH groups of GO and –OH, –NH2 groups of DOX. In this study it has been found a faster kinetic of adsorption at pH 3 media. However, the dynamic of adsorption at pH 7.7 is lower within the first 24 hours.

With regard to the results by FTIR-ATR spectroscopy analysis, it indicate that π-π stacking interactions exist between developed material and DOX. In conclusion, the adsorption of DOX on GO was determined, and evidenced interesting adsorption capacity, which was improved through the incubation time and experimental conditions. The developed material GO resulted very interesting nanomaterial for nanomedicine application, this approach will probably allow

the development of new synthesis of GO to test DOX to enhancing the adsorption process. The high adsorption level permits to use GO in combination with other biopolymers to produce effective nanocarriers, and could have a cheap production and wide scalability.

CHAPTER 5

Applications with Graphene Oxide

REMOVAL OF POLLUTANTS FROM WATER

5. Environmental Application: Removal of Pollutants Adsorption

Dyes are one of the major contaminants of water and many research groups developed their studies by finding ways to removal pollutants from water.[147][109]. They are usually used in manufacturing textile and are unfortunately part of industrial wastewaters. Thus, from an environmental point of view, the removal of dyes is of great concern, and recent applications using carbon-based materials showed high adsorption ability.

Acridine dyes are widely used in the field of printing, stain, leather, printing and lithography processes [148]. Acridine Orange (AO) is a selective cationic dye for nucleic acids and useful for measurements on the cell cycle acids; it interacts with DNA and RNA by intercalation within the molecule or by electrostatic attraction, respectively [108]. Fluorochrome acridine orange has the property to bind with the nucleic acids to be stained. [149]

In this work, graphene oxide (GO) was used for adsorption of acridine orange dye (AO) in water. GO is a material containing functional groups such as carboxyl, epoxy, ketone, and hydroxyl, therefore it can potentially adsorb the cationic dyes.

5.1. Materials and Methods

Graphene Oxide was previously prepared as described in section 3.1.2, while AO dye was purchased from Sigma–Aldrich (CAS Number 10127-02-3; linear formula $C_{17}H_{20}ClN_3 \bullet HCl \bullet 1/2ZnCl_2$; molecular weight 369.96; dye content of 90%) and used without further purification.

Spectrophotometric quantitative analyses were carried out to evaluate the adsorption performance of GO material using the depletion method and an UV- 160A Shimadzu UV-Visible spectrophotometer instrument.

FTIR spectra of the samples were recorded from 4000 cm^{-1} to 500 cm^{-1} using a Perkin Elmer Spectrum 100 FTIR spectrophotometer using the "Attenuated Total Reflection" (ATR) technique.

Field emission Scanning Electron Microscopy (FESEM) images were obtained using a microscope model QUANTA FEG 400 F7 (FEI) with resolution up to 10 nm. Scans were performed with accelerating voltage in the 10-20 kV range. Energy Dispersive X-ray Analyzer (EDS) allowed elementals analysis.

5.2. Acridine Orange (AO) Adsorption

The adsorption study of AO on GO was performed using experimental tests in conjunction with UV-visible spectroscopy analysis. In order to obtain information about the interaction between the dye and the prepared GO, various experimental parameters were varied such as the concentration of aqueos solutions, the contact time, the temperature of experiments and the amount of adsorbent used. In particular, the AO concentration in water used was varied from 0.02 mg/mL to 0.10 mg/mL with a 0.02 mg/mL increment interval, the contact time from 10 minutes to 66 hours, while the temperature values used were Room Temperature (RT), 2 °C and 50 °C, and the graphene oxide weight was changed from 1 to 20 mg, respectively.

The adsorption capacity was determined by spectrophotometric quantitative analysis of the remaining AO concentration observed using the characteristic band having λ_{max} at 496 nm. For this purpose, a series of concentrations with well-known quantity of AO were prepared in distilled water, and their UV-vis absorbance was measured, in order to obtain a calibration curve.

To determine the saturation concentration adsorption experiments were carried out by using the depletion method in vials containing 1 mg of GO and 2.5 mL of AO solution at different initial concentrations. The vials were placed in an analogic vortex mixed (VWR, 58816-123) at 1200 rpm constant agitation and at room temperature for predefined time intervals. All adsorption experiments were performed in equilibrium conditions.

In the second stage, the studied parameter was the amount of GO. The AO solution in a volume of 2.5 mL was added in 5 vials; these containing 1 mg, 2 mg, 5 mg, 10 mg, 15 mg and 20 mg of GO respectively. To this proposes the major concentration (0.10 mg/mL) was tested, and the vials, each one, were put under agitation for 24 h at Room Temperature (RT).

Lastly, the temperature dependence of adsorption process was tested as follows. The GO in amount of 1 mg were prepared in various vials. Afterwards, AO solution with concentration of 0.02 mg/mL was prepared in a volume of 2.5 mL into each vial. The vials were placed under static conditions for different interval times (15 30, 60, 120 and 180 minutes), in order to check the behavior at three different temperatures: rt, 4 °C and 50 °C

5.3. Adsorption Results

The adsorption experiments performed demonstrated the high capacity of GO as an adsorbent of AO [106][116]. Figure 5.1 shows the photography test of adsorption: vials in (a) contain the AO solution at different initial concentration (0.10 mg/mL left, 0.06 mg/mL right) with 1 mg of

GO and in (b) the same vials after 6h, it is evident that turned colorless. Visually, GO is a good adsorbent of AO.

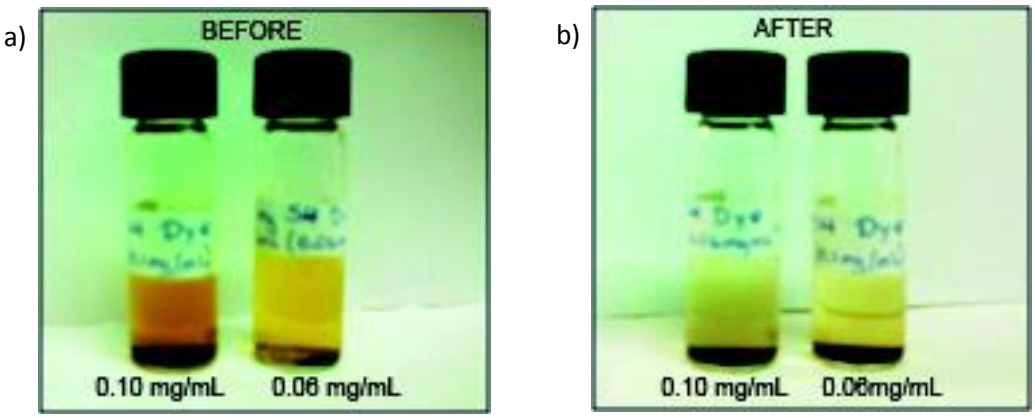

Figure 5.1 Adsorption processes of two different Acridine Orange concentrations (a) Initial concentration 0.01 mg/mL and 0.06 mg/mL (b) Final concentrations reached after 6h of adsorption process.

5.3.1.Uv- Visible characterization

UV-visible spectra of AO initial concentrations were performed, and it revealed the characteristic absorption bands centered at wavelengths comprise in the range from 440 nm to 510 nm according to the literature references [148][123]. In particular, in this study for perform the quantitative analysis, the wavelength of the maximum intensity of band selected was λ_{max} = 496 nm. Similar results were obtained for all different initial concentrations used in this study.

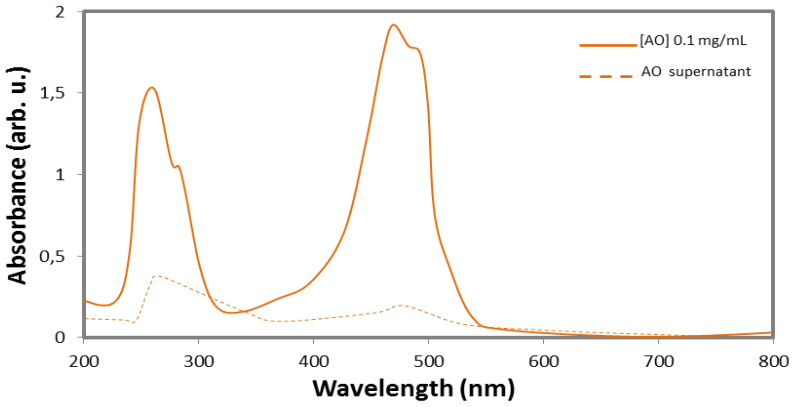

Figure 5.2 UV-vis spectrum of acridine orange solution at 0.1 mg/mL before and after contact with GO

5.3.2.FTIR –ATR Spectroscopy

FTIR spectroscopy is an important technique to understand the chemical interactions between the dye and the adsorbent involved in the adsorption process. The GO/AO adducts were obtained after the adsorption process and analyzed in order to compare the obtained vibrational bands with the characteristic spectra of GO and AO then to evidence structural variations obtained produced some, see figure 5.2 .

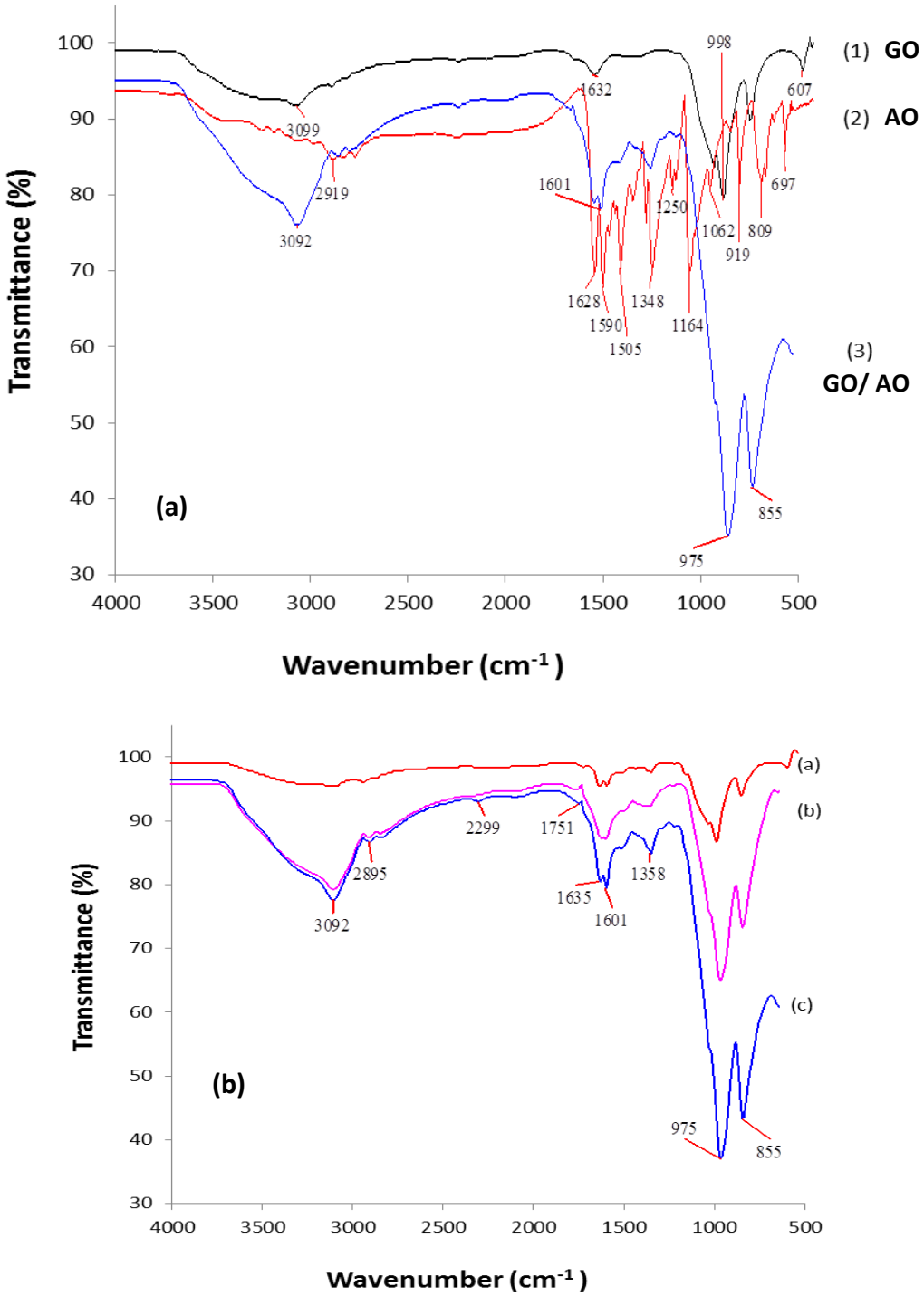

Figure 5.2 FTIR spectra in (a): (1) GO, (2) AO and (3) GO/AO. In (b): (a) GO with adsorbed 0.02 mg/mL [AO], (b) GO with adsorbed 0.06 mg/mL [AO], and (c) GO adsorbed with adsorbed 0.10 mg/mL [AO].

In order to establish a comparison, figure 5.2(a) presents the FTIR spectra of the AO, the GO, and the GO/AO composite obtained after adsorption process, respectively. It can be observed that the main change of the composite GO/AO is localized at 3092 cm^{-1}, band typical of the hydroxyl groups [8]. The band intensity of these groups increases with respect to GO similar bands. A notable difference can be observed at 975 cm^{-1} in the amine domains due to the interaction between the NH_2 group of the dye and the carbonyl groups of the adsorbent material.

The FTIR spectra of GO containing different amounts of AO are reported in figure 5.2(b). In the spectra of GO/AO composites can be observed an increase of the intensity of carboxyl group at 1736 cm^{-1} and of hydroxyl group at 3095 cm^{-1}. Moreover it can be evidenced that the intensity of the vibrational bands centered around 1630 cm^{-1}, related to –C-C– and –C-N– stretching, and around 1360 cm^{-1}, due to and–C–N–stretching increase. This behavior may be attributed, in a first time, to the electrostatic interaction of AO with the –COO group of GO [150].

5.3.3. Adsorption Capacity

Experimental conditions were optimized in order to optimize the dye removal. There were evidenced of adsorption effects, due to the temperature and changes in the amount of GO. Figure 5.3 shows the effect of contact time on AO adsorption by GO, using five different initials concentration of AO. The amount of AO adsorbed on GO, see figure 5.3 (a), depends on the initial concentration of AO, and the adsorption reaches the equilibrium in less than one hour for lower concentrations, while for the highest concentration (0.10 mg/mL) the equilibrium is reached in twenty hours, that could be happens due to agitation applied and the mass transfer between GO/AO.

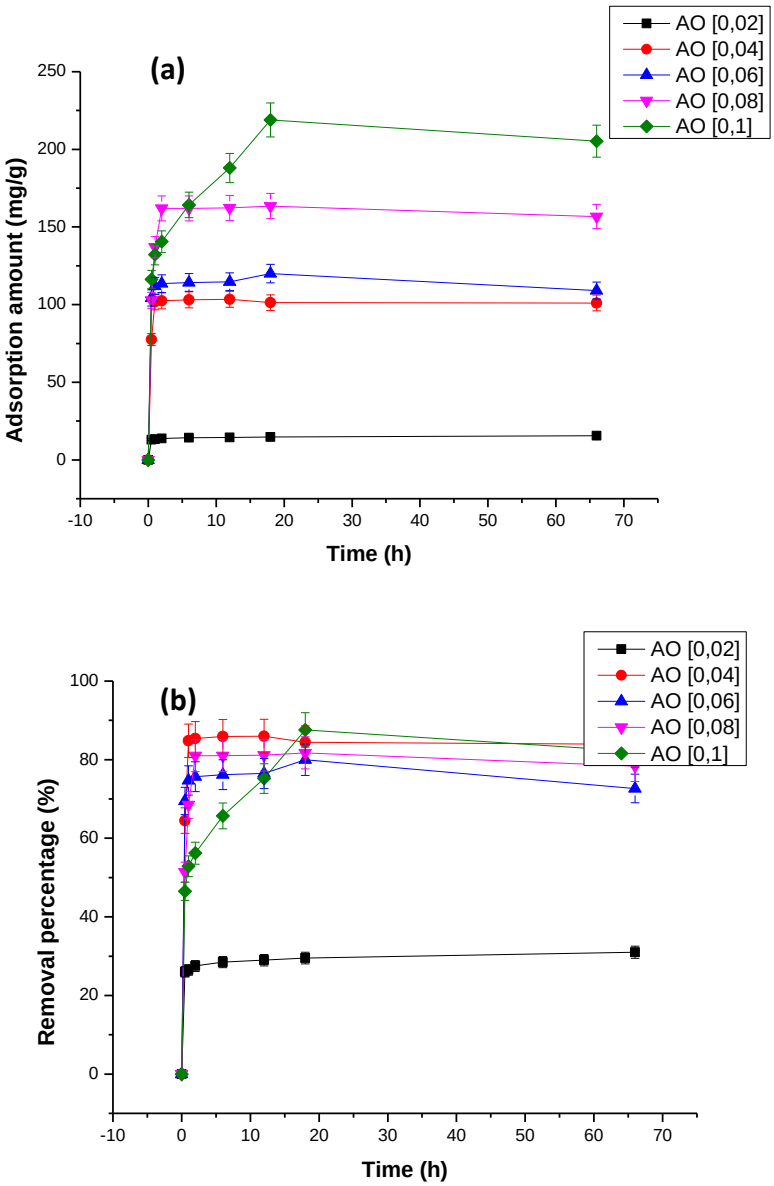

Figure 5.3 Dynamic adsorption of AO on GO. (a) The amount of adsorbent loaded on AO for different initials concentrations. (b) The removal percentage at different intervals of time.

The oxygen functionalities introduced in GO (chapter 3, section 3.1.2); it improves the adsorption of AO onto graphene oxide layer. The removal percentage achieved for AO is displayed in Fig. 5.3(b), and it exhibits optimal values, these values are in the range of 70% to 95%. The higher initial concentrations, showed a maximum of percentage of 92 %, that means that GO material adsorbed almost all molecules of AO onto it surface. Only for the lowest concentration of 0.02 mg/mL the removal percentage is noticeably lower. Thus removal of AO by GO is mainly due to not physical adsorption, but rather to the surface chemistry of GO. Is worth to note that the obtain percentage is higher respect to other works carried out for MWCNT [151], as well as the amount loading onto GO in the first 20 min reached a value of 205 mg/g higher than magnetic nanoparticles [152], MWCNT [151] and clays [153][154].

GO Amount (mg)	[AO] initial (mg/mL)	Volume (mL)	Time (h)	[AO] Final (mg/mL)	AO removal amount (mg)	AO removal Percentage
1	0.1	2.5	24	0.0081	0.2298	91.9
2	0.1	25	24	0.0031	0.2423	96.9
5	0.1	2.5	24	0.0027	0.2433	97.3
10	0.1	2.5	24	0.0026	0.2435	97.4
20	0.1	2.5	24	0.0025	0.2438	97.5

Table 14. Adsorption amount by using different GO weight

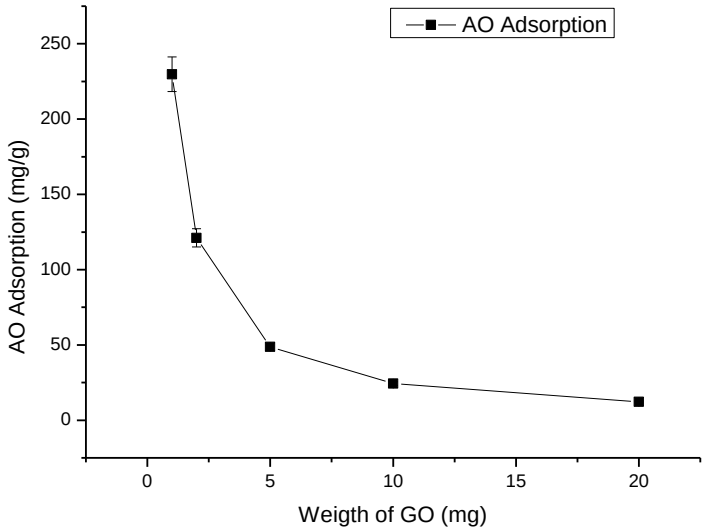

Figure 5.4 Adsorption AO amount in several GO weight

With regards the amount of GO and the adsorption capacity, the table 1 shows the different weight using for GO with an initial concentration of 0.1 mg/mL of AO. It was tested at room temperature in static conditions. The GO reveals a slow increment of percentage as the weight increases up to reach higher loadings of GO. Such effect is displayed in figure 5.4; so that, AO adsorption exhibits the highest value for 0.1 mg of GO, this fact can be ascribed to the slow mass transfer between adsorbate and adsorbent.

Figure 5.5 show that the adsorption is strongly influenced by temperature and initial concentration. It is evident that the kinetic of adsorption is faster at 50 °C than at other temperatures used, see figure 5.5 (a). The amount loading onto GO vs the initial concentration of AO is depicted in figure 5.5 (b), it is evident that the loading is produce almost linearity as the concentration increases.

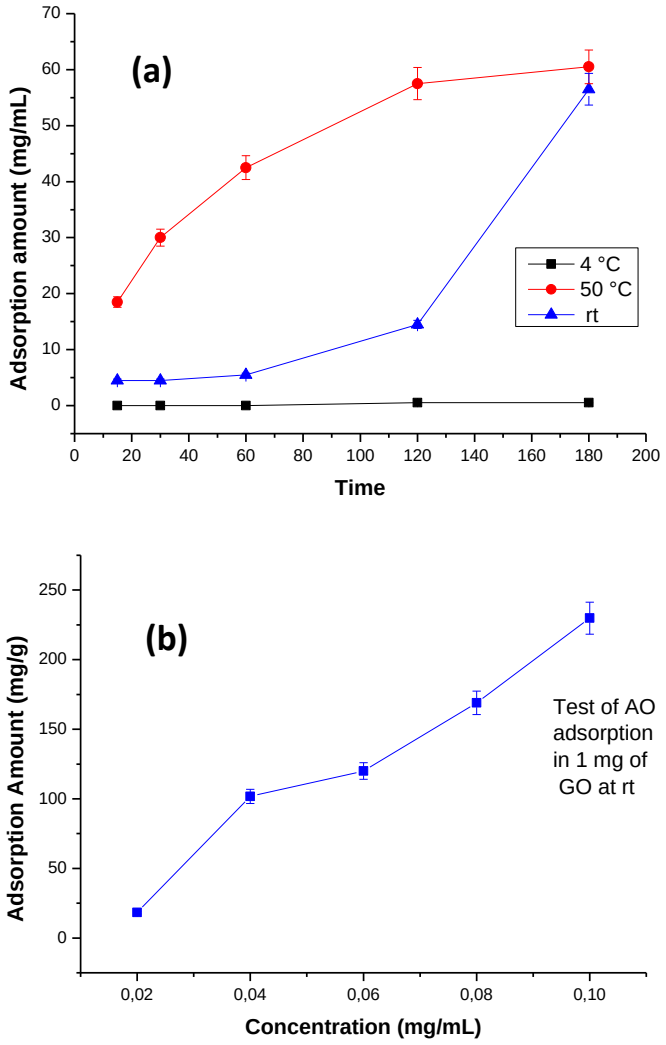

Figure 5.5 Adsorption effects due to (a) temperature and (b) AO concentration

5.4. Conclusions

Graphene oxide prepared from natural graphite by oxidation process was successfully applied as adsorbent for acridine orange, due to the wide area of graphene oxide structure and the presence of oxygen-containing functional groups.

The FTIR analysis showed that the adsorption process causes an appreciable interaction between the hydroxyl groups of GO and amine groups of AO. Regarding the GO adsorption and temperature, it can be evidenced that AO percentage adsorption increases increasing the temperature value. Moreover it is evident that the kinetic of adsorption process is faster at 50 °C than at other temperatures used.

Obtained results shown that the adsorption equilibrium, with the removal of 40% of the dye, is reached in approximately 1 hour, and the adsorption capacity increases at higher initial concentrations.

The GO exhibits good ability to adsorb AO in aqueous solution. The adsorption capacity of AO by graphene oxide reaches 230 mg/g, much higher than clays and MWCNT materials. The proposed method to remove acridine orange from water is simple and cheap; the GO without additional functionalization could be employed as a low-cost alternative in the removal of AO dye from wastewater. The dye adsorbed in GO was not released, then this material has a great potential to be used in environmental applications.

Conclusions

Few layer graphene was successfully produced. In the mixture of solvents, natural graphite was exfoliated by sonication using different ratio of solvents. The Uv-visible analysis showed an increment in the absorbance in the domain of C=C bonds, moreover the Raman spectroscopy demonstrated an existence of Few layers Graphene (FLG).

In the second stage, the zeolite 4A improved the exfoliation and stability. The experiments were characterized by Field Emission Scanning Electron Microscopy (FE-SEM), Transmission Electron Microscopy (TEM), Electron Diffration, and Raman Spectroscopy. At the end, the 3_BS suspension and the 7_F suspension showed the best results; these reached the greatest amount of days in suspension. In the electrical characterization, the suspensions demonstrated a high conductivity; it presented excellent characteristics to be used in composites, as well as, in the field of electronic, such as sensors, transparent electrodes and solar cells.

Graphene Oxide was produced from natural graphite flakes using Hummer's method and Improved Hummer's method. A mix of them produced a well-oxidized material. The characterization was made by Field Emission Scanning Electron Microscopy (FE-SEM), Ultraviolet–visible (UV-vis) spectroscopy, Fourier Transform Infrared spectroscopy (FTIR), Energy Dispersive Spectroscopy (EDS), and Raman Spectroscopy. The UV- vis analysis showed bands that belong to C=C and C=O bonds. Raman spectrum displayed a disruption in the crystal lattice, and FTIR spectroscopy indicates presence of functional groups such as hydroxyl, carboxyl, ether and epoxides. The results showed a good level of oxidation in the material and small flakes of graphene oxide.

The adsorption process for drug delivery was tested using Doxorubicin (DOX) hydrochloride in conjunction with GO. The study was carried out by using different initial concentrations of DOX, different pH values, and diverse incubation times. All experiments were carried out under agitation in dark conditions at room temperature. The percentage of adsorption was reported at 95% for each concentration and pH value. The high capacity of adsorption for DOX was achieved in acidic conditions; where in only 24 hours of interaction the amount achieved is 400 μg/mg. Therefore, GO shows a very interesting behavior which makes it a good candidate as nanomaterial for nanomedicine application.

About the environmental application, the adsorption study was conducted using a commercial dye Acridine Orange (AO). AO was prepared in aqueous solution at different concentrations,

these solutions were placed under centrifugation and dark conditions in combination with GO to evaluate the kinetic of adsorption. Additionally, the GO was analyzed at different weight and temperatures to find out the best conditions for the adsorption process. The nanohybrid AO/GO were recovered from the bottom of the supernatant solution, in order to establish the chemical structure by FTIR; where the results shown a strong interaction between the hydroxyls groups and amine groups present in AO. The kinetic of adsorption showed a percentage from 75% to 95% for higher concentrations and the amount of AO loading on GO was 230 mg/g. GO showed a better adsorption with higher temperatures. This material has a great potential to be used in environmental applications.

References

[1] X. Li, W. Cai, J. An, S. Kim, J. Nah, and D. Yang, “Large-Area Synthesis of High-Quality and Uniform Graphene Films on Copper Foils,” vol. 2009, pp. 1–12, 2009.

[2] A. Reina, X. Jia, J. Ho, D. Nezich, H. Son, V. Bulovic, M. S. Dresselhaus, and J. Kong, “Large Area, Few-Layer Graphene Films on Arbitrary Substrates by Chemical Vapor Deposition,” *Nano Lett.*, vol. 9, no. 1, pp. 30–35, 2009.

[3] H. Fukidome, Y. Miyamoto, H. Handa, E. Saito, and M. Suemitsu, “Epitaxial Growth Processes of Graphene on Silicon Substrates,” *Jpn. J. Appl. Phys.*, vol. 49, no. 1, p. 01AH03, 2010.

[4] W. a. de Heer, C. Berger, X. Wu, P. N. First, E. H. Conrad, X. Li, T. Li, M. Sprinkle, J. Hass, M. L. Sadowski, M. Potemski, and G. Martinez, “Epitaxial graphene,” *Solid State Commun.*, vol. 143, no. 1–2, pp. 92–100, 2007.

[5] J. W. S. Hummers and R. E. Offeman, “Preparation of graphitic oxide.” Journal American Chemical Society, p. 1339, 1958.

[6] D. C. Marcano, D. V Kosynkin, J. M. Berlin, a Sinitskii, Z. Z. Sun, a Slesarev, L. B. Alemany, W. Lu, and J. M. Tour, “Improved Synthesis of Graphene Oxide,” *ACS Nano*, vol. 4, no. 8, pp. 4806–4814, 2010.

[7] S. Stankovich, D. a. Dikin, R. D. Piner, K. a. Kohlhaas, A. Kleinhammes, Y. Jia, Y. Wu, S. T. Nguyen, and R. S. Ruoff, “Synthesis of graphene-based nanosheets via chemical reduction of exfoliated graphite oxide,” *Carbon N. Y.*, vol. 45, no. 7, pp. 1558–1565, 2007.

[8] L. Guardia, J. I. Paredes, P. Solı, and J. M. D. Tasco, “Vitamin C Is an Ideal Substitute for Hydrazine in the Reduction of Graphene Oxide Suspensions.pdf,” pp. 6426–6432, 2010.

[9] Y. Hernandez, V. Nicolosi, M. Lotya, F. M. Blighe, Z. Sun, S. De, I. T. McGovern, B. Holland, M. Byrne, Y. K. Gun’Ko, J. J. Boland, P. Niraj, G. Duesberg, S. Krishnamurthy, R. Goodhue, J. Hutchison, V. Scardaci, A. C. Ferrari, and J. N. Coleman, “High-yield production of graphene by liquid-phase exfoliation of graphite.,” *Nat. Nanotechnol.*, vol. 3, no. 9, pp. 563–568, 2008.

[10] M. Lotya, Y. Hernandez, P. J. King, R. J. Smith, V. Nicolosi, L. S. Karlsson, M. Blighe, S. De, Z. Wang, I. T. Mcgovern, G. S. Duesberg, J. N. Coleman, and F. M. Blighe, “Liquid Phase Production of Graphene by Exfoliation of Graphite in Surfactant / Water Solutions Liquid Phase Production of Graphene by Exfoliation of Graphite in Surfactant / Water Solutions,” no. 11, pp. 3611–3620, 2009.

[11] U. Khan, A. O’Neill, M. Lotya, S. De, and J. N. Coleman, “High concentration solvent-exfoliation of graphene,” *Small*, vol. 1, no. 6, p. 864, 2012.

[12] J. I. Paredes, a Marti, J. M. D. Tasco, and a Martı, “Graphene Oxide Dispersions in Organic Solvents Graphene Oxide Dispersions in Organic Solvents,” vol. 24, no. August, pp. 10560–10564, 2008.

[13] K. Parvez, Z. S. Wu, R. Li, X. Liu, R. Graf, X. Feng, and K. Müllen, “Exfoliation of graphite into graphene in aqueous solutions of inorganic salts,” *J. Am. Chem. Soc.*, vol. 136, no. 16, pp. 6083–6091, 2014.

[14] D. R. Dreyer, S. Park, C. W. Bielawski, and R. S. Ruoff, “The chemistry of graphene oxide.,” *Chem. Soc. Rev.*, vol. 39, no. 1, pp. 228–240, 2010.

[15] S. Park and R. S. Ruoff, “Chemical methods for the production of graphenes.,” *Nat.*

Nanotechnol., vol. 4, no. 4, pp. 217–224, 2009.

[16] S. V. Tkachev, E. Y. Buslaeva, a. V. Naumkin, S. L. Kotova, I. V. Laure, and S. P. Gubin, "Reduced graphene oxide," *Inorg. Mater.*, vol. 48, no. 8, pp. 796–802, 2012.

[17] C. Y. Su, Y. Xu, W. Zhang, J. Zhao, A. Liu, X. Tang, C. H. Tsai, Y. Huang, and L. J. Li, "Highly efficient restoration of graphitic structure in graphene oxide using alcohol vapors," *ACS Nano*, vol. 4, no. 9, pp. 5285–5292, 2010.

[18] H. C. Arora, M. P. Jensen, Y. Yuan, A. Wu, S. Vogt, T. Paunesku, and G. E. Woloschak, "Nanocarriers enhance doxorubicin uptake in drug-resistant ovarian cancer cells," *Cancer Res.*, vol. 72, no. 3, pp. 769–778, 2012.

[19] G. Tubón Usca, C. Vacacela Gómez, D. Fiallos Coello, P. Tavolaro, G. Martino, L. S. Caputi, and A. Tavolaro, "Preparation of graphene oxide as biomaterials for drug adsorption," no. October, pp. 79–86, 2015.

[20] Y. Chen, L. Chen, H. Bai, and L. Li, "Graphene oxide–chitosan composite hydrogels as broad-spectrum adsorbents for water purification," *J. Mater. Chem. A*, vol. 1, no. 6, p. 1992, 2013.

[21] D. Coello Fiallos, C. Vacacela Gómez, G. Tubón Usca, D. Cid Pérez, P. Tavolaro, G. Martino, L. S. Caputi, and A. Tavolaro, "Removal of acridine orange from water by graphene oxide," no. August 2015, pp. 38–45, 2015.

[22] W. Yuan and G. Shi, "Graphene-based gas sensors," *J. Mater. Chem. A*, vol. 1, no. 35, p. 10078, 2013.

[23] S. Wang, P. K. Ang, Z. Wang, A. L. L. Tang, J. T. L. Thong, and K. P. Loh, "High Mobility, Printable, and Solution-Processed Graphene Electronics," *Nano Lett.*, vol. 10, no. 1, pp. 92–98, 2010.

[24] S. D. Bergin, Z. Sun, D. Rickard, P. V. Streich, J. P. Hamilton, and J. N. Coleman, "Multicomponent solubility parameters for single-walled carbon nanotube-solvent mixtures," *ACS Nano*, vol. 3, no. 8, pp. 2340–2350, 2009.

[25] J. N. Coleman, "Liquid exfoliation of defect-free graphene," *Acc. Chem. Res.*, vol. 46, no. 1, pp. 14–22, 2013.

[26] G. P. Keeley, a O'Neill, N. McEvoy, N. Peltekis, J. N. Coleman, and G. S. Duesberg, "Electrochemical ascorbic acid sensor based on DMF-exfoliated graphene," *J. Mater. Chem.*, vol. 20, no. 36, pp. 7864–7869, 2010.

[27] S. Pang, Y. Hernandez, X. Feng, and K. Müllen, "Graphene as transparent electrode material for organic electronics," *Adv. Mater. (Weinheim, Ger.*, vol. 23, no. 25, pp. 2779–2795, 2011.

[28] P. G. Collins, "Extreme Oxygen Sensitivity of Electronic Properties of Carbon Nanotubes," *Science (80-.).*, vol. 287, no. 5459, pp. 1801–1804, 2000.

[29] J. H. Warner, F. Schaffel, A. Bachmatiuk, and M. H. Rummeli, *Graphene: Fundamentals and Emergent Applications.*, Vol.1 ed. Elsevier, 2013.

[30] R. Cowan, "Nuclear Power Reactors: A Study in Technological Lock-in," *J. Econ. Hist.*, vol. 50, no. 03, p. 541, 1990.

[31] R. M. R. S. Ruoff Doris S. Tse and D. C. Lorents, "Solubility of C60 in a Variety of Solvents," *J. Phys. Chem.*, vol. 97, pp. 3379–3383, 1993.

[32] B. I. Yakobson and R. E. Smalley, "graphite in the carbon family Fullerene Nanotubes : C1000000 and Beyond with tantalizing Some unusual new molecules ? long , hollow electronic fibers and mechanical properties ? have joined diamonds and graphite in the

carbon family," *Society*, 2012.

[33] R. Martel, T. Schmidt, H. R. Shea, T. Hertel, and P. Avouris, "Single- and multi-wall carbon nanotube field-effect transistors," vol. 73, no. 17, pp. 2447–2449, 1998.

[34] M. J. Biercuk, M. C. Llaguno, M. Radosavljevic, J. K. Hyun, a T. Johnson, and J. E. Fischer, "Carbon nanotube composites for thermal management," *Appl. Phys. Lett.*, vol. 80, no. 15, pp. 2767–2769, 2002.

[35] A. K. Geim and K. S. Novoselov, "The rise of graphene.," *Nat. Mater.*, vol. 6, no. 3, pp. 183–191, 2007.

[36] A. Malesevic, R. Vitchev, K. Schouteden, A. Volodin, L. Zhang, G. Van Tendeloo, A. Vanhulsel, and C. Van Haesendonck, "Synthesis of few-layer graphene via microwave plasma-enhanced chemical vapour deposition.," *Nanotechnology*, vol. 19, no. 30, p. 305604, 2008.

[37] A. a Balandin, S. Ghosh, W. Bao, I. Calizo, D. Teweldebrhan, F. Miao, and C. N. Lau, "Superior Thermal Conductivity of Single-Layer Graphene 2008," *Nano Lett.*, vol. 8, pp. 902–907, 2008.

[38] C. Lee, X. Wei, J. W. Kysar, and J. Hone, "Measurement of the elastic properties and intrinsic strength of monolayer graphene.," *Science*, vol. 321, no. 5887, pp. 385–388, 2008.

[39] R. R. Nair, P. Blake, a. N. Grigorenko, K. S. Novoselov, T. J. Booth, T. Stauber, N. M. R. Peres, and a. K. Geim, "Fine Structure Constant Defines Visual Transperency of Graphene," *Science (80-.).*, vol. 320, no. June, p. 2008, 2008.

[40] C. N. R. Rao, a. K. Sood, K. S. Subrahmanyam, and a. Govindaraj, "Graphene: The new two-dimensional nanomaterial," *Angew. Chemie - Int. Ed.*, vol. 48, no. 42, pp. 7752–7777, 2009.

[41] T. Kobayashi, M. Bando, N. Kimura, K. Shimizu, K. Kadono, N. Umezu, K. Miyahara, S. Hayazaki, S. Nagai, Y. Mizuguchi, Y. Murakami, and D. Hobara, "Production of a 100-m-long high-quality graphene transparent conductive film by roll-to-roll chemical vapor deposition and transfer process," *Appl. Phys. Lett.*, vol. 102, no. 2, p. 023112, 2013.

[42] A. Ciesielski and P. Samorì, "Grapheneviasonication assisted liquid-phase exfoliation," *Chem. Soc. Rev.*, vol. 43, no. 1, pp. 381–398, 2014.

[43] B. C. Brodie, "Sur le poids atomique du graphite." Ann.Chim., pp. 466–472, 1860.

[44] L. Staudenmaier, "Verfahren zur darstellung der graphitsaure." Ber. Dtsch. Chem. Ges., pp. 1481–1487, 1898.

[45] Y. Zhu, S. Murali, M. D. Stoller, A. Velamakanni, R. D. Piner, and R. S. Ruoff, "Microwave assisted exfoliation and reduction of graphite oxide for ultracapacitors," *Carbon N. Y.*, vol. 48, no. 7, pp. 2118–2122, 2010.

[46] Y. Zhu, S. Murali, W. Cai, X. Li, J. W. Suk, J. R. Potts, and R. S. Ruoff, "Graphene and Graphene Oxide: Synthesis, Properties, and Applications," *Adv. Mater.*, vol. 22, no. 35, pp. 3906–3924, 2010.

[47] K. Erickson, R. Erni, Z. Lee, N. Alem, W. Gannett, and A. Zettl, "Determination of the local chemical structure of graphene oxide and reduced graphene oxide," *Adv. Mater.*, vol. 22, no. 40, pp. 4467–4472, 2010.

[48] C. Zhu, S. Guo, Y. Fang, and S. Dong, "Reducing sugar: New functional molecules for the green synthesis of graphene nanosheets," *ACS Nano*, vol. 4, no. 4, pp. 2429–2437, 2010.

[49] J. N. Israelachvili, *Intermolecular and Surface Forces*. (Academic Press, Harcourt Brace

Jovanovich), 2011.

[50] S. R. Solomon HM1, Burgess BA, Kennedy GL Jr, "1-Methyl-2-pyrrolidone (NMP): reproductive and developmental toxicity study by inhalation in the rat," *Drug Chem Toxicol*, vol. 18, no. 4, pp. 271–293, 1995.

[51] R. Tolando, a Zanovello, R. Ferrara, J. N. Iley, and M. Manno, "Inactivation of rat liver cytochrome P450 (P450) by N,N-dimethylformamide and N,N-dimethylacetamide.," *Toxicol. Lett.*, vol. 124, no. 1–3, pp. 101–11, 2001.

[52] A. O'Neill, U. Khan, P. N. Nirmalraj, J. Boland, and J. N. Coleman, "Graphene dispersion and exfoliation in low boiling point solvents," *J. Phys. Chem. C*, vol. 115, no. 13, pp. 5422–5428, 2011.

[53] Y. Hernandez, M. Lotya, D. Rickard, S. D. Bergin, and J. N. Coleman, "Measurement of multicomponent solubility parameters for graphene facilitates solvent discovery," *Langmuir*, vol. 26, no. 5, pp. 3208–3213, 2010.

[54] Q. Cheng, S. Debnath, E. Gregan, and H. J. Byrne, "Ultrasound-Assisted swnts dispersion: Effects of sonication parameters and solvent properties," *J. Phys. Chem. C*, vol. 114, no. 19, pp. 8821–8827, 2010.

[55] J. Raso, P. Mañas, R. Pagán, and F. J. Sala, "Influence of different factors on the output power transferred into medium by ultrasound.," *Ultrason. Sonochem.*, vol. 5, no. 4, pp. 157–162, 1999.

[56] G. Ralston and G. Ralston, "Introduction to Analytical Ultracentrifugation," pp. xi, 87p, 1993.

[57] K. M. Brakke, *Die Ultrazentrifuge*, Vol. 2. Springer, 1953.

[58] A. V. Alaferdov, A. Gholamipour-Shirazi, M. a. Canesqui, Y. a. Danilov, and S. a. Moshkalev, "Size-controlled synthesis of graphite nanoflakes and multi-layer graphene by liquid phase exfoliation of natural graphite," *Carbon N. Y.*, vol. 69, pp. 525–535, 2014.

[59] A. Balandin, "Review of the Low-Frequency 1/f Noise in Graphene Devices," *arXiv Prepr. arXiv1307.4797*, pp. 1–25, 2013.

[60] E. Perkins, L. Barreto, J. Wells, and P. Hofmann, "Surface-sensitive conductivity measurement using a micro multi-point probe approach," *Rev. Sci. Instrum.*, vol. 84, no. 3, p. 033901, 2013.

[61] F. J. Tölle, K. Gamp, and R. Mülhaupt, "Scale-up and purification of graphite oxide as intermediate for functionalized graphene," *Carbon N. Y.*, vol. 75, no. i, pp. 432–442, 2014.

[62] J. Chen, B. Yao, C. Li, and G. Shi, "An improved Hummers method for eco-friendly synthesis of graphene oxide," *Carbon N. Y.*, vol. 64, no. 1, pp. 225–229, 2013.

[63] B. Faust, "Modern Chemical Techniques (3rd edition)," 1997.

[64] G. Eda, J. Ball, C. Mattevi, M. Acik, L. Artiglia, G. Granozzi, Y. Chabal, T. D. Anthopoulos, and M. Chhowalla, "Partially oxidized graphene as a precursor to graphene," *J. Mater. Chem.*, vol. 21, no. 30, p. 11217, 2011.

[65] C. S. R. Ingle James D. J, *Spectrochemical Analysis*, vol. 33. Englewood Cliffs, NJ 07632: Prentice-Hall, 1988.

[66] D. D. Nguyen, N. H. Tai, Y. L. Chueh, S. Y. Chen, Y. J. Chen, W. S. Kuo, T. W. Chou, C. S. Hsu, and L. J. Chen, "Synthesis of ethanol-soluble few-layer graphene nanosheets for flexible and transparent conducting composite films.," *Nanotechnology*, vol. 22, no. 29,

p. 295606, 2011.

[67] M. Xu, W. Zhang, Z. Yang, F. Yu, Y. Ma, N. Hu, D. He, Q. Liang, Y. Su, and Y. Zhang, “One-pot liquid-phase exfoliation from graphite to graphene with carbon quantum dots,” *Nanoscale*, pp. 10527–10534, 2015.

[68] A. C. Ferrari, J. C. Meyer, V. Scardaci, C. Casiraghi, M. Lazzeri, F. Mauri, S. Piscanec, D. Jiang, K. S. Novoselov, S. Roth, and a. K. Geim, “Raman spectrum of graphene and graphene layers,” *Phys. Rev. Lett.*, vol. 97, no. 18, pp. 1–4, 2006.

[69] L. M. Malard, M. a. Pimenta, G. Dresselhaus, and M. S. Dresselhaus, “Raman spectroscopy in graphene,” *Phys. Rep.*, vol. 473, no. 5–6, pp. 51–87, 2009.

[70] A. C. Ferrari, “Raman spectroscopy of graphene and graphite: Disorder, electron-phonon coupling, doping and nonadiabatic effects,” *Solid State Commun.*, vol. 143, no. 1–2, pp. 47–57, 2007.

[71] S. Gayathri, P. Jayabal, M. Kottaisamy, and V. Ramakrishnan, “Synthesis of few layer graphene by direct exfoliation of graphite and a Raman spectroscopic study,” *AIP Adv.*, vol. 4, no. 2, pp. 0–12, 2014.

[72] D. R. Lenski and M. S. Fuhrer, “Raman and optical characterization of multilayer turbostratic graphene grown via chemical vapor deposition,” *J. Appl. Phys.*, vol. 110, no. 1, 2011.

[73] Z. H. Ni, H. M. Wang, Y. Ma, J. Kasim, Y. H. Wu, and Z. X. Shen, “Tunable stress and controlled thickness modification in graphene by annealing,” *ACS Nano*, vol. 2, no. 5, pp. 1033–1039, 2008.

[74] V. Chabot, B. Kim, B. Sloper, C. Tzoganakis, and A. Yu, “High yield production and purification of few layer graphene by gum arabic assisted physical sonication.,” *Sci. Rep.*, vol. 3, p. 1378, 2013.

[75] A. Reina, X. Jia, J. Ho, D. Nezich, H. Son, V. Bulovic, M. S. Dresselhaus, and J. Kong, “LETTERS Large Area , Few-Layer Graphene Films on Arbitrary Substrates by Chemical Vapor Deposition,” vol. xx, no. x, pp. 30–35, 2009.

[76] I. F. Cheng, Y. Xie, R. Allen Gonzales, P. R. Brejna, J. P. Sundararajan, B. a. Fouetio Kengne, D. Eric Aston, D. N. McIlroy, J. D. Foutch, and P. R. Griffiths, “Synthesis of graphene paper from pyrolyzed asphalt,” *Carbon N. Y.*, vol. 49, no. 8, pp. 2852–2861, 2011.

[77] C. T. J. Low, F. C. Walsh, M. H. Chakrabarti, M. a. Hashim, and M. a. Hussain, “Electrochemical approaches to the production of graphene flakes and their potential applications,” *Carbon N. Y.*, vol. 54, no. APRIL, pp. 1–21, 2013.

[78] K. Arapov, A. Goryachev, G. De With, and H. Friedrich, “A simple and flexible route to large-area conductive transparent graphene thin-films,” *Synth. Met.*, vol. 201, pp. 67–75, 2015.

[79] Z. Ni, Y. Wang, T. Yu, and Z. Shen, “Raman spectroscopy and imaging of graphene,” 2008.

[80] H. Search, C. Journals, A. Contact, M. Iopscience, and I. P. Address, “Spectroscopic Raman Nanometrology of Graphene and Graphene Multilayers on Arbitrary Substrates,” vol. 012008.

[81] a Das, S. Pisana, B. Chakraborty, S. Piscanec, S. K. Saha, U. V Waghmare, K. S. Novoselov, H. R. Krishnamurthy, a K. Geim, a C. Ferrari, and a K. Sood, “Monitoring dopants by Raman scattering in an electrochemically top-gated graphene transistor.,” *Nat. Nanotechnol.*, vol. 3, no. 4, pp. 210–215, 2008.

[82] M. M. Hossain, O. K. Park, J. R. Hahn, and B. C. Ku, “High yield and high concentration few-layer graphene sheets using solvent exfoliation of graphite with pre-thermal treatment in a sealed bath,” *Mater. Lett.*, vol. 123, pp. 90–92, 2014.

[83] L. Reimer, *Transmission Electron Microscopy Physics of Image Formations and Microanalysis*, Verlag Ber., vol. 36. New York Tokio: Springer Open Ltd, 1984.

[84] K. S. Novoselov, “Electric Field Effect in Atomically Thin Carbon Films,” *Science (80-.).*, vol. 666, no. October, pp. 666–669, 2007.

[85] Y. Wu, B. Wang, Y. Ma, Y. Huang, N. Li, F. Zhang, and Y. Chen, “Efficient and large-scale synthesis of few-layered graphene using an arc-discharge method and conductivity studies of the resulting films,” *Nano Res.*, vol. 3, no. 9, pp. 661–669, 2010.

[86] F. Bonaccorso, Z. Sun, T. Hasan, and a C. Ferrari, “Graphene Photonics and Optoelectronics,” *Nat. Photonics*, vol. 4, no. 9, pp. 611–622, 2010.

[87] S. Stankovich, D. a. Dikin, G. H. B. Dommett, K. M. Kohlhaas, E. J. Zimney, E. a. Stach, R. D. Piner, S. T. Nguyen, and R. S. Ruoff, “Graphene-based composite materials,” *Nature*, vol. 442, no. 7100, pp. 282–286, 2006.

[88] H. a. Becerril, J. Mao, Z. Liu, R. M. Stoltenberg, Z. Bao, and Y. Chen, “Evaluation of solution-processed reduced graphene oxide films as transparent conductors,” *ACS Nano*, vol. 2, no. 3, pp. 463–470, 2008.

[89] J. Wu, M. Agrawal, a Becerril, Z. Bao, Z. Liu, Ќ. Y. Chen, and P. Peumans, “Organic Light-Emitting Diodes on,” vol. 4, no. 1, pp. 43–48, 2010.

[90] V. C. Tung, L. Chen, M. J. Allen, K. Wassei, K. Nelson, R. B. Kaner, Y. Yang, V. C. Tung, L. Chen, M. J. Allen, J. K. Wassei, K. Nelson, R. B. Kaner, and Y. Yang, “Low-Temperature Solution Processing of Graphene− Carbon Nanotube Hybrid Materials for High-Performance Transparent Conductorsvincent_graphene_cnt_nanoletter.pdf,” 2009.

[91] X. Wang, L. Zhi, N. Tsao, Ž. Tomović, J. Li, and K. Müllen, “Transparent carbon films as electrodes in organic solar cells,” *Angew. Chemie - Int. Ed.*, vol. 47, no. 16, pp. 2990–2992, 2008.

[92] P. Blake, P. D. Brimicombe, R. R. Nair, T. J. Booth, D. Jiang, and F. Schedin, “Graphene-Based Liquid Crystal Device,” pp. 1–13.

[93] A. a. Green and M. C. Hersam, “Solution phase production of graphene with controlled thickness via density differentiation,” *Nano Lett.*, vol. 9, no. 12, pp. 4031–4036, 2009.

[94] S. A. Abraham, D. N. Waterhouse, L. D. Mayer, P. R. Cullis, T. D. Madden, and M. B. Bally, “The Liposomal Formulation of Doxorubicin,” in *METHODS IN ENZYMOLOGY*, vol. 391, Elsevier, 2005, pp. 71–97.

[95] S. Wu, X. Zhao, Y. Li, Q. Du, J. Sun, Y. Wang, X. Wang, Y. Xia, Z. Wang, and L. Xia, “Adsorption properties of doxorubicin hydrochloride onto graphene oxide: Equilibrium, kinetic and thermodynamic studies,” *Materials (Basel).*, vol. 6, no. 5, pp. 2026–2042, 2013.

[96] S. Liu, A. C.-T. Ko, W. Li, W. Zhong, and M. Xing, “NIR initiated and pH sensitive single-wall carbon nanotubes for doxorubicin intracellular delivery,” *J. Mater. Chem. B*, vol. 2, no. 9, p. 1125, 2014.

[97] I. F. Tannock and D. Rotin, “Acid pH in tumors and its potential for therapeutic exploitation.,” *Cancer Res.*, vol. 49, no. 16, pp. 4373–4384, 1989.

[98] M. F. McCarty and J. Whitaker, “Manipulating tumor acidification as a cancer treatment strategy,” *Altern. Med. Rev.*, vol. 15, no. 3, pp. 264–272, 2010.

[99] J. Chen, A. C. Ko, W. Liao, and M. Xing, “Reducible polyamidoamine-magnetic iron oxide self-assembled nanoparticles for doxorubicin delivery,” no. September 2015, 2013.

[100] Y. Tian, A. Glogowska, W. Zhong, T. Klonisch, and M. Xing, “Polymeric mesoporous silica nanoparticles as a pH-responsive switch to control doxorubicin intracellular delivery,” *J. Mater. Chem. B*, vol. 1, no. 39, p. 5264, 2013.

[101] J. Chen, J. Ouyang, J. Kong, W. Zhong, and M. M. Xing, “Photo-cross-linked and pH-sensitive biodegradable micelles for doxorubicin delivery,” *ACS Appl. Mater. Interfaces*, vol. 5, no. 8, pp. 3108–3117, 2013.

[102] S. Liu, A. C.-T. Ko, W. Li, W. Zhong, and M. Xing, “NIR initiated and pH sensitive single-wall carbon nanotubes for doxorubicin intracellular delivery,” *J. Mater. Chem. B*, vol. 2, no. 9, p. 1125, 2014.

[103] Z. Liu, S. Tabakman, K. Welsher, and H. Dai, “Carbon nanotubes in biology and medicine: In vitro and in vivo detection, imaging and drug delivery,” *Nano Res.*, vol. 2, no. 2, pp. 85–120, 2009.

[104] J. S. Mattson and H. B. Mark, “Infrared internal reflectance spectroscopic determination of surface functional groups on carbon,” *J. Colloid Interface Sci.*, vol. 31, no. 1, pp. 131–144, 1969.

[105] D. W. Lee, L. De Los Santos V., J. W. Seo, L. L. Felix, a. Bustamante D., J. M. Cole, and C. H. W. Barnes, “The structure of graphite oxide: Investigation of its surface chemical groups,” *J. Phys. Chem. B*, vol. 114, no. 17, pp. 5723–5728, 2010.

[106] H. He, J. Klinowski, M. Forster, and A. Lerf, “A new structural model for graphite oxide,” *Chem. Phys. Lett.*, vol. 287, no. 1–2, pp. 53–56, 1998.

[107] A. Lagutschenkov and O. Dopfer, “Infrared spectrum of a protonated fluorescence dye: Acridine orange,” *J. Mol. Spectrosc.*, vol. 268, no. 1–2, pp. 66–77, 2011.

[108] A. Orange, S. Solution, P. Description, and C. Form, “Acridine Orange Product information,” pp. 2–3.

[109] M. Shaikh, J. Mohanty, P. K. Singh, W. M. Nau, and H. Pal, “Complexation of acridine orange by cucurbit[7]uril and beta-cyclodextrin: photophysical effects and pKa shifts.,” *Photochem. Photobiol. Sci.*, vol. 7, no. 4, pp. 408–414, 2008.

[110] J. Han and K. Burgess, “Fluorescent indicators for intracellular pH,” *Chem. Rev.*, vol. 110, no. 5, pp. 2709–2728, 2009.

[111] I. Ali and V. K. Gupta, “Advances in water treatment by adsorption technology.,” *Nat. Protoc.*, vol. 1, no. 6, pp. 2661–2667, 2006.

[112] V. K. Gupta, P. J. M. Carrott, M. M. L. Ribeiro Carrott, and Suhas, “Low-Cost Adsorbents: Growing Approach to Wastewater Treatment—a Review,” *Crit. Rev. Environ. Sci. Technol.*, vol. 39, no. 10, pp. 783–842, 2009.

[113] B. H. Hameed, a. L. Ahmad, and K. N. a Latiff, “Adsorption of basic dye (methylene blue) onto activated carbon prepared from rattan sawdust,” *Dye. Pigment.*, vol. 75, no. 1, pp. 143–149, 2007.

[114] B. Fugetsu, S. Satoh, T. Shiba, T. Mizutani, Y. B. Lin, N. Terui, Y. Nodasaka, K. Sasa, K. Shimizu, T. Akasaka, M. Shindoh, K. I. Shibata, A. Yokoyama, M. Mori, K. Tanaka, Y. Sato, K. Tohji, S. Tanaka, N. Nishi, and F. Watari, “Caged multiwalled carbon nanotubes as the adsorbents for affinity-based elimination of ionic dyes,” *Environ. Sci. Technol.*, vol. 38, no. 24, pp. 6890–6896, 2004.

[115] P. Bradder, S. K. Ling, S. Wang, and S. Liu, “Dye Adsorption on Layered Graphite Oxide,”

J. Chem. Eng. Data, vol. 56, no. 1, pp. 138–141, 2011.

[116] N. A. Travlou, G. Z. Kyzas, N. K. Lazaridis, and E. A. Deliyanni, "Functionalization of graphite oxide with magnetic chitosan for the preparation of a nanocomposite dye adsorbent," *Langmuir*, vol. 29, no. 5, pp. 1657–1668, 2013.

[117] J. Zhao, W. Ren, and H.-M. Cheng, "Graphene sponge for efficient and repeatable adsorption and desorption of water contaminations," *J. Mater. Chem.*, vol. 22, no. 38, p. 20197, 2012.

[118] G. K. Ramesha, a. Vijaya Kumara, H. B. Muralidhara, and S. Sampath, "Graphene and graphene oxide as effective adsorbents toward anionic and cationic dyes," *J. Colloid Interface Sci.*, vol. 361, no. 1, pp. 270–277, 2011.

[119] T. J. Mason and J. P. Lorimer, *Applied Sonochemistry: The Uses Of Power Ultrasound in Chemistry and Processing*, vol. 0. 2002.

[120] K. R. Paton, E. Varrla, C. Backes, R. J. Smith, U. Khan, A. O'Neill, C. Boland, M. Lotya, O. M. Istrate, P. King, T. Higgins, S. Barwich, P. May, P. Puczkarski, I. Ahmed, M. Moebius, H. Pettersson, E. Long, J. Coelho, S. E. O'Brien, E. K. McGuire, B. M. Sanchez, G. S. Duesberg, N. McEvoy, T. J. Pennycook, C. Downing, A. Crossley, V. Nicolosi, and J. N. Coleman, "Scalable production of large quantities of defect-free few-layer graphene by shear exfoliation in liquids.," *Nat. Mater.*, vol. 13, no. 6, pp. 624–30, 2014.

[121] U. Khan, H. Porwal, A. Óneill, K. Nawaz, P. May, and J. N. Coleman, "Solvent-exfoliated graphene at extremely high concentration," *Langmuir*, vol. 27, no. 15, pp. 9077–9082, 2011.

[122] Y. Hernandez, M. Lotya, D. Rickard, S. D. Bergin, N. Jonathan, and J. N. A. C. S. Nano, "Supporting Information Multi-component solubility parameters for graphene School of Physics , Trinity College Dublin , Dublin 2 , Ireland Centre for Research on Adaptive Nanostructures and Nanodevices (CRANN), Trinity College Dublin , Dublin 2 , Ireland," pp. 9–11.

[123] R. E. Schirmer, "UV and Visible Adsorption Techniques," in *Modern Methods of Pharmaceutical Analysis*, Volume I., B. R. CRC Press Inc., Ed. 1982, p. 304 pp.

[124] S. Gayathri, P. Jayabal, M. Kottaisamy, and V. Ramakrishnan, "Synthesis of few layer graphene by direct exfoliation of graphite and a Raman spectroscopic study," *AIP Adv.*, vol. 4, no. 2, p. 027116, 2014.

[125] a C. Ferrari, J. C. Meyer, V. Scardaci, C. Casiraghi, M. Lazzeri, S. Piscanec, K. S. Novoselov, S. Roth, and a K. Geim, "The Raman Fingerprint of Graphene," *Evolution (N. Y).*, vol. 1, pp. 1–5, 2007.

[126] Q.-Q. Li, X. Zhang, W.-P. Han, Y. Lu, W. Shi, J.-B. Wu, and P.-H. Tan, "Raman spectroscopy at the edges of multilayer graphene," *Carbon N. Y.*, vol. 85, pp. 221–224, 2015.

[127] J. R. Williams, L. DiCarlo, and C. M. Marcus, "Quantum Hall Effect in a Graphene p-n Junction," no. 2, pp. 1–4, 2007.

[128] H. Wang, Y. Wu, C. Cong, J. Shang, and T. Yu, "Hysteresis of electronic transport in graphene transistors," *ACS Nano*, vol. 4, no. 12, pp. 7221–7228, 2010.

[129] X. Li, Y. Zhu, W. Cai, M. Borysiak, B. Han, D. Chen, R. D. Piner, L. Colomba, and R. S. Ruoff, "Transfer of large-area graphene films for high-performance transparent conductive electrodes," *Nano Lett.*, vol. 9, no. 12, pp. 4359–4363, 2009.

[130] S. L. Rumyantsev, D. Coquillat, R. Ribeiro, M. Goiran, W. Knap, M. S. Shur, a. a. Balandin, and M. E. Levinshtein, "The effect of a transverse magnetic field on 1/f noise

in graphene," *Appl. Phys. Lett.*, vol. 103, no. 17, pp. 2011–2015, 2013.

[131] Y. Lu, X.-Y. Yang, and B.-L. Su, "Self-assembly to monolayer graphene film with high electrical conductivity," *J. Energy Chem.*, vol. 22, no. 1, pp. 52–57, 2013.

[132] C. Ciofi, F. Crupi, C. Pace, and G. Scandurra, "Micro-prober for wafer-level low-noise measurements in MOS devices," *IEEE Trans. Instrum. Meas.*, vol. 52, no. 5, pp. 1533–1536, 2003.

[133] C. P. -, J. L. H. A. -, D. D. P. -, and G. C. -, "Instrumentation for Innovative Semiconductor Power Devices Reliability Tests," *Int. J. Eng. Ind.*, vol. 4, no. 2, pp. 70–78, 2013.

[134] J. Martin, N. Akerman, G. Ulbricht, T. Lohmann, J. H. Smet, K. von Klitzing, and A. Yacoby, "Observation of Electron-Hole Puddles in Graphene Using a Scanning Single Electron Transistor," *Nat. Phys.*, no. 4, pp. 144 – 148, 2008.

[135] M. M. Fogler, "Neutrality point of graphene with coplanar charged impurities," *Phys. Rev. Lett.*, vol. 103, no. 23, 2009.

[136] D. Schroeder, T. Ostermann, and O. Kalz, "Nonlinear Contact Resistance and Inhomogeneous Current Distribution at Ohmic Contacts," *Simul. Semicond. Devices …*, vol. 5, no. September, pp. 3–6, 1993.

[137] J. Gao, F. Liu, Y. Liu, N. Ma, Z. Wang, and X. Zhang, "Environment-friendly method to produce graphene that employs vitamin C and amino acid," *Chem. Mater.*, vol. 22, no. 7, pp. 2213–2218, 2010.

[138] D. Zhang, L. Fu, L. Liao, N. Liu, B. Dai, and C. Zhang, "Preparation, characterization, and application of electrochemically functional graphene nanocomposites by one-step liquid-phase exfoliation of natural flake graphite with methylene blue," *Nano Res.*, vol. 5, no. 12, pp. 875–887, 2012.

[139] D. a Dikin, S. Stankovich, E. J. Zimney, R. D. Piner, G. H. B. Dommett, G. Evmenenko, S. T. Nguyen, and R. S. Ruoff, "Preparation and characterization of graphene oxide paper.," *Nature*, vol. 448, no. 7152, pp. 457–460, 2007.

[140] X. Z. Xiaoying Yang Zunfeng Liu, Yanfeng Ma, Yi Huang,and and Y. Chen, "High-Efficiency Loading and Controlled Release of Doxorubicin Hydrochloride on\rGraphene Oxide," *J Phys Chem C*, vol. 112, p. 17554, 2008.

[141] D. Depan, J. Shah, and R. D. K. Misra, "Controlled release of drug from folate-decorated and graphene mediated drug delivery system: Synthesis, loading efficiency, and drug release response," *Mater. Sci. Eng. C*, vol. 31, no. 7, pp. 1305–1312, 2011.

[142] Q. Zhang, W. Li, T. Kong, R. Su, N. Li, Q. Song, M. Tang, L. Liu, and G. Cheng, "Tailoring the interlayer interaction between doxorubicin-loaded graphene oxide nanosheets by controlling the drug content," *Carbon N. Y.*, vol. 51, no. 1, pp. 164–172, 2013.

[143] J. Zhang, X. G. Chen, Y. Y. Li, and C. S. Liu, "Self-assembled nanoparticles based on hydrophobically modified chitosan as carriers for doxorubicin," *Nanomedicine Nanotechnology, Biol. Med.*, vol. 3, no. 4, pp. 258–265, 2007.

[144] G. Das, A. Nicastri, M. L. Coluccio, F. Gentile, P. Candeloro, G. Cojoc, C. Liberale, F. De Angelis, and E. Di Fabrizio, "FT-IR, Raman, RRS measurements and DFT calculation for doxorubicin," *Microsc. Res. Tech.*, vol. 73, no. 10, pp. 991–995, 2010.

[145] T. Szabó, E. Tombácz, E. Illés, and I. Dékány, "Enhanced acidity and pH-dependent surface charge characterization of successively oxidized graphite oxides," *Carbon N. Y.*, vol. 44, no. 3, pp. 537–545, 2006.

[146] Y. Lu, X. Yang, Y. Ma, Y. Huang, and Y. Chen, "A novel nanohybrid of daunomycin and

single-walled carbon nanotubes: photophysical properties and enhanced electrochemical activity," *Biotechnol. Lett.*, vol. 30, no. 6, pp. 1031–1035, 2008.

[147] L. Sun, H. Yu, and B. Fugetsu, "Graphene oxide adsorption enhanced by in situ reduction with sodium hydrosulfite to remove acridine orange from aqueous solution.," *J. Hazard. Mater.*, vol. 203–204, pp. 101–10, 2012.

[148] Y. Xie, F. Chen, J. He, J. Zhao, and X. Hu, "Photoassisted degradation of dyes in the presence of Fe3+ and H2O2 under visible irradiation.," vol. 41, no. 136, pp. 235–240, 2000.

[149] G. K. Meffe, "Author Guidelines," *Conserv. Biol.*, vol. 24, pp. 3–9, 2006.

[150] T. Hartono, S. Wang, Q. Ma, and Z. Zhu, "Layer structured graphite oxide as a novel adsorbent for humic acid removal from aqueous solution," *J. Colloid Interface Sci.*, vol. 333, no. 1, pp. 114–119, 2009.

[151] H. Yu and B. Fugetsu, "A novel adsorbent obtained by inserting carbon nanotubes into cavities of diatomite and applications for organic dye elimination from contaminated water.," *J. Hazard. Mater.*, vol. 177, no. 1–3, pp. 138–45, 2010.

[152] S. Qadri, A. Ganoe, and Y. Haik, "Removal and recovery of acridine orange from solutions by use of magnetic nanoparticles," *J. Hazard. Mater.*, vol. 169, no. 1–3, pp. 318–323, 2009.

[153] D. Garfinkel-Shweky and S. Yariv, "Metachromasy in Clay Dye Systems: The Adsorption of Acridine Orange by Na-Beidellite," *Clay Miner.*, vol. 34, pp. 459–467, 1999.

[154] D. M. Salh, "Removal of Acridine Orange from Waste Water using Different Natural clays," no. 05, pp. 2–6, 2013.

Publications

- Alternative method to obtained Liquid-Phase Exfoliated Graphene Self-Assembled Films: Low-Frequency Noise and Thermal-Electric Characterization, G. Tubon Usca, J. Hernandez Ambato, A. Tavolaro, C. Pace and L. S. Caputi, Applied Surface Science, 2015, submitted.
- Preparation of graphene oxide as biomaterials for drug adsorption, G. Tubón Usca, C. Vacacela Gómez, D. Coello Fiallos, P. Tavolaro, G. Martino, L. S. Caputi and A. Tavolaro AIP Conf. Proc. 1646 , 79 (2015). DOI: 10.1063/1.4908586
- Removal of acridine orange from water by graphene oxide, D. Coello Fiallos, C. Vacacela Gómez, G. Tubón Usca, D. Cid Pérez, P. Tavolaro, G. Martino, L. S. Caputi and A. Tavolaro, AIP Conf. Proc. 1646 , 38 (2015). DOI: 10.1063/1.4908580

Conferences

Oral Presentations

- "Alternative method to obtained Liquid-Phase Exfoliated Graphene Self-Assembled Films: Low-Frequency Noise and Thermal-Electric", G. Tubon Usca, J. Hernandez Ambato, C. Pace, L. S. Caputi and A. Tavolaro, ITM days and seminars, November 2015, Rende - Italy.
- "Noise and Thermal Characterization of Exfoliated Graphene Films", G. Tubon Usca, J. Hernandez Ambato, A. Tavolaro, C. Pace & L. S. Caputi, NANOSMAT 2015, Manchester Conference Centre, September 2015, Manchester - United Kingdom.
- "Preparation of graphene oxide as biomaterials for drug adsorption", D. Coello, C. Vacacela, G. Tubon, P.Tavolaro, G. Martino, L. Caputi, A.Tavolaro, NN14 Conference, July 2014, Thessaloniki – Grecee.
- Environmental application of graphite oxide in acridine orange adsorption for water remediation, D. Coello, C. Vacacela, G. Tubon, P.Tavolaro, G. Martino, L. Caputi, A.Tavolaro, NN14 Conference, July 2014, Thessaloniki – Grecee.

Posters presentations

- Hard Templated hydrothermal synthesis of mel zeolite crystals, ITM days seminars and conference, Rende, Italy, 2014.
- Graphene Oxide as novel adsorbent for waste containing dyes, Nanotech Italy conference, Venecia, Italy, 2014.
- “Preparation of graphite oxide materials preparation for drug adsorption” at the NN14 Conference, Thessaloniki, Grecee, 2014.
- “Hydrothermal Exfoliation of Graphite to Produce Few-Layer Graphene” at 4th edition of Graphene Conference series, Toulouse, 2014.
- “Synthetic inorganic materials for drug adsorption” “ G.Tubón and A. Tavolaro at the Early-stage and experienced researchers – Rende, Italy, 2013.